공학박사학위논문

Optimization of Cable System for a Cable-stayed Suspension Bridge using a Simplified Analysis Model

간략화 구조해석모델을 적용한 사장-현수교 케이블 시스템의 최적화

2017 년 2 월

서울대학교 대학원

건설환경공학부

최 현 석

Optimization of Cable System for a Cable-stayed Suspension Bridge using a Simplified Analysis Model

지도교수 고 현 무

이 논문을 공학박사학위논문으로 제출함

2016년 12월

서울대학교 대학원

건설환경공학부

최 현 석

최현석의 공학박사학위논문을 인준함

2016년 12월

위 원 장 金 錦 卿 (인)

부 위 원 장 高 銳 武 (인)

위 원 李 海 成 (인)

위 원 朴 垣 錫 (인)

위 원 趙 京 提 (인)

ABSTRACT

A cable-stayed suspension bridge is a hybrid structural system that is a combination of a cable-stayed bridge and a suspension bridge. In the cable-stayed suspension bridge, the cable-stayed system is generally allocated near pylons to reduce the loads supported by the suspension cables and to improve the stiffness of the bridge. Therefore, the span length can be extended and the structural behavior can be improved. Since the suspension system and the cable-stayed system present different structural behaviors due to the discrepancy in their load carrying path and the structural discontinuity taking place at the border between both systems, the design of the cable system is a complex and time consuming work. Particularly, designers should deal with the design variables of both cable-stayed system and suspension system and analyze various combinations of the variables to secure safety, stability, and economic feasibility. However, there is no generally optimized cable system for such a structural type since a few projects have been just completed in the past century and because of the scarcity of related researches. Accordingly, in this study, an optimization procedure to find an optimal cable system with minimized construction cost of superstructure for a cable-stayed suspension bridge using Genetic Algorithm (GA) is presented, and the optimal cable systems for a roadway bridge and a railway bridge are proposed. The proposed optimal cable system is defined using several design variables including a side span length (L_s), a main span length (L_{sp}), an overlapping length (L_{ov}), a cable sag (f), and a dead load distribution factor (r). The application of the proposed optimal cable system to the practical design can enhance

the efficiency of the design process as well as reduce much time, cost and manpower for numerous iteration works.

Generally, the optimization procedure based on a GA dealing with several design variables necessitates a lot of iteration works mobilizing tremendous time, cost and manpower. This study proposes a new simplified analysis model enabling to analyze efficiently a cable-stayed suspension bridge. The proposed simplified analysis model uses the two-dimensional truss elements for all members, and the cables in the side spans are replaced with an equivalent horizontal cable spring at the pylon top. Through the comparison with FEM analysis using a commercial software, the applicability of the proposed model to the structural analysis of cable supported bridges is verified, and the simplified analysis model is employed to the proposed optimization procedure. As a result, time for assembling and analyzing a structural model for a cable-stayed suspension bridge is remarkably reduced.

Using the simplified analysis model, parametric investigations are performed to understand the effects of design modifications including the change of a side span length, the composition of a suspension section and an overlapping section, the cable sag, and the dead load distribution factor on the structural behavior under traffic load and rail load. The 3rd Bosphorus Bridge with a main span length of 1,408 m is adopted as example bridge. The results of the parametric investigations are applied to set the range of design variables in the proposed optimization procedure.

Finally, the optimization problem for the design of the cable system of a cable-stayed suspension bridge is defined as a cost optimization for finding the minimum

construction cost of superstructures. GA is employed for the optimization, design criteria for stress and deformation from the design specification of KBDC and Eurocode are employed to examine the structural safety in the optimization procedure. The optimal cable systems are proposed for both roadway and railway bridges, and a sensitivity analysis is performed to investigate the effects of the change of design constraints and variables on the optimized result. It appears that the angular change of suspension cables among the constraints and the suspension section length among the design variables are very dominant on the optimal design of cable system.

The proposed optimization procedure to find an optimal cable system for a cable-stayed suspension bridge using the simplified analysis model is so reasonable and efficient that it can be applied to the practical design process with reduced time, cost and manpower for numerous iteration works. Also, the proposed optimal cable systems for a roadway bridge and a railway bridge help design engineers avoid heavy iteration works to find a conceptual design in the preliminary design stage.

Keywords : Cable system, cable-stayed suspension bridge, cost optimization, simplified analysis model, parametric investigation, genetic algorithm, sensitivity analysis

Student Number : 2011-30985

Table of Contents

List of Figures

List of Tables

1. INTRODUCTION

1.1 Background

Since the suspension bridges using iron chain bars as suspended members were developed in the late 1700s, cable supported bridges have been generally employed to connect two faraway places and overcome long spans during the past century. In the early 1800s, cables using thousands of parallel wires with circular cross section were firstly applied to the main cable of suspension bridges, but several suspension bridges unfortunately collapsed due to wind-induced motions or crowd loads. Thus, a new suspension system strengthened by a fan-shaped stay system near the towers was developed and applied to many suspension bridges in Europe and USA. This strengthened bridge marked the beginning of the cable-stayed suspension bridge with generally main span length shorter than 300 meters. A representative suspension bridge is Brooklyn Bridge completed in 1883 which had the world's longest main span length, 486 meters, at the moment. Brooklyn Bridge has an overlapping section near each pylon, and this type is called as Roebling system. On the other hand, a structural type that has no overlapping section between a stayed system and a suspended system is called as Dischinger system, as illustrated in Figure 1.1. However, one had to wait until early 1900s to see the construction of cable-stayed suspension bridges because it was very difficult to analyze such a highly indeterminate structure and install both cables without any error in tension (Bounopane, 2006). Meanwhile, new analytical methods to analyze the cable system were developed. Therefore, suspension bridges and cable-stayed bridges became the general structural types for long span cable supported bridges as shown in Figure 1.2.

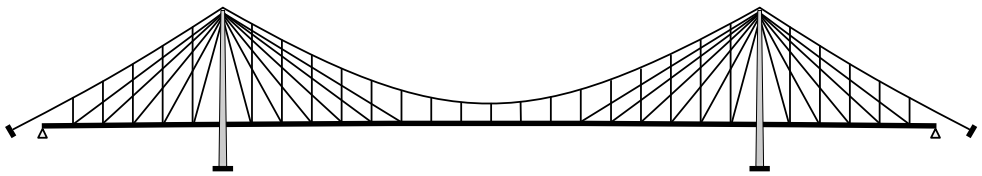

(a) Roebling system

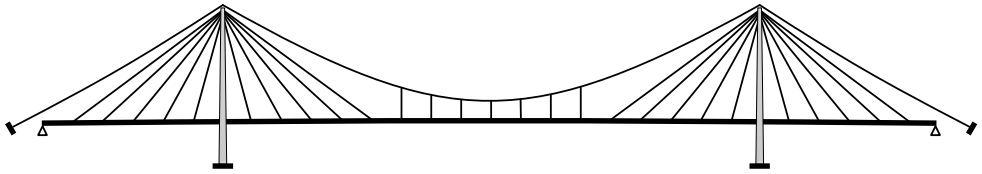

(b) Dischinger system

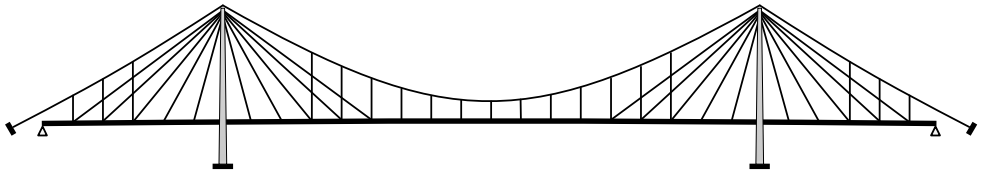

(c) Combined system

Figure 1.1 Configuration of cable-stayed suspension bridges

Recently, the cable-stayed suspension bridge combining the suspension system and cable-stayed system has been receiving attention again due to some benefits brought by reasonable structural behaviors, improved torsional stiffness and aerostatic stability for long span bridges. In addition, the cable-stayed suspension bridge can guarantee stable and safe erection stages, and improve the deformability of the deck due to the reinforcement effect of inclined stay cables especially for railway bridges (Bruno *et al.*, 2009). The remarkable example of this combination is the 3rd Bosphorus Bridge, Yavuz Sultan Selim Bridge, completed in 2016 in Turkey which has a main span length of 1,408 m for 8 traffic lanes and two railways.

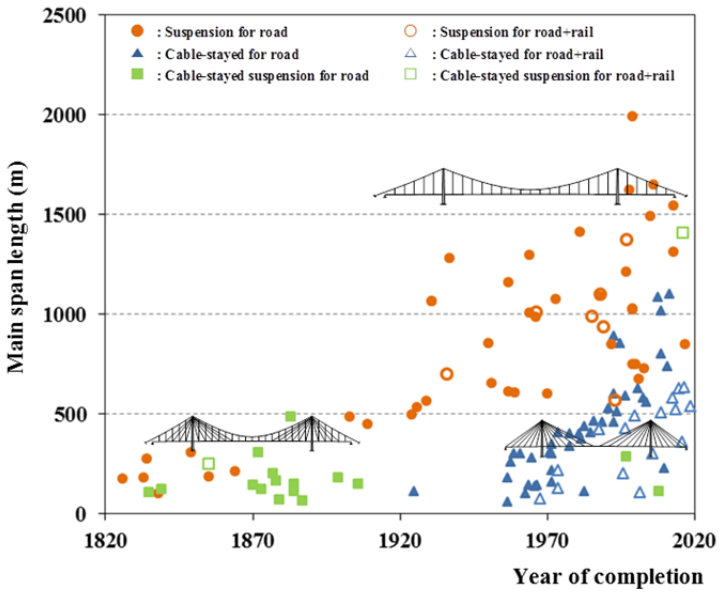

Figure 1.2 Completion of cable supported bridges since 19C

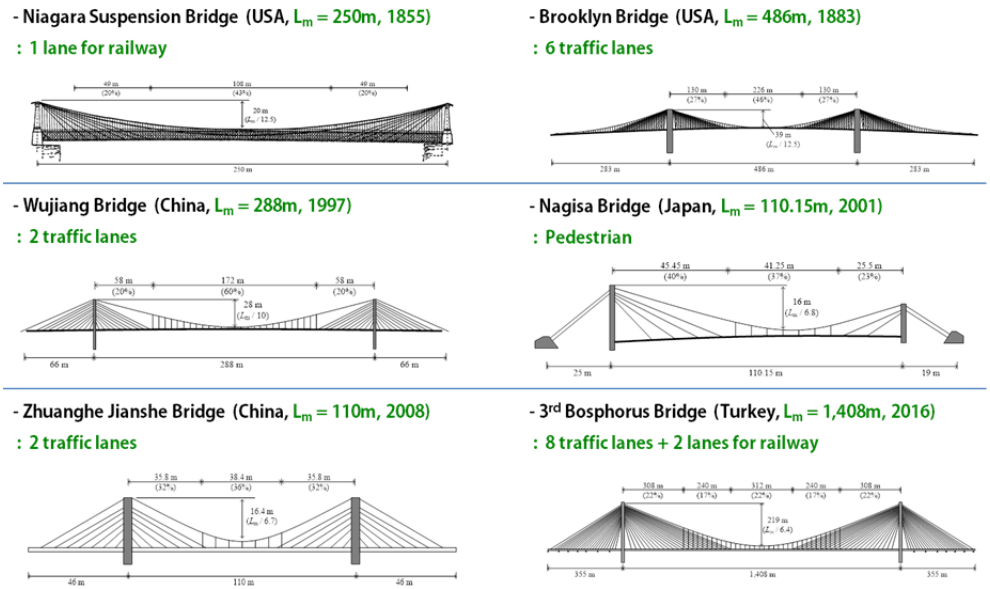

Figure 1.3 Geometric configuration of completed cable-stayed suspension bridges

A cable-stayed suspension bridge, basically, has structural discontinuity problem at the border between the stayed cable system and the suspended cable system due to the discrepancy in their structural behaviors under live loads. In case of the 3rd Bosphorus Bridge, the design of overlapping sections in the main span was revised during the detail design stage to solve the discontinuity problem. The number of hangers in the overlapping sections was increased from 8 hangers to 11 hangers, and the cross sectional area of the suspension cables was enlarged from 0.358 m^2 to 0.407 m^2 as illustrated in Figure 1.4. The increment of the overlapping hangers means the loading section supported the dead and live load of deck is increased in suspension cables, and the increment will affect the cable behavior.

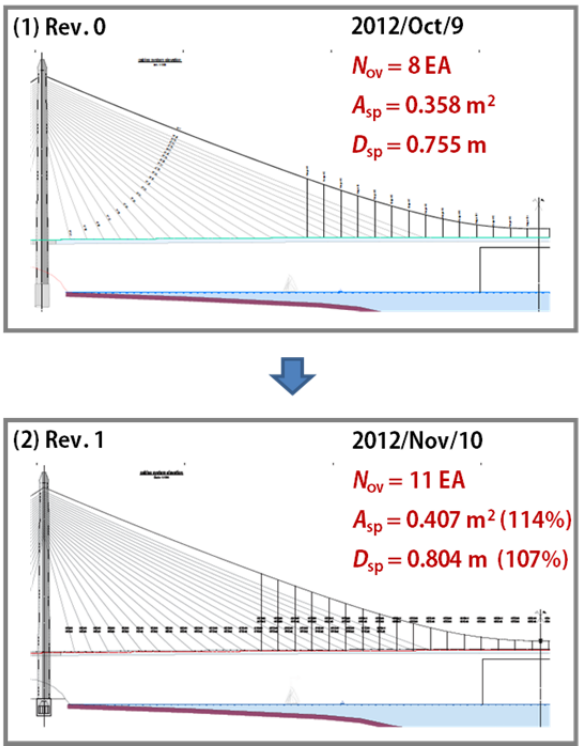

Figure 1.4 Design revision of the overlapping section for the 3rd Bosphorus Bridge

For example, a suspended cable is assumed to support a uniform distributed load with a span length of 1,500m, a sag ratio of 1/9, and a loading length of *b* as illustrated in Figure 1.5. When the uniform load is 180 kN/m and the loading length, *b*, is changed from 0 m to 1,500 m, the cable's behaviors including the vertical displacement and the angular change are investigated and plotted in Figure 1.6.

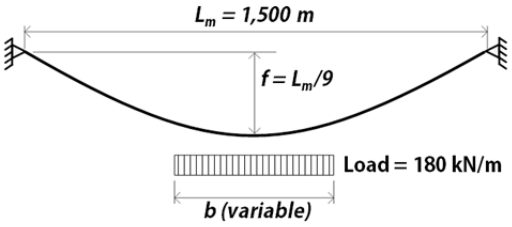

Figure 1.5 Suspended cable subjected to a uniform distributed load

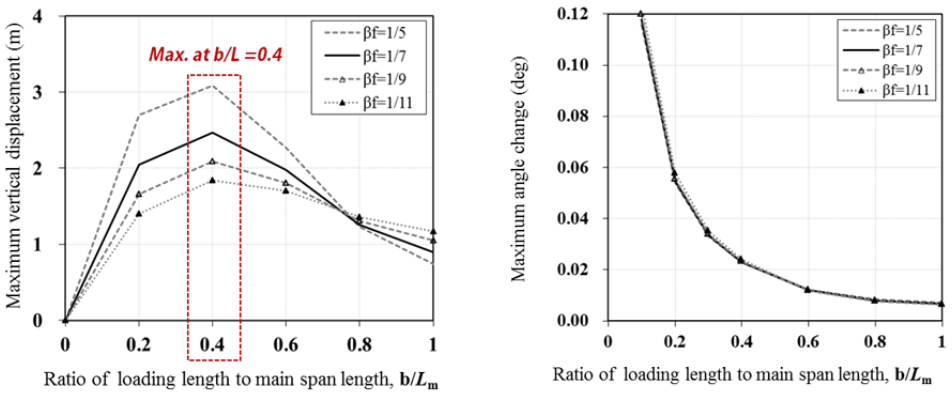

(a) Maximum vertical displacement (b) Maximum angular change

Figure 1.6 Deformation of suspended cable with various sag ratios

The maximum vertical displacement and angular change of the suspended cable

depend significantly on the loading length. As the loading length decreases, the vertical displacement and the angular change are increased, but the vertical displacement is decreased when the ratio of the loading length to the total span length is less than 0.4. Because the cable's vertical displacement and the angular change are directly related to the deformation of the deck and the inner stress of the suspended cable, respectively, it is very important to decide the portion of the loading section for the design of a cable-stayed suspension bridge. Besides, as the loading length decreases, the cross sectional area of the suspended cable may be decreased due to the reduction of the supported loads. Therefore, the design of the suspended portion for a cable-stayed suspension bridge has a trade-off problem between the performance of the bridge and the quantity of cables.

Most cable supported bridges should be designed by using iterative methods to satisfy the design criteria in a preliminary design stage. In this design process, the modelling and nonlinear cable analysis including initial shape finding analysis and live loads analysis are generally performed by 3D FEM program such as MIDAS, RM, and SAP. The finite element method has been extensively used to analyze the cable supported bridges, but it takes much time, cost, and manpower to perform the iteration works in preliminary and conceptual designs. In case of a suspension bridge or a cable-stayed bridge, designers can reduce the iteration works by using cable configurations of similar projects because the bridge's cable configuration has been optimized through a number of completed projects since 1900s. The main span length is about 200-1,000 m for cable-stayed bridge and about 500-2,000 m for suspension bridge, and the sag to span ratio is about 1/5.5~1/3.5 and about 1/11~1/9, respectively.

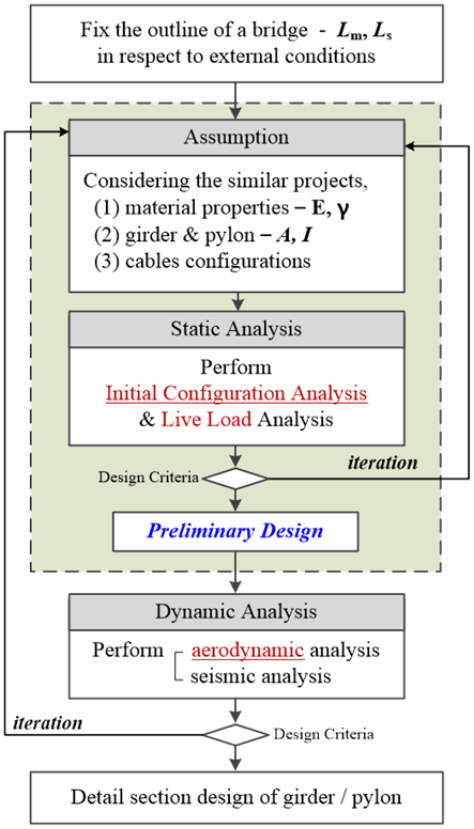

Figure 1.7 Design process of cable supported bridge

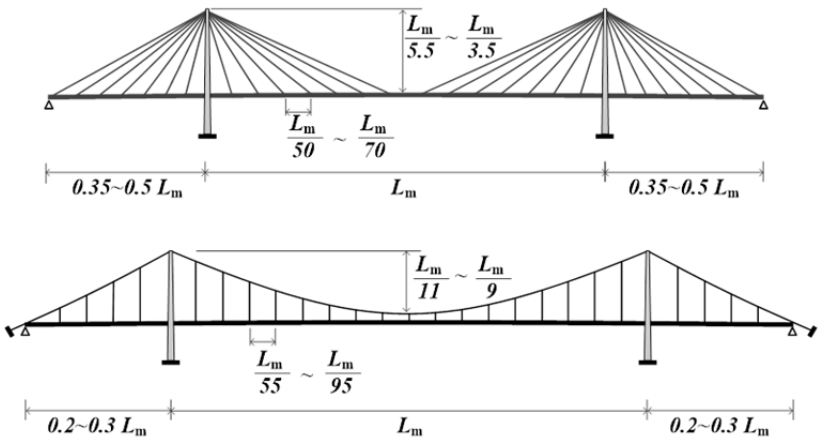

Figure 1.8 Optimized configuration of cable-stayed and suspension system

In contrast, the design of a cable-stayed suspension bridge is much complicated because the bridge involves all the design variables of both cable-stayed and suspension systems, and the absence of optimal cable configuration to secure the deformability, safety, and stability under live loads due to the very few number of completed projects as shown in Figure 1.3. A number of iterations should be performed to confirm the optimal cable system of a cable-stayed suspension bridge in a preliminary design, and it may lead to take much time, cost and designer's manpower. As a result, a relatively simple analysis model can make the design process for a cable-stayed suspension bridge reasonable and efficient, and the reasonable and efficient analysis method can suggest an optimal cable system through a number of iteration works with various combinations of design variables.

1.2 Literature Review

In this section, the previous research works on the analysis of cable-stayed suspension bridges and the optimum design of cable supported bridges are reviewed briefly. Since the early 2000s, research on the cable-stayed suspension bridges focused on the development of an initial equilibrium shape finding method, the optimization of cable tension under dead load, the structural behavior analysis under live loads. These studies dealt with three different types of systems – Roebling system, Dischinger system, combined system, and the live loads include traffic load, train load, wind load or a combination of them.

Table 1.1 Recent researches for cable-stayed suspension bridges

Title	Year	Cable System			Subject			Analysis		Live Load			Others		Publication		
		Dischinger	Combined	Roebling	Initial Configuration	Behavior Analysis	Optimization	Static	Dynamic	Traffic	Rail	Wind	Mode Analysis	Critical Wind Speed	Dissertation	Paper on Journal	Proceeding
Initial equilibrium configuration analysis for bridges supported with stayed and suspended cables	2011	•			•			•							•		
A study on initial shape finding of cable-stayed suspension bridges	2011	•			•			•							•		
Initial equilibrium configuration analysis for bridges supported with stayed and suspended cables	2011	•			•			•									•
Initial shape analysis for bridges supported with stayed and suspended cables by initial force method	2012	•			•			•									•
Initial equilibrium state analysis and buckling analysis using a fictitious axial force for cable-stayed suspension bridge	2013	•			•			•									•
Initial shape finding of a cable-stayed suspension bridge	2013		•		•			•									•
Geometric nonlinear analysis of self-anchored cable-stayed suspension bridges	2013	•				•		•		•						•	
Study on the joint part of self-anchored cable-stayed suspension bridge with hybrid girder	2013	•				•		•		•						•	
Static characteristics analysis of cable-stayed suspension bridges using CFRP cables	2013	•				•		•		•						•	
Case study on 4000m-span cable-stayed suspension bridge, Research Journal of Applied Sciences	2014	•				•		•		•						•	
吊り区間を含むＰＣ斜張橋「ハイブリッド斜張橋」の検討	2000	•				•		•		•						•	
Optimum span-ratio of cable stayed-suspension bridge	2011	•				•		•		•							•
Structural characteristics of the Nagisa-bridge (cable-stayed suspension bridge)	2005	•				•		•	•	•			•				•
Static and dynamic structural characteristics and economic efficiency of ultra long-span cable-stayed suspension bridges	2002	•				•		•	•	•		•		•		•	
Parametric analysis for systemic behavior of cable stayed-suspension bridge	2013	•				•		•	•	•		•	•				•
Applicability of Dischinger-type to ultra-long span bridges	1998	•				•		•	•				•				•
Aerodynamic stability of cable-stayed-suspension hybrid bridges	2005	•				•			•				•	•		•	
The Influence of Cable Sag on the dynamic behaviour of cable-stayed suspension bridge with variable suspension to main span ratio	2015	•				•			•				•			•	
Static and Dynamic Analysis of Cable-stayed Suspension Hybrid Bridge & Validation	2015	•				•			•				•			•	
Analysis strategy and parametric study of cable-stayed-suspension bridge	2013		•			•		•		•		•				•	
Exploration of structural form of hybrid cable-supported structures	2014		•			•		•									•
The behavior of the third Bosporus bridge related to wind and railway loads	2015		•			•			•		•						•
Structural behavior of cable-stayed suspension bridge structure	2009			•		•		•							•		
A parametric study on the dynamic behavior of combined cable-stayed and suspension bridges under moving loads	2009			•		•			•		•					•	
A mathematical model for a combined cable system of bridges	2010			•		•			•							•	
Static analysis of a self-anchored cable-stayed-suspension bridge with optimal cable tensions	2010	•					•	•								•	
Optimum design analysis of hybrid cable-stayed suspension bridges	2014			•			•	•		•						•	

For the initial equilibrium shape finding method, Kim *et al.* (2011) and Kim (2011) proposed a separation analysis method for Dischinger system by using TCUD. The method separates the initial equilibrium configuration of cable-stayed suspension bridge into three parts: the cable stayed bridge, the suspension bridge, and the hangers. The author concluded that the separation analysis method is more efficient than the lump analysis method, but the method cannot be applied to the analysis of a combined system or a Roebling system. Seo *et al.* (2013) studied an initial shape finding method considering the overlapping section. Although the method used the same separation analysis method, the initial shape for a cable-stayed suspension bridge with overlapping section was available by adopting a dead load distribution factor. The dead load distribution factor is equal to the fraction of the total dead load of the deck carried by the cable-stayed system in the regions where both the suspension and the cable stayed systems are present.

Maeda *et al.* (2002), Sun *et al.* (2013) and Cho *et al.* (2013) presented the effect of cable configuration for Dischinger system on the static structural behavior including cable tension, vertical deflection and moment of deck under traffic load. The design variables for cable configuration were the longitudinal length of suspension system in the center span and pylon height. Zhang and Sun (2005) analyzed the natural frequency and the flutter speed of Dischinger system with changing cable configuration of sag and suspension portion length in the center span. Also, Bruno *et*

al. (2009) formulated dynamic equilibrium equations for moving loads and performed a parametric study on the dynamic behavior of Roebling system under moving train loads.

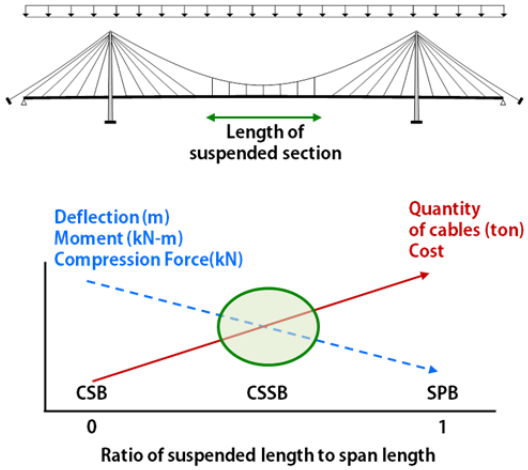

Figure 1.9 Previous research for the effect of the suspended portion on the behaviors

Lonetti and Pascuzzo (2014) proposed an optimization procedure to minimize the cable quantity of Roebling system considering the performance under traffic loads. Venkat *et al.* (2011) and Olfat (2012) used the genetic algorithm to find the optimal design of a cable-stayed bridge by minimizing the total cost of the bridge, and design constraints satisfying certain design criteria under traffic loads were adopted to the optimization process.

There is a clear lack of studies on the behavior analysis and the optimization of cable system or cost for a combined system since as described above, most of previous studies on cable-stayed suspension bridges focused on the structural analysis of Dischinger system or Roebling system under dead load and live loads.

1.3 Research Objective and Scope

In the design of a cable-stayed suspension bridge, the performance and the construction cost depend sensitively on the arrangement of cable system. However, there is currently no general cable system or geometric configuration for the cable system design of a cable-stayed suspension bridge due to a lack of completed project and the abundance of design variables. Much cost, time, and manpower should be consumed at the preliminary design stage. Therefore, this study proposes an optimal cable system for a cable-stayed suspension bridge considering the geometric configuration or cable sag, the lengths of the side and center spans, the composition of overlapping section, and cross-sectional area of the cables. Also, the optimal result should satisfy the design criteria for stress and deformation as well as the economic feasibility. Such optimal cable system can provide a design guide for the cable-stayed suspension bridge in a preliminary design stage that will reduce the cost, time and manpower of design engineers.

For developing the optimal cable system, some assumptions on the structural type of the cable-stayed suspension bridge are considered. Firstly, the main span length is longer than 1,500 m, and the geometric configuration is symmetric with respect to the center of the main span. The suspension cable is anchored to the earth, and the stay cables are fixed to the top of pylon like a fan-type. Also, the overlapping section exists only in the main span, and the side span is supported by the inner piers as illustrated in Figure 1.10.

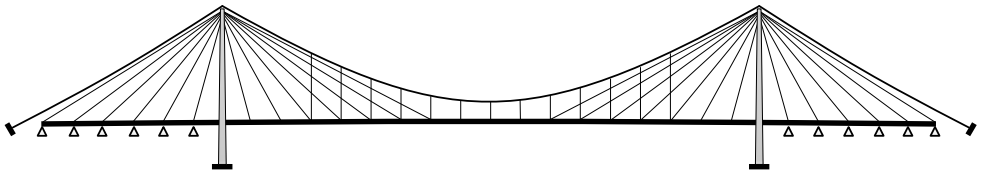

Figure 1.10 Configuration of a basic cable system applied to this research

In addition, to improve the procedure finding an optimal cable system, a simplified analysis model for a cable-stayed suspension bridge is proposed. The proposed simplified analysis model is based on the two dimensional truss elements considering the geometric nonlinearity. That is so efficient and reasonable that bridge designers can remarkably save much time, cost and a lot of manpower for a number of iteration works. Finally, the optimization procedure is proposed to find the best solution by minimizing the construction cost for cable system. The optimization method uses

Genetic Algorithm known to be powerful, efficient, and capable of handling large number of variables (Olfat, 2012). Through the proposed optimization procedure, case studies for a combined system with main span length over 1,500 m are performed considering two combinations of live loads for traffic and train loads.

1.4 Overview

This dissertation consists of five chapters. The outline is summarized as follows.

Chapter 1 provides the research background, the literature review on related topics, the research objective and scope, and the overview of this dissertation. Chapter 2 proposes a new simplified analysis model for analyzing a cable-stayed suspension bridge. An initial equilibrium configuration analysis under dead loads and a structural analysis under live loads using the simplified analysis model are described. For a verification of the proposed model, a suspension bridge with a main span length of 850 m and a combined system with a main span length of 1,408 m are used as example bridges. The resulting initial equilibrium configurations and behaviors under live loads are compared with the results obtained by a commercial FEM software, RM Bridge. Chapter 3 shows parametric investigations of the effects of the design variables on the behavior of a combined system under live loads. The design variables include the side span length, the composition of the suspension section and the

overlapping section, the cable sag, and the dead load distribution factor. For a sensitivity analysis, the variations of design variables normalized by the main span length are compared with the results normalized by the structural behavior under the original design value of the example bridge. Chapter 4 defines the optimization problem to find an optimal cable system of a cable-stayed suspension bridge. The objective function is expressed as the total construction cost for the superstructure only. As an optimization tool, Genetic Algorithm (GA) based on the theory of biological evolution and adaptation is employed to improve the efficiency when handling large number of variables. The optimal cable systems for a road-railway bridge and a roadway bridge with main span length over 1,500 m are proposed by the simplified analysis model and GA, and the sensitivity for each design variable is analyzed. Finally, Chapter 5 summarizes and concludes this study.

2. A PROPOSED SIMPLIFIED ANALYSIS MODEL FOR A CABLE-STAYED SUSPENSION BRIDGE

2.1 Structural Analysis Model of a Combined System

At present, generally, cable supported bridges are designed through the structural analysis by commercial FEM softwares such as MIDAD Civil, SAP, and RM Bridge which are based on the element stiffness matrix method. They can deal with static and dynamic analysis under dead and live loads including traffic, wind, earthquake, and so on. The catenary cable elements or nonlinear truss elements are normally used to simulate the cables, and pylons and decks are modelled by frame elements. For considering the large displacement due to the flexible behavior's features of cable structures, the FEM softwares reflect the geometric nonlinearity to the calculation. These commercial softwares give designers reasonable analysis results for initial equilibrium shape of cables and the member forces and deformations under live loads.

When the commercial softwares are applied to analyze a combined system, however, there are some critical disadvantages due to the existence of the overlapping section. Firstly, because the cable supported bridges have own stiffness from the cable tension, designers should find the initial equilibrium configuration and tension of the cable under the dead load. The commercial softwares, generally, calculate the cable tension for the initial equilibrium state by solving the simultaneous equation which consists of the unknown cable tensions and the known displacement constraints.

Namely, the number of cables and the number of displacement constraints should be the same. As shown in Figure 2.1, the equilibrium equation at the node in the overlapping section has two unknown cable tensions, T_{CS} and T_{HG} while the only constraint is a vertical displacement under dead load. Therefore, this situation interrupts to find a unique solution for cable tensions, and designers should manually assume and fix the tension for one cable of two cables under dead load before the analysis.

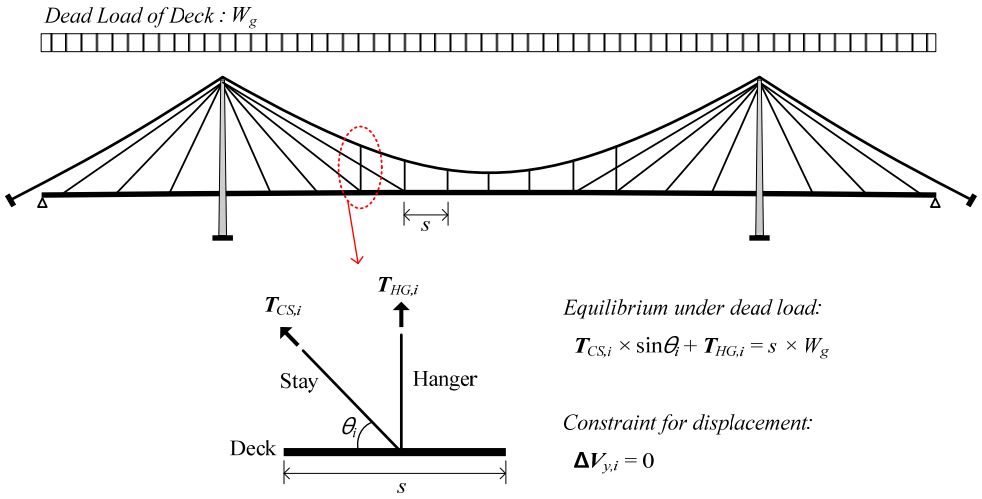

Figure 2.1 Equilibrium in overlapping section

Secondly, as the development of the commercial FEM softwares, they have been extensively used to analyze cable supported bridges, but it is not suitable to deal with

a number of case studies including the iteration works with the variation of design variables because it takes much times for assembling and analyzing FEM models. In case of suspension bridges and cable-stayed bridges, there is the optimized cable configuration through a number of completed projects over 100 years, and the iteration works can be reduced. However, when designers plan a preliminary design for a cable-stayed suspension bridge, numerous iteration works are necessary to find an optimal design because a few projects have been completed and there is no general optimum design. Namely, there is an obvious need for a simplified structural analysis model and method to understand the structural behaviors and decrease the time and cost as shown in Figure 2.2.

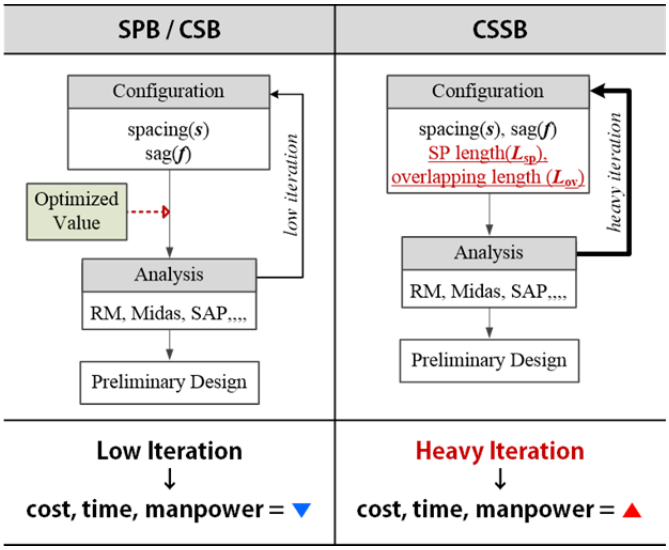

Figure 2.2 Iteration works for the design of cable supported bridges

In this research, a reasonable simplified analysis model is proposed for modelling a cable-stayed suspension bridge efficiently. The proposed analysis model is useful in a preliminary design and suitable to calculate the member force and deformation. For developing the new efficient analysis model, a configuration of cable system is assumed as shown in Figure 2.3, and the assumptions are described below.

- A geometric configuration is symmetric with respect to the center of a bridge.
- Overlapping sections exist only in the main span
- Stay cables and hanger ropes in the overlapping sections are anchored to the same point on the deck.
- Suspension cables have a constant area along the length in each span and are anchored to the earth.
- All stay cables are fixed to the pylon top.
- The deck has a constant cross section and does not connect with the pylons.
- Side spans are supported by inner piers.

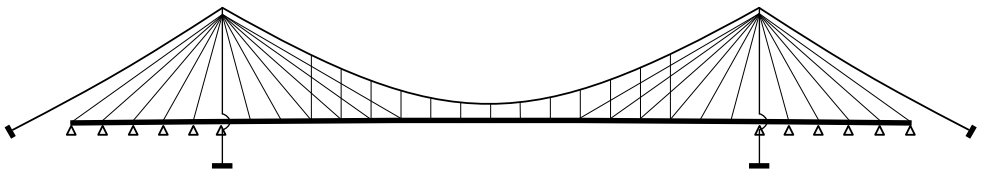

Figure 2.3 General scheme of a combined system applied to this study

The proposed analysis model consists of design variables for assembling a structural model and analysis theory, and they are described in Chapter 2.2 and Chapter 2.3, respectively.

2.2 Design Variables

2.2.1 Design variables for a cable-stayed suspension bridge

As shown in Figure 2.4, there are a number of design variables to define a cable-stayed suspension bridge including a geometric configuration and material properties. The configuration variables include span lengths, pylon heights, a sag, a length of suspension section in the center span, a length of overlapping section, a cable spacing, the number of stayed cables, areas and inertia moments of each member, and the material properties include elastic modulus, specific weight and strength of each material. Each variable can be expressed as vectors of $\mathbf{V}_{geo}$ and $\mathbf{V}_{mat}$.

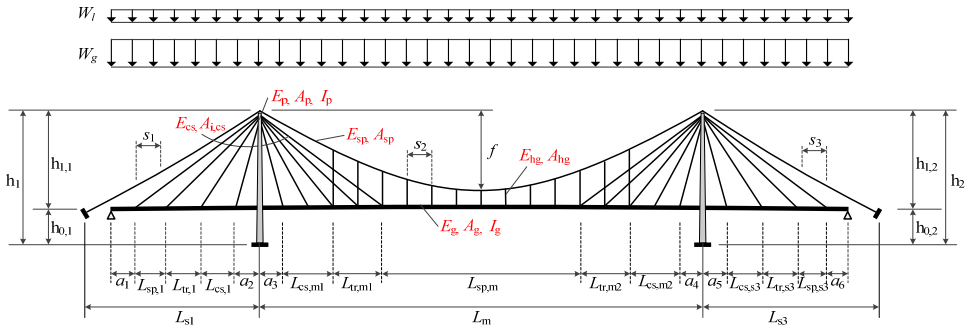

Figure 2.4 Design variables of a combined system

$$\mathbf{V}_{geo} = \{ L_m, L_s, L_{sp}, L_{ov}, L_{cs}, s, n, h_1, f, A_{sp}, A_{hg}, A_{cs}, A_d, A_p, I_d, I_p, r\} \quad (2.1)$$

$$\mathbf{V}_{mat} = \{ E_{sp}, E_{hg}, E_{cs}, E_{steel}, E_{concrete}, \gamma_{sp}, \gamma_{hg}, \gamma_{cs}, \gamma_{steel}, \gamma_{concrete}, f_{u\_sp}, f_{u\_hg}, f_{u\_cs}, f_{y\_steel}, f_{ck\_concrete} \} \quad (2.2)$$

where, L is a length of each span and zone, s is a interval between stay cables and hangers, n is the number of stay cables, h is a height of pylon, A is an area of each cable, I is a moment of inertia, E is the elastic modulus, γ is the specific weight, f_u is the tensile strength of cables, f_y is the yield strength of structural steel, and f_{ck} is the compressive strength of concrete. For the cable-stayed suspension bridge, particularly, a dead load distribution in the overlapping section is of special importance, because the stay and suspension system support total dead load of the girder simultaneously and the distributed dead loads determine the cable areas. When the total dead load of deck is W_g and a fraction of dead load carried by the stay system is W_{cs}, the dead load distribution factor, r, can be expressed by Equation 2.3.

$$r = \frac{Dead\ load\ of\ deck\ supported\ by\ stay\ cables}{Dead\ load\ of\ deck} = \frac{W_{cs}}{W_g} \quad (2.3)$$

The factor, r, is able to change from 0 to 1, and the combined bridge refers to a perfect suspension bridge when r equals to 0 or a perfect cable-stayed bridge when r equals to 1. The distributed dead load condition of a combined system is illustrated in Figure 2.5.

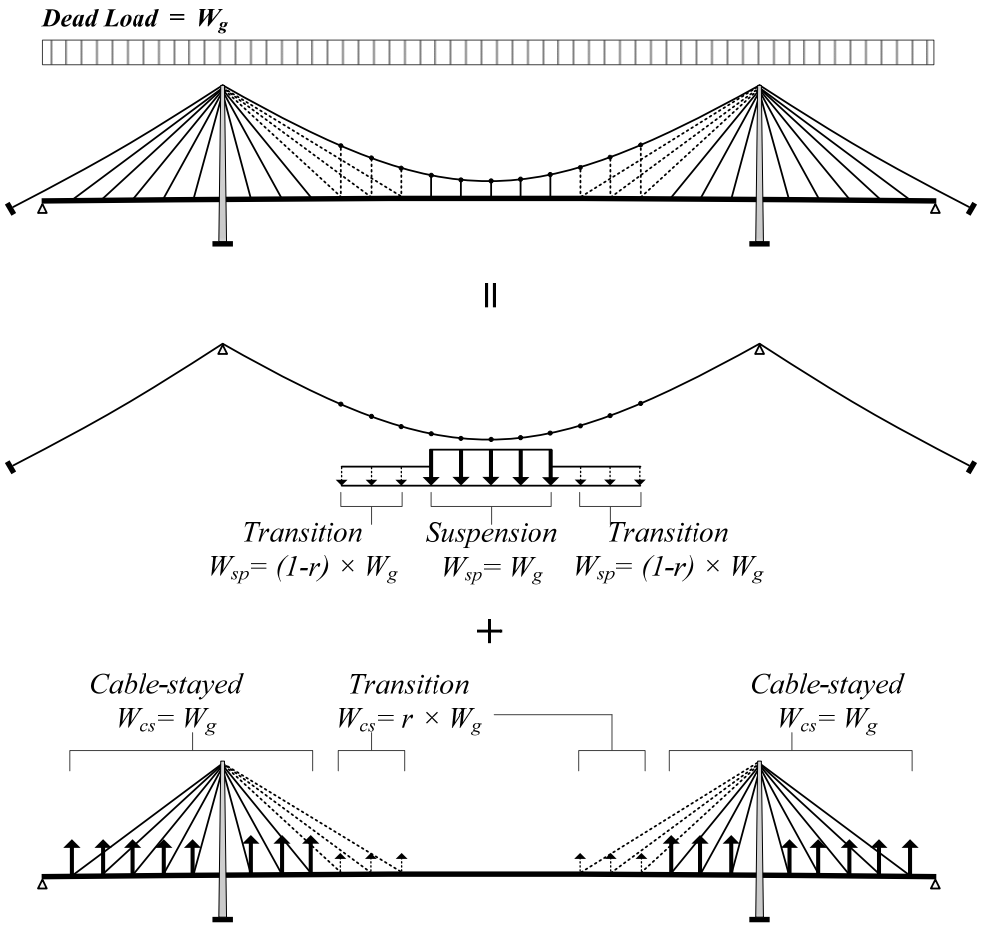

(a) Load distribution by the distribution factor, *r*

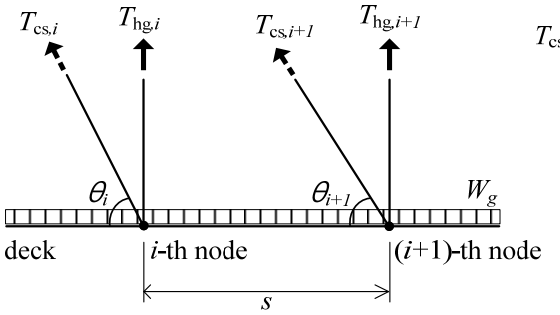

$$T_{cs,i} \times \sin\theta_i + T_{hg,i} = s \times W_g$$

$$T_{cs,i} = \frac{r \times \{s \times W_g\}}{\sin\theta_i}$$

$$T_{hg,i} = (1\text{-}r) \times \{s \times W_g\}$$

(b) Equilibrium in overlapping section by the load distribution factor, *r*

Figure 2.5 Dead load distribution factor, *r*

2.2.2 Variables for a material property

Material properties for main structural members of long span cable supported bridges are very similar at present, and the strength of materials is getting higher to decrease the dead load and increase the span length. The recently general material properties for cable supported bridges are listed in Table 2.1. Here, E is the elastic modulus, γ is the specific weight, f_u is the tensile strength of cables, f_y is the yield strength of structural steel, and f_{ck} is the compressive strength of concrete.

Table 2.1 Material properties applied to recent cable supported bridges

Material	E (GPa)	γ (kN/m^3)	f (MPa)	Remarks
Wire for suspension	200	77	f_u=1,860~1,960	
Strand for stay cable	200	77	f_u=1,860~1,960	
Rope for hanger	200	77	f_u=1,570~1,770	
Structural steel	200	77	f_y=335~460	S355~S460
Concrete	33~37	25	f_{ck}=30~50	C30~C50

2.2.3 Principal design variables for a combined system

The areas of cables are calculated by an initial equilibrium configuration analysis when dead loads of all members are confirmed. Also, the areas of deck and pylon and

moment inertia are generally confirmed by structural analysis based on an engineering sense of designers in a preliminary design stage. As a result, the most important variables for cable supported bridges are a length of main span, L_m and sag, f, because the values determine quantities and area of cable and girder section, and so on. The second one is a ratio of side span length, L_s to L_m, which is strongly related to the deflection of girder under live loads. In particular case of a cable-stayed suspension bridge with an overlapping section, a length of suspension section, L_{sp}, a length of overlapping section, L_{ov}, and a dead load distribution factor, r are expected to affect the structural features and behaviors. Thus, design variables vectors, $\mathbf{V}_{geo}$ and $\mathbf{V}_{mat}$ can be integrated and revised as $\mathbf{V}_{CSSB}$. The new variables, β, mean a ratio of each variable's value to the main span length.

$$\mathbf{V}_{CSSB}=\{ L_m, \quad \beta_s, \quad \beta_{sp} \quad \beta_{ov}, \quad \beta_f, \quad r \} \tag{2.4}$$

$$\beta_s = \frac{L_s}{L_m} \tag{2.5a}$$

$$\beta_{sp} = \frac{L_{sp}}{L_m} \tag{2.5b}$$

$$\beta_{ov} = \frac{2 \times L_{ov}}{L_m - L_{sp}} \tag{2.5c}$$

$$\beta_f = \frac{f}{L_m} \tag{2.5d}$$

The variables, β_{sp} and β_{ov}, can define various configurations of cable supported bridges by changing the value of variables, and both variables have a bound from 0 to 1. The bridge is a perfect cable-stayed bridge when β_{sp} is zero, and the bridge becomes a pure suspension bridge when β_{sp} is one. Also, the bridge has a Dischinger system when β_{ov} is zero, and the bridge becomes a Roebling system when β_{ov} is one as shown in Figure 2.7.

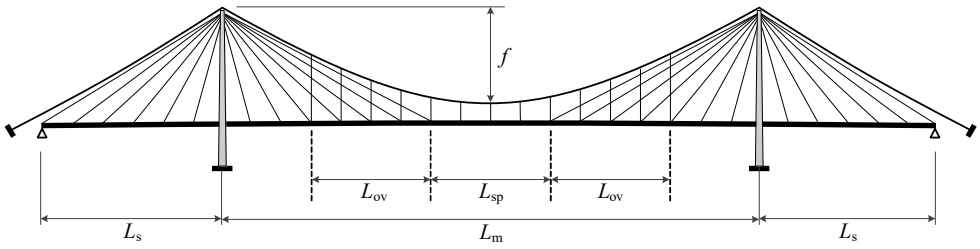

Figure 2.6 Scheme of a combined system with principal design variables

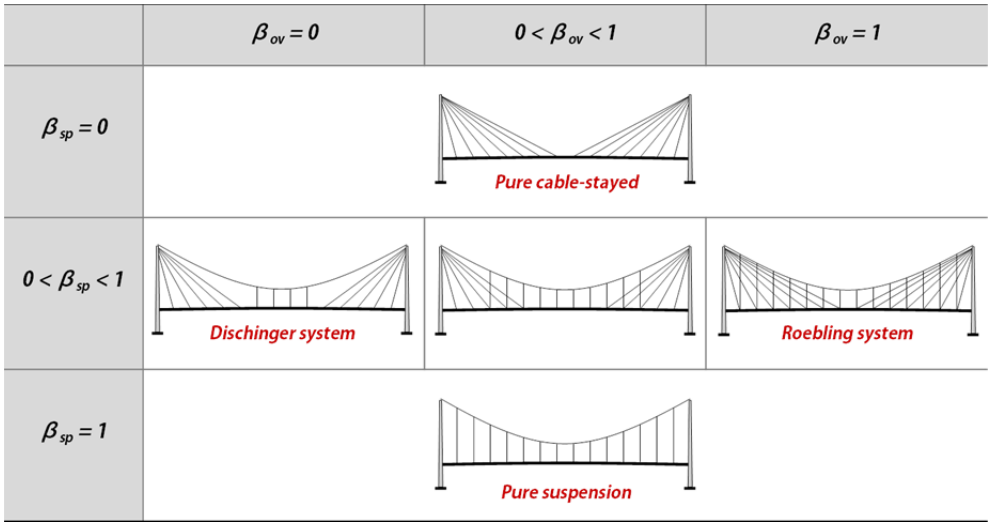

Figure 2.7 Variation of geometric configuration through the change of variables

2.3 A Proposed Simplified Structural Analysis Model

This chapter proposes a simple and efficient structural analysis model to analyze a cable-stayed suspension bridge. This proposed method can remarkably decrease the time to assemble and analyze a model for a combined system, and confirm the reasonable analysis results with respect to the results by commercial FEM softwares. The method includes a set-up of a structural analysis model, an initial equilibrium configuration analysis and live loads analysis by two dimensional truss elements based on a stiffness matrix method as illustrated in Figure 2.8.

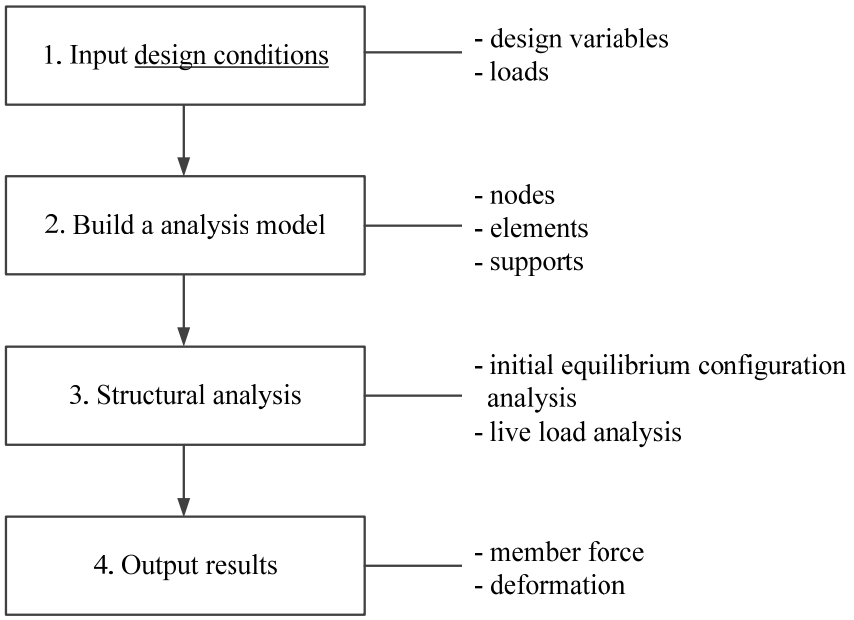

Figure 2.8 Composition of the proposed numerical analysis method

2.3.1 A simplified analysis model

The proposed structural analysis model for a combined system is a simplified two-dimensional structure as illustrated in Figure 2.9. The most important features of the proposed model are the application of truss elements for all members, the replacement of cables in side spans with cable springs, and the elimination of pylons. Also, the flexural stiffness of the deck is neglected to verify the effect of the combined cable system on the structural behavior in this study, which gives a reasonable result when designers analyze the behavior of cable supported bridges under live loads (Gimsing, 2012).

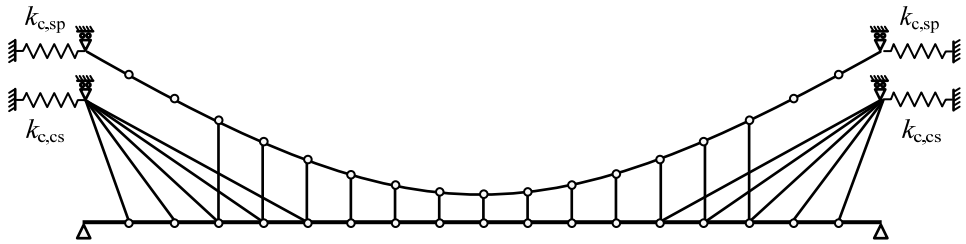

Figure 2.9 Simplified structural analysis model using truss elements

(1) Truss elements

First of all, truss elements have the simplest local stiffness matrix, and the analysis is very efficient. When the structural member has a geometric nonlinearity as like

suspension cables or stay cables, a simple matrix can reasonably deal with the nonlinearity using a tension and a length of the member. Therefore, a truss element for cables makes the structural analysis of a cable-stayed suspension bridge efficient. A local element stiffness matrix, $\boldsymbol{k}^{e}$, for a cable truss element includes an elastic stiffness part (k_E) and a geometric stiffness part (k_G) as expressed in Equation 2.6, and it is able to consider the geometric nonlinearity of cables easily.

$$[k]^{e} = [k]_{E} + [k]_{G} = \frac{EA}{L_0}\begin{bmatrix} 1 & 0 & -1 & 0 \\ 0 & 0 & 0 & 0 \\ -1 & 0 & 1 & 0 \\ 0 & 0 & 0 & 0 \end{bmatrix} + \frac{T}{L}\begin{bmatrix} 0 & 0 & 0 & 0 \\ 0 & 1 & 0 & -1 \\ 0 & 0 & 0 & 0 \\ 0 & -1 & 0 & 1 \end{bmatrix} \tag{2.6}$$

where EA is an axial stiffness, L_0 is a non-stressed length, L is a length with a tension, and T is a tension of a cable. Although the cables are modelled by truss elements, the error of calculation between the truss elements and catenary elements can be ignored if the cable tension is high enough such as the completed state under dead load (Moon, 2008). Moreover, the Ernst formula in Equation 2.7 for the equivalent elastic modulus is applied to modify the elastic modulus of stay cables due to the effect of sag by self weight. Generally, the elastic modulus considering the sag effect is lower than the original material's elasticity, and the decline increases when the tension of stay cables is low and the span length is long as shown in Figure 2.10. The horizontal axis of Figure 2.10 means the ratio of axial stress to tension strength. Because the stress ratio is about 0.4~0.6 under live load for recent cable-stayed bridges, the elastic modulus

decreases by 5~ 10%. The Ernst formula is expressed in Equation 2.7.

$$E_{eq} = \frac{E_{cs}}{1 + E_{cs} \times \frac{(\gamma_{cs} L)^2}{12\sigma^3}} \tag{2.7}$$

where, E_{cs} is the elastic modulus of strands for a stay cable, γ_{cs} is the specific weight of stay cable, L is the span length, and σ is the axial stress of stay cable.

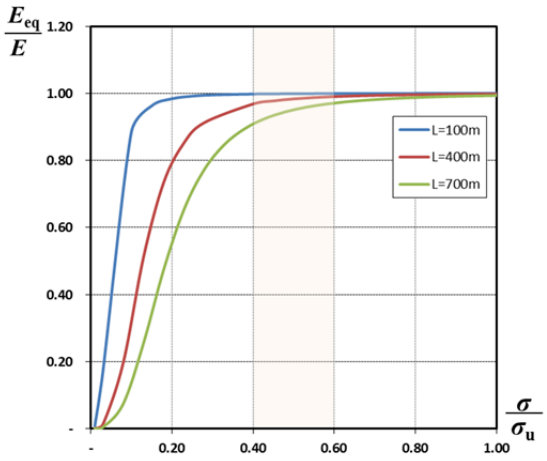

Figure 2.10 Effect of span length and axial stress on the elastic modulus

(2) Horizontal cable spring

When a traffic load is applied on deck, the vertical displacement of deck in the main span is related to the horizontal displacement at the pylon top. Also, the horizontal displacement is affected by the horizontal stiffness of cables in the side span and the

flexural stiffness of the pylon which is expressed by $k_p = \frac{3EI_{pylon}}{h_p^3}$ where h_p is the height of pylon. Since it is much lesser than the horizontal stiffness of cables in the side span, the horizontal stiffness of cables and pylon in the side span can replaced with the equivalent horizontal cable spring for the simplification of the analysis model, and the stiffness of pylon is neglected as shown in Figure 2.11.

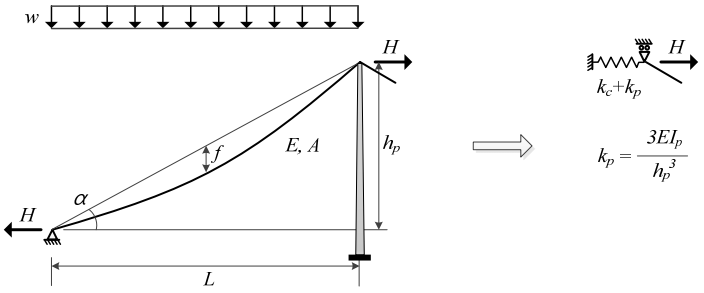

Figure 2.11 Replacement of an inclined cable with an equivalent horizontal spring

Chai *et al* (2012) proposed the k_c from the energy method with neglecting the elongation of cable, which is expressed in Equation 2.8.

$$k_c = \frac{3w}{128}\left(\frac{L}{f}\right)^3 + \frac{w}{4}\left(\frac{L}{f}\right) \tag{2.8}$$

Also, Choi *et al* (2014) proposed the k_c that is derived from the derivative of $\frac{dH}{dL}$

with assuming the cable configuration as the parabola curve, and the stiffness is expressed in Equation 2.9.

$$k_c = \frac{H^2\cos\alpha + \frac{(wL)^2}{8}\cos^3\alpha\left(1+\sin^2\alpha\right) - \frac{H^3}{EA}\left(1-\tan^2\alpha\right) - \frac{H(wL)^2}{4EA}}{\frac{LH^2}{EA}\left(1+\tan^2\alpha\right) + \frac{L(wL)^2}{12H}\cos^3\alpha - \frac{L(wL)^2}{12EA}} \tag{2.9}$$

In this study, for the simplicity and efficiency of the numerical model and analysis, a new expression of k_c is proposed by using the Ernst equivalent modulus. When the inclined cable with the sag under loads is considered as the truss with the stiffness of E_{eq} as shown in Figure 2.12, the Hooke's law of the truss is expressed by Equation 2.10.

$$\Delta T = \frac{E_{eq}A}{L}\Delta L \tag{2.10}$$

where ΔT is the increment of cable tension and ΔL is the elongation of cable.

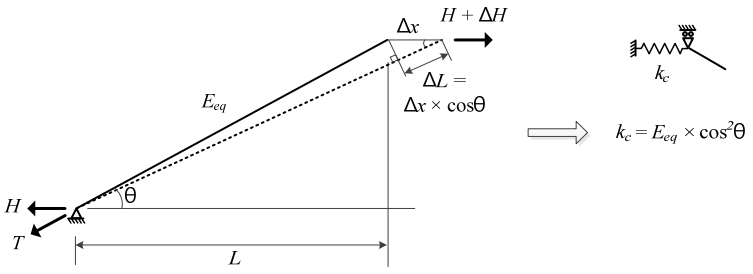

Figure 2.12 Proposed equivalent spring stiffness by E_{eq}

Similarly, the horizontal stiffness, k_c, can be expressed by Equation 2.11. When the relations of the horizontal force of cable (ΔH) to the tension and the horizontal deformation of cable's elongation (Δx) to the elongation is applied to the Equation 2.11, the k_c can be easily expressed by Equation 2.13.

$$\Delta H = k_c \Delta x \tag{2.11}$$

$$\Delta H = \Delta T \times \cos\theta = \frac{E_{eq} A}{L} \Delta L \times \cos\theta = \left(\frac{E_{eq} A}{L} \cos^2 \theta \right) \Delta x \tag{2.12}$$

$$k_c = \frac{E_{eq} A}{L} \times \cos^2 \theta \tag{2.13}$$

For verifying an application of the horizontal cable spring, three suspension bridges with different structural types are applied to examples. Table 2.2 shows the specification of the example bridges including two suspension bridges and one cable-stayed suspension bridge.

Table 2.2 Design values of example bridges

Example Bridge	Description	Span Length		Pylon			
		Main Span (m)	Side Span (m)	Height (m)	E (Gpa)	A (m^2)	I (m^4)
YSS	3-span SPB	1,545	357.5	266	30	23 ~ 68	132 ~ 1,851
JG	1-span SPB	850	255	135	30	13 ~ 22	15 ~ 67
BOS3	3-span CSSB	1,408	355	317	30	36 ~ 72	555 ~ 1,843

First of all, the horizontal stiffness at the top of pylon with cables in the side span is compared to the flexural stiffness of the only pylon by FEM software. Both stiffness results are calculated by a ratio of various horizontal forces to horizontal displacements at the top when various horizontal forces are loaded at the top of pylon. Table 2.3 shows the results of the horizontal stiffness for three bridges, and the portion of the only pylon's flexural stiffness is significantly small. Therefore, it is reasonable that the flexural stiffness of pylon can be ignored in the simplified analysis model in Figure 2.11, the simplified analysis model can be revised as Figure 2.13.

Table 2.3 Calculated horizontal stiffness of example bridges

Bridge	Case 1 : Cable + Pylon  (A)	Case 2 : Pylon Only  (B)	Ratio (B/A)
YSS	59,456 kN/m	1,479 kN/m	2.5 %
JG	83,713 kN/m	710 kN/m	0.8 %
BOS3	161,562 kN/m	1,458 kN/m	0.9 %

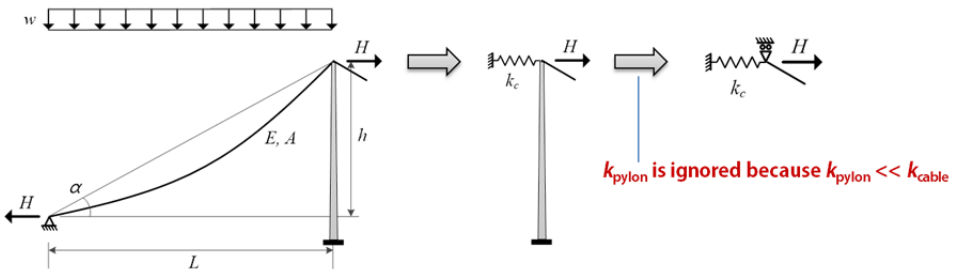

Figure 2.13 Replacement of a side span with an equivalent horizontal spring

Secondly, the stiffness of a horizontal cable spring by Equation 2.9 for each example bridge is compared to the horizontal stiffness by FEM software. In case of the cable-stayed suspension bridge, the cable spring stiffness can be calculated by a summation of horizontal stiffness for all stay cables and suspended cable as expressed by Equation 2.14.

$$k_c = k_{c,sp} + \sum_{n=1}^{n} k_{c,cs,n-th} \tag{2.14}$$

Table 2.4 shows the results of the horizontal stiffness for three bridges, and the error of the horizontal stiffness, k_c, is under 2.4% and it is nonsignificant at a preliminary design stage. Therefore, the application of the simplified cable spring is reasonable for this research.

Table 2.4 Comparison of horizontal stiffness by both methods

Bridge	α (rad)	w (kN/m)	L (m)	h (m)	H (kN)	E (GPa)	A (m2)	k_c (kN/m) by proposal	k_c (kN/m) by FEM(*)	Error
YSS	0.447	90.8	376	180	157,565	200	0.2877	60,897	*59,456*	2.4 %
JG	0.443	11.5	255	121	65,521	200	0.1495	82,203	*83,713*	1.8 %

Cable	α (rad)	w (kN/m)	L (m)	h (m)	H (kN)	E (GPa)	A (m^2)	k_c (kN/m) by proposal		k_c (kN/m) by FEM		Error
SP	0.560	27.3	381	239	157, 300	200	0.3549	105,698				
CS01	1.419	0.11	35	220.1	1220	203	0.0145	332				
CS02	1.356	0.09	50	220.1	1630	203	0.0120	517				
:	:	:	:	:	:	:	:	:	57,938	163,636	161,562	1.2 %
CS21	0.602	0.13	335	220.1	9,440	203	0.0165	5,196				
CS22	0.581	0.13	350	220.1	9,850	203	0.0165	5,134				

2.3.2 Initial equilibrium configuration analysis

For the analysis of cable structures, the tension and geometry of cables under dead load should be known because the structural stiffness of cable system comes from the cable tension and the tension determines the geometry of cables. The analysis process to find the tension and geometry of cables under dead load is called as the initial equilibrium configuration analysis.

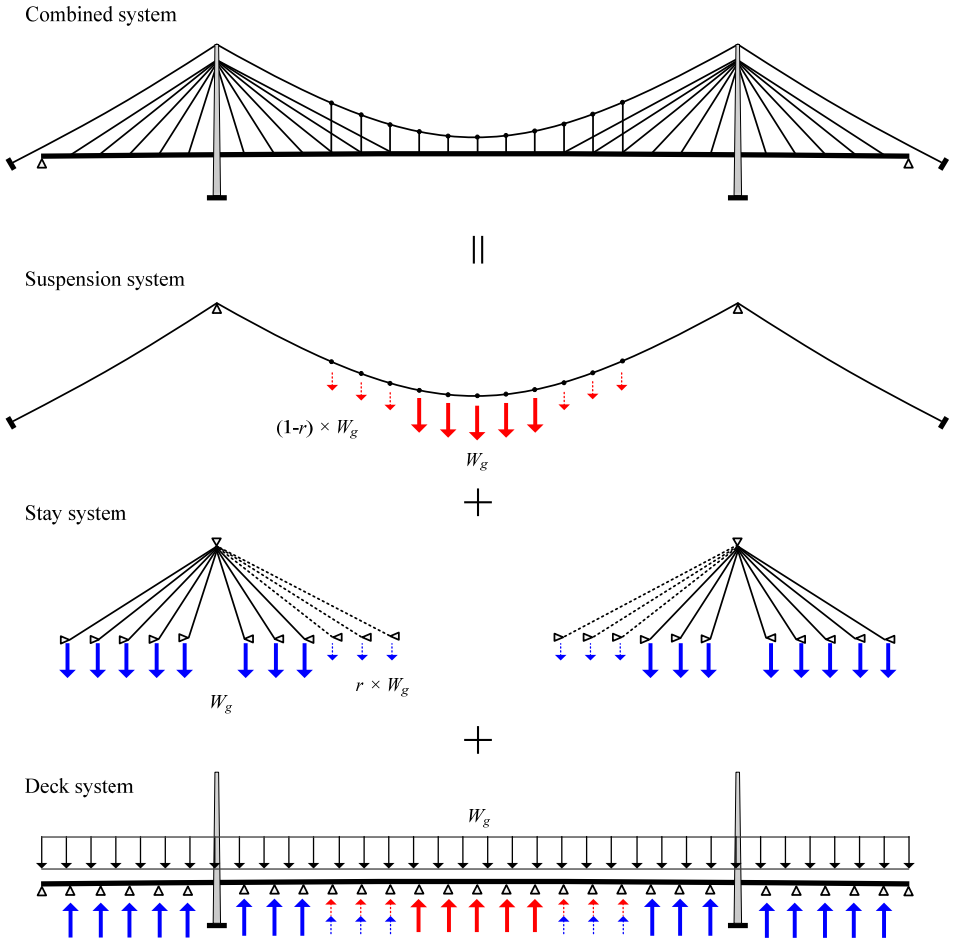

Figure 2.14 Separation analysis method for a combined system

For the initial equilibrium configuration analysis for a cable-stayed suspension bridge, there are a lump analysis method which considers the cable-stayed suspension bridge as one structure and a separation analysis method which considers the bridge as two separated structures of a suspension system and a stay system. This research uses the separation analysis which is revealed that it is efficient to save the analysis time by Kim(2011). As shown in Figure 2.14 the separation analysis method divides a combined system to a suspension system and a stay system, and performs the equilibrium analysis separately. The cable tension and configuration of each system is evaluated by the dead load of deck, W_g with a dead load distribution factor, r.

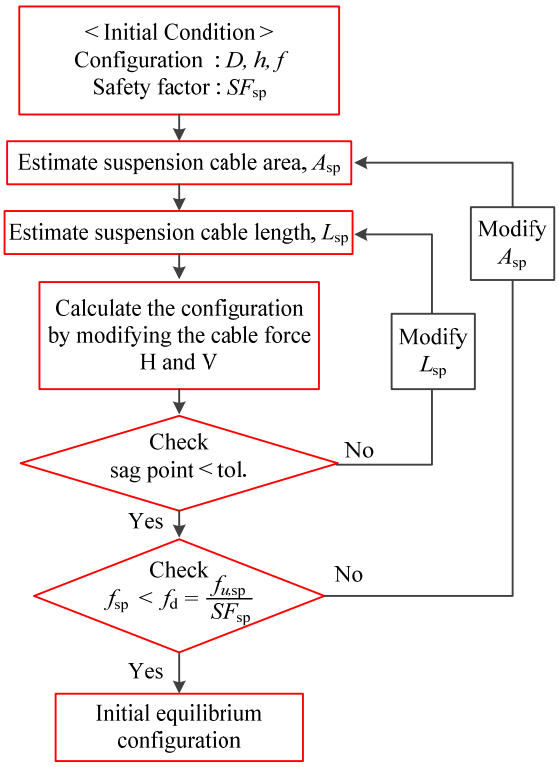

Figure 2.15 Flow chart of initial configuration analysis for suspension cable

Firstly, the initial equilibrium configuration analysis for design of suspension cable includes two processes, the determination of the cable's area and the total length between both supports. Because the dead load of suspension cable is calculated by the product of the area and the length, the process needs a number of iteration calculations. Figure 2.15 shows the flow to find an initial equilibrium configuration of a suspension cable. For the initial assumption of cable area and cable length, the suspension cable can be considered as a parabola with a sag of f under the dead load, W_g and the live load W_l of deck as illustrated in Figure 2.16.

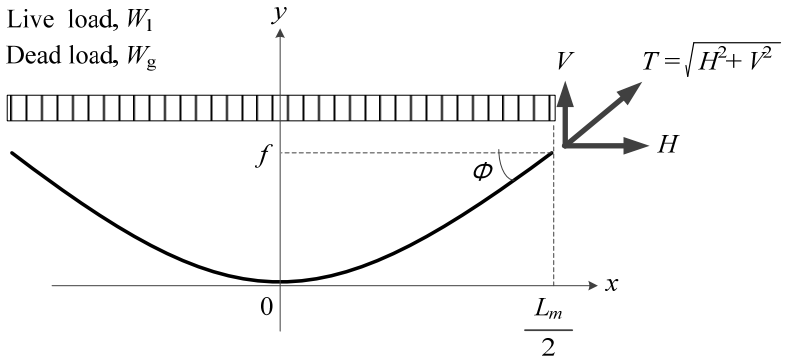

Figure 2.16 Suspension cable assumed by a parabola

From the parabola equation, the geometry of the suspension cable in Figure 2.15 is expressed as Equation 2.15, and the tension at the top of the cable can be calculated by Equation 2.16.

$$y=\frac{8f}{L_m{}^2}x^2 \tag{2.15}$$

$$T = \sqrt{H^2 + V^2} \tag{2.16}$$

where, the horizontal and vertical fraction of the tension can be defined by the force equilibrium. γ_{sp} is the specific weight of the suspension cable.

$$H = \frac{qL_m{}^2}{8f} = \frac{\left(A_{sp}\gamma_{sp} + W_g + W_l\right)L_m{}^2}{8f} \tag{2.17}$$

$$V = \frac{qL_m}{2} = \frac{A_{sp}\gamma_{sp}L_s + \left(W_g + W_l\right)L_m}{2} \tag{2.18}$$

The initially assumed area of suspension cable may satisfy the design stress calculated by the safety factor in Equation 2.19. Solving the equations, the initially assumed area of suspension cable for the initial configuration analysis is Equation 2.20.

$$f_{sp} = \frac{T}{A_{sp}} = \frac{f_u}{SF} \tag{2.19}$$

$$A_{sp} = \frac{W_g L_m{}^2 \sqrt{1+16\beta_f{}^2}}{\frac{f_u}{SF}8f - \gamma_{sp}L_m{}^2\sqrt{1+16\beta_f{}^2}} \tag{2.20}$$

where, W_g is the dead load of deck, L_m is the length of main span, β_f is the ratio of sag to main span length as expressed in Equation 2.5, f_u is the tensile strength of the cable wire, and SF is the safety factor for the cable design. However, this equation is suitable to the suspension bridge which supports the loads of deck along the entire span, and the case of a combined system which supports the fraction of loads at the middle of the center span.

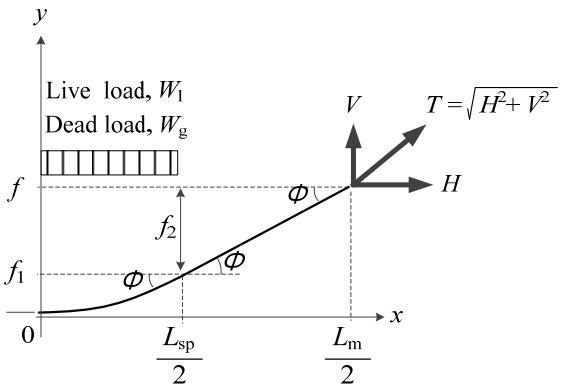

Figure 2.17 Suspension cable assumed by a partial parabola

The suspension cable of a combined system can be illustrated as Figure 2.16, and the cable is considered as two parts – the suspension section with hangers and the freehanging section without hangers. The configuration of suspension cable is assumed as the parabola in the suspension section and the straight line in the freehanging section. From the parabola equation, the geometry of the suspension section in Figure 2.17 is expressed as Equation 2.21, and the slope of the cable in the freehanging section is in Equation 2.22.

$$y = \frac{4f_1}{L_{sp}^{\ 2}} x^2 \tag{2.21}$$

$$\tan\Phi = y'_{x=\frac{L_{sp}}{2}} = \frac{4f_1}{L_{sp}} \tag{2.22}$$

Also, the height of the freehanging section, f_2, can be expressed by using f_1, and the sag, f_1, in the suspension section is derived from the compatibility condition of the sag, f, is the summation of f_1 and f_2.

$$f = f_1 + f_2 = f_1 + \frac{L_m - L_{sp}}{2}\tan\Phi = \frac{2L_m - L_{sp}}{L_{sp}} f_1 \tag{2.23}$$

where, f equals f_1 when the L_{sp} is the same as L_m or the bridge is a pure suspension bridge along the entire span. The tension of cable at the top can be defined by the force equilibrium.

$$T = \frac{H}{\cos\Phi} = \left[\frac{A_{sp} r_{sp} {L_m}^2}{8f} + \frac{W_g {L_{sp}}^2}{16f}\left(\frac{2}{\beta_{sp}} - 1\right)\right]\sqrt{1 + \left(\frac{4\beta_f}{2 - \beta_{sp}}\right)^2} \tag{2.24}$$

$$A_{sp} = \frac{W_g {L_{sp}}^2 \left(\frac{2}{\beta_{sp}} - 1\right)\sqrt{1 + \left(\frac{4\beta_f}{2 - \beta_{sp}}\right)^2}}{\frac{f_u}{SF} 8f - r_c {L_m}^2 \sqrt{1 + \left(\frac{4\beta_f}{2 - \beta_{sp}}\right)^2}} \tag{2.25}$$

The initial assumption of suspension cable's area, A_{sp}, for a combined system is modified as the Equation 2.25, and the equation is the same as the Equation 2.20 for the entire suspension cable when the L_{sp} equals to the L_m. Finally, the initial assumption of the cable length is calculated by Equation 2.26.

$$L_s = L_{sp}\left[1 + \frac{8}{3}\left(\frac{f_1}{2L_m - L_{sp}}\right)^2\right] + \left(L_m - L_{sp}\right)\sqrt{1 + \left(\frac{4\beta_f}{2 - \beta_{sp}}\right)^2} \tag{2.26}$$

This study uses the force method which calculates the suspension cable's tension and geometry in a short iteration process by using an integrated flexibility matrix of truss elements (Moon, 2008). This method deals with only two variables, horizontal force, H_0 and vertical forces, V_0 at one support as illustrated in Figure 2.18. When the horizontal distance and the vertical height of each truss is defined as D_i and h_i, they

can be expressed as Equation 2.27 and 2.28.

$$D_i = L_i \cos\theta_i = L_{0,i}\left(1+\frac{T_i}{EA}\right)\frac{H_i}{T} = \frac{H_i L_{0,i}}{EA} + L_{0,i}\cos\theta_i \tag{2.27}$$

$$h_i = L_i \sin\theta_i = L_{0,i}\left(1+\frac{T_i}{EA}\right)\frac{H_i}{T_i} = \frac{H_i L_{0,i}}{EA} + L_{0,i}\sin\theta_i \tag{2.28}$$

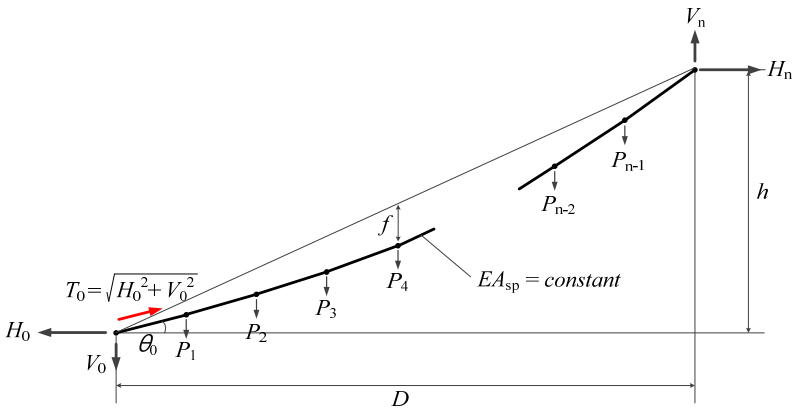

Figure 2.18 Scheme of truss elements for suspension cables

The flexibility matrix of a truss element is defined as Equation 2.29, and the flexibility matrix for the suspension cable can be evaluated by the summation of the flexibility matrix of each truss as noted in Equation 2.30.

$$\mathbf{f}^e = \begin{bmatrix} \frac{\partial D_i}{\partial H_i} & \frac{\partial D_i}{\partial V_i} \\ \frac{\partial h_i}{\partial H_i} & \frac{\partial h_i}{\partial V_i} \end{bmatrix} = \begin{bmatrix} \frac{L_{0,i}}{EA} + \frac{L_{0,i}}{T}\sin^2\theta_i & -\frac{L_{0,i}}{T_i}\cos\theta_i\sin\theta_i \\ -\frac{L_{0,i}}{T_i}\cos\theta_i\sin\theta_i & \frac{L_0}{EA} + \frac{L_{0,i}}{T_i}\cos^2\theta_i \end{bmatrix} \tag{2.29}$$

$$\mathbf{f} = \begin{bmatrix} \sum_{i=1}^{n} \frac{\partial D_i}{\partial H_i} & \sum_{i=1}^{n} \frac{\partial D_i}{\partial V_i} \\ \sum_{i=1}^{n} \frac{\partial h_i}{\partial H_i} & \sum_{i=1}^{n} \frac{\partial h_i}{\partial V_i} \end{bmatrix} \tag{2.30}$$

The initial equilibrium configuration analysis by the flexibility matrix is very simple and quick because the update of the geometry is performed by the product of the inverse matrix of the flexibility matrix and the discrepancies of the coordination between the objective point and the calculated point as expressed in Equation 2.31.

$$\begin{pmatrix} \Delta H_0 \\ \Delta V_0 \end{pmatrix} = \mathbf{f}^{-1} \begin{pmatrix} \Delta x_n \\ \Delta y_n \end{pmatrix} \tag{2.31}$$

In case of the stay cable, the tension is estimated by the dead load of deck and the dead load distribution factor, *r* in Equation 2.32and the initial assumption of the area can be expressed in Equation 2.33.

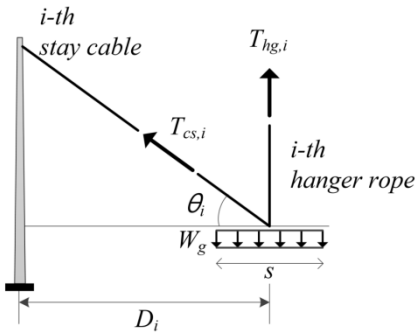

Figure 2.19 Tension of hanger rope and stay cable due to the dead load

$$T_{CS,i} = \frac{r \times s \times \left(W_g + W_l\right)}{\sin\theta_i} \tag{2.32}$$

$$A_{cs,i} = \frac{r \times s \times \left(W_g + W_l\right)}{\frac{f_{u,cs}}{SF}\sin\theta_i - \gamma_{cs} D_i \tan\theta_i} \tag{2.33}$$

where s is the interval of cable anchorage on the deck, W_g and W_l is the dead load and live load, θ_i is the angle of i-th stay cable, and D_i is the span length. SF is the the safety factor for stay cable's design. Similarly, the initial assumption for the area of hanger rope can be expressed in Equation 2.34 and Equation 2.35.

$$T_{HG} = \left(1 - r\right) \times s \times \left(W_g + W_l\right) \tag{2.34}$$

$$A_{hg,i} = \frac{\left(1 - r\right) \times s \times \left(W_g + W_l\right)}{\frac{f_{u,hg}}{SF} - \gamma_{hg} L_{hg,i}} \tag{2.35}$$

2.3.3 Live load analysis

After the initial equilibrium configuration analysis, the live load analysis is performed sequentially. It is very important to verify whether the cross section of members for the assumed design can resist the live load and the deformation of the structure can satisfy the design criteria or not. The safety of section for cables is confirmed by checking the tension, and the calculation of tension is calculated easily from the matrix analysis with the truss elements. Also, the vertical displacement of deck using truss elements is very similar to the result of FEM analysis using frame elements for the cable supported bridges. Since the truss elements for the deck have no flexural

stiffness, however, the live load analysis cannot calculate the bending stress on deck expressed in Equation 2.36. This research proposes an efficient method to calculate the curvature of deck from the analysis result using truss element. Firstly, the rotation angle of truss elements under the live load can be calculated by Equation 2.37.

$$f = \frac{M}{I} y \tag{2.36}$$

$$\Delta\theta_i = \tan^{-1}\left(\frac{V_{y,i+1} - V_{y,i}}{s}\right) \tag{2.37}$$

where, $V_{y,i}$ is the vertical displacement at the i-th node, and s is the interval between hangers or stay cables. The curvature of deck, κ, defines as the inverse of the radius of the tangent sector with the central angle of $\Delta\theta_i$ the as illustrated in Figure 2.20, and the curvature can be expressed as Equation 2.38. When the relationship between moment and curvature is applied to the Equation 2.36, the bending stress on deck can be calculated although the analysis is performed by truss elements.

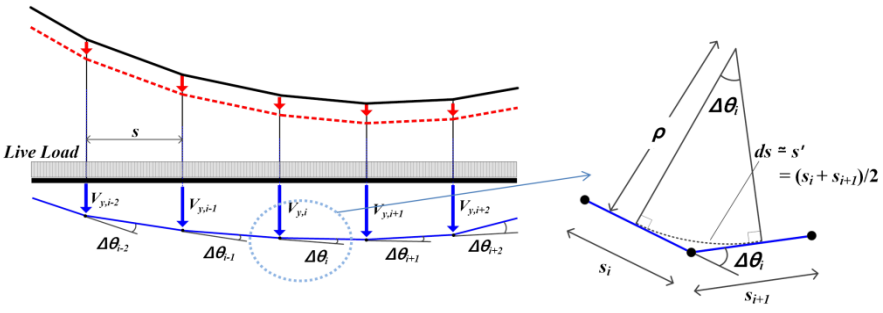

Figure 2.20 Calculation of deck's curvature from the truss elements

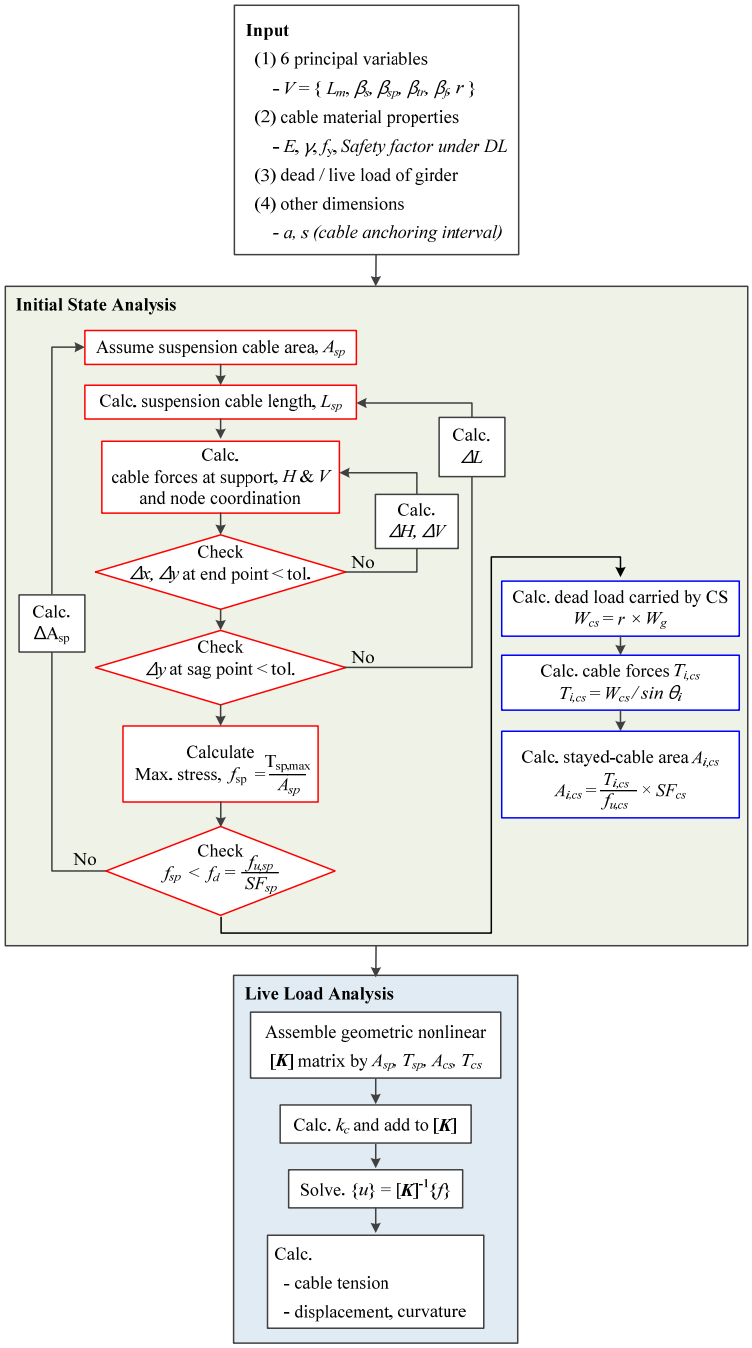

Figure 2.21 Flow chart of the proposed numerical analysis method

$$\kappa = \frac{1}{\rho} = \frac{d\theta}{\rho\, d\theta} = \frac{d\theta}{ds} \approx \frac{\Delta\theta_i}{s'} \tag{2.38}$$

$$f = \frac{M}{I} y = \frac{EI\kappa}{I} y = E\kappa y \tag{2.39}$$

2.3.4 Algorithm of structural analysis

Figure 2.21 shows the flow of the structural analysis process using the simplified analysis model. The process has an order of input, initial state analysis, and live load analysis.

2.4 Verification of the Simplified Analysis Model

The proposed simplified analysis model using nonlinear truss elements can be applied to an initial equilibrium configuration analysis under dead loads as well as a structural behavior analysis under live loads. The two-dimensional truss elements can analyze, in a simple way, the geometric nonlinearity and deformation of cable structures using the simple element stiffness matrix. These features are very efficient and suitable to a preliminary design of complex cable supported bridges because the method can dramatically decrease the cost and time to plan and analyze a number of conceptual designs. This chapter, therefore, verifies and confirms the accuracy of structural analysis results by the proposed structural analysis model through the comparison with the structural behavior including the member force and deformation by a

commercial FEM software. As the commercial software, *RM Bridge* which has been widely being used to the cable supported bridge's design is adopted to this study. Also, a single-span suspension bridge with a main span length of 850 m and a cable-stayed suspension bridge with a main span length of 1,408 m are considered as the examples of this verification, and an initial equilibrium configuration under dead load and a tension and deformation under live load for each bridge are analyzed.

2.4.1 Application to a suspension bridge

A suspension bridge with a main span length of 850 m illustrated in Figure 2.22 is analyzed by both methods. The suspension bridge has a single span in the center span, and a height of pylons with H-shaped concreate legs is 138 m, and a ratio of a cable sag to the main span length is $\frac{1}{9}$. A deck has two lanes for traffic, and hanged by hangers with a interval of 17.5 m. A cross section of the deck is designed as a streamlined box girder with 19.7 m wide and 3.0 m high.

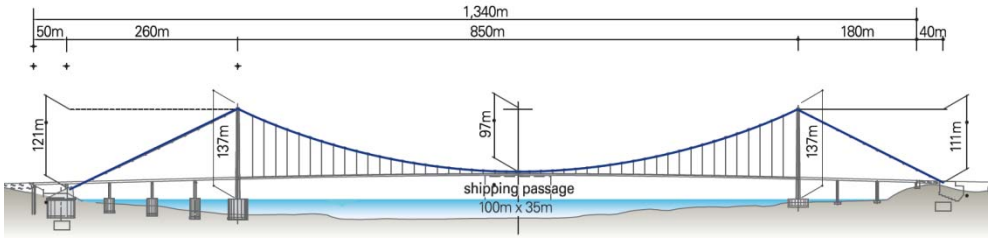

Figure 2.22 Scheme of Pal-young Bridge

The sectional and material properties are listed in Table 2.5, and a tensile strength of the suspension cable is 1,770 MPa. Figure 2.23 shows three dimensional model for the FEM software and the simplified model. The dimension of the bridge, the area of cross section for cables and deck, and the dead loads of both analysis models correspond with each other.

Table 2.5 Material and sectional properties of a suspension bridge

Spec.			Cable				Girder			Pylon		
L_m (m)	L_s (m)	h (m)	E (GPa)	A (m^2)	s (m)	f (m)	E (GPa)	A (m^2)	I (m^4)	E (GPa)	A (m^2)	I (m^4)
850	255	138	200	0.1475	17.5	94	200	0.786	1.155	30	18	40

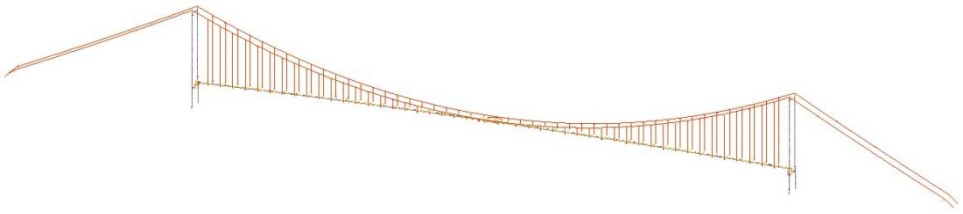

(a) FEM model by RM Bridge

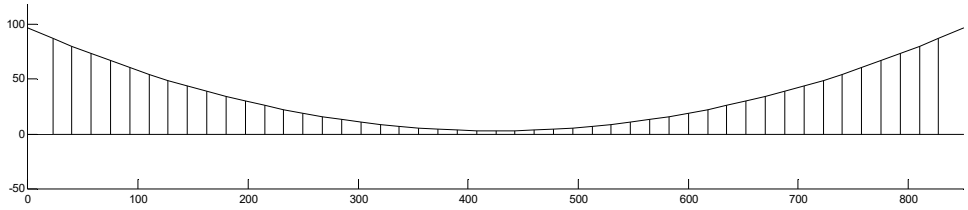

(b) Simplified analysis model

Figure 2.23 Analysis model for the example of a suspension bridge

The results of the initial equilibrium configuration analysis are plotted in Figure 2.24. First of all, in case of the geometry of main cable, both results are very similar, and the discrepancy of an elevation between two models is under ±10 mm. Also, the error of the suspension cable's tension is about 70 kN which is the same as 0.1 % of the axial tension.

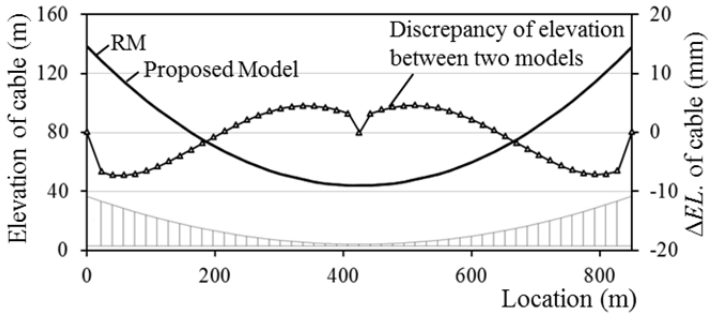

(a) Geometry of suspension cable

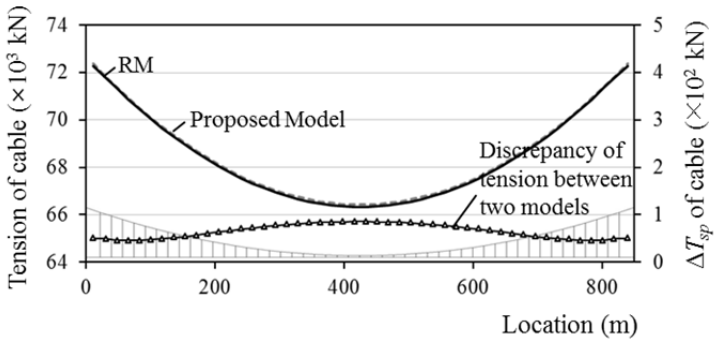

(b) Tension of suspension cable

Figure 2.24 Result of the initial equilibrium configuration for Pal-young Bridge

For a verification of structural analysis under live loads, a uniformly distributed traffic load of 20 kN/m is applied to both models. The results of the deformation of the cable system are summarized in Table 2.6, and the error is under 2.0 %. It is reasonable to develop a concept of cable system at a preliminary design stage without a detail design, and the simplified analysis model is suitable to be applied to this study.

Table 2.6 Result of displacements under live load for Pal-young Bridge

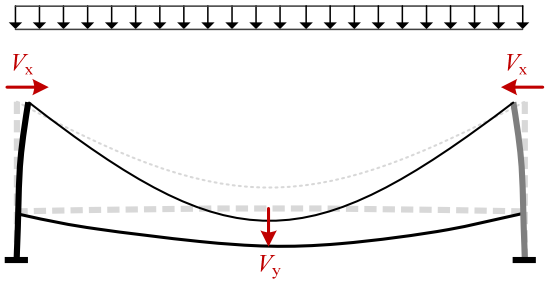

Displacement	RM Bridge	Simplified Model	Error
V_x at Pylon top	103 mm	101 mm	2.0 %
V_y at the center of span	862 mm	848 mm	1.7 %

2.4.2 Application to a cable-stayed suspension bridge

The 3rd Bosphorus Bridge, Yavuz Sultan Selim Bridge, in Turkey is selected as an example for a cable-stayed suspension bridge. The bridge has a combined cable system, a main span length of 1,408 m, and two side spans of 378 m as shown in Figure 2.25. The height of pylons with A-shape concreate leg is 322 m, and the ratio

of the cable sag to the center span length is $\frac{1}{6.4}$. The main span consists of a suspension section of 312 m including 12 hangers in the middle, two overlapping portions of 240 m including 11 hangers and 11 stay cables, and two pure cable-stayed portions of 308 m including 11 stay cables. In the side span, four intermediate piers are installed in order to increase in-plane flexural rigidity of bridge. The deck has eight lanes for traffic outside and two tracks for train in the center. The stay cables and hanger cables are spaced at 24m in the center span, and the 22 stay cables in the side span are anchored to the deck at 15m intervals. The deck is designed a streamlined box girder with 58.5 m wide and 5.2 m high.

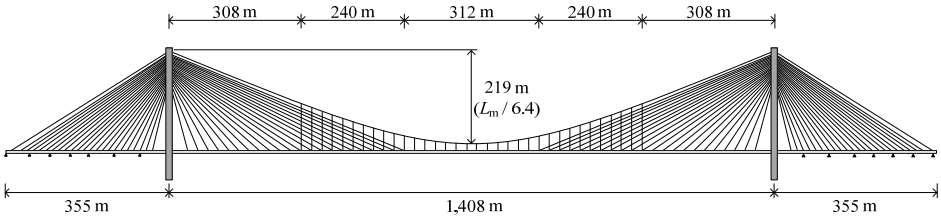

(a) Elevation view

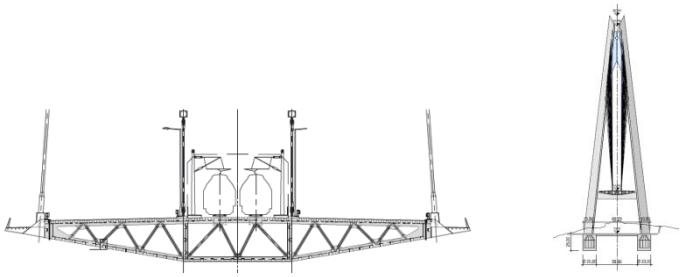

(b) General cross section of deck (c) Tower

Figure 2.25 The 3rd Bosphorus Bridge (Yavuz Sultan Selim Bridge)

Table 2.7 Material and sectional properties of the example bridge

Spec.			Cable (SP/CS)				Girder (S / C)			Pylon		
L_m (m)	L_s (m)	h (m)	E (GPa)	A (m^2)	s (m)	f (m)	E (GPa)	A (m^2)	I (m^4)	E (GPa)	A (m^2)	I (m^4)
1,408	355	308.3	200	0.3287	24	218	200	3.6~3.1	15~12	20	72~36	1,843~555
			200	0.013~0.021	24	219	200	54	162			

The main span and side span decks consist of steel and pre-stressed concrete, respectively, and the sectional and material properties are listed in Table 2.7. The tensile strength of suspension cables and stay cables is 1,860 MPa. Also, the dead load distribution factor, *r*, in the overlapping section is considered as the constant ratio for all stay cables, 0.67.

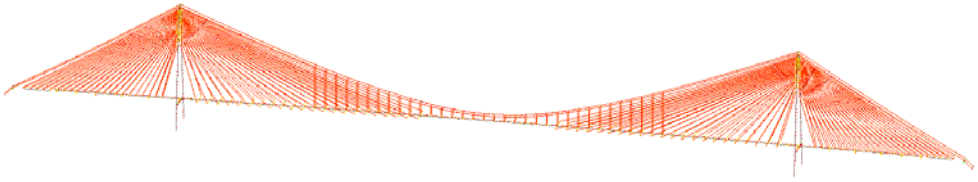

(a) 3-dimensional FEM model by RM Bridge

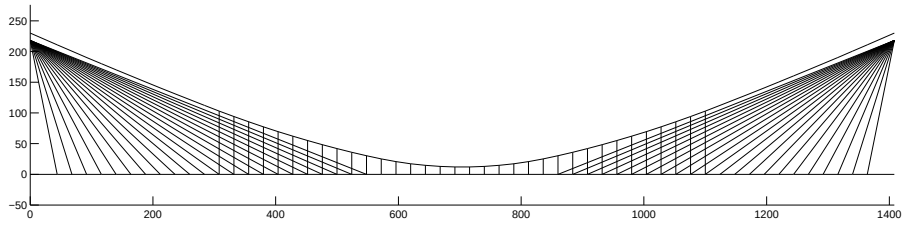

(b) Simplified numerical model

Figure 2.26 Analysis model for the example of a cable-stayed suspension bridge

The results of the initial equilibrium configuration analysis are plotted in Figure 2.27. In case of the geometry of main cable, both results are very similar, and the discrepancy of an elevation between two models is under ±25 mm. Also, the error of the suspension cable's tension is about 2,200 kN which is the same as 1.3 % of the axial tension.

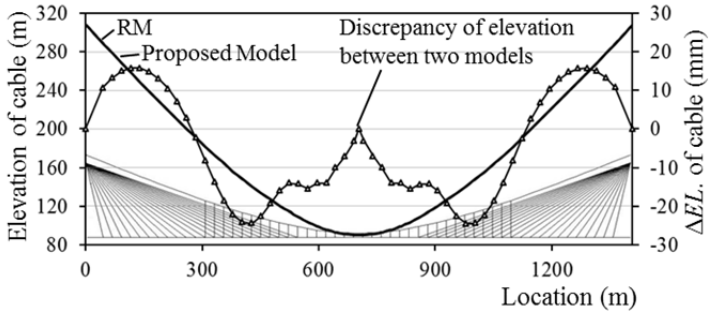

(a) Geometry of suspension cable

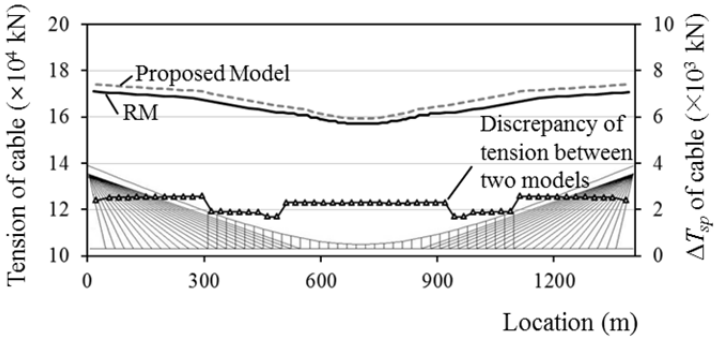

(b) Tension of suspension cable

Figure 2.27 Result of the initial equilibrium configuration for 3rd Bosphorus Bridge

For a verification of structural analysis under live loads, a uniformly distributed traffic load of 48 kN/m for eight lanes and a combination load of a uniform load 80 kN/m and a point load of 1,000 kN for two tracks are considered as shown in Figure 2.28. This railway load uses a train load model, LM71, defined in Eurocode.

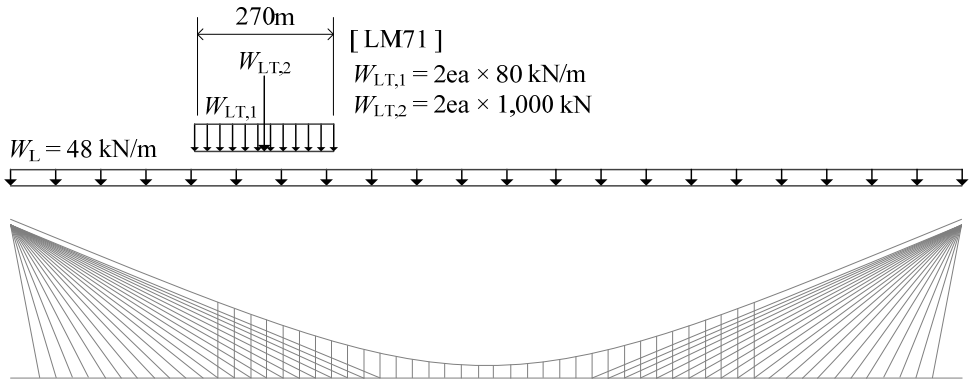

Figure 2.28 Live loads for the verification of 3rd Bosphorus Bridge

For the verification, the results including a tension of suspension cable, stayed cable, and vertical displacement of deck are shown in Figure 2.29 and Figure 2.30. In case of cable tension, both results are very similar, and the discrepancy of the tension between two models is about 2.0 % for suspension cable and 4.1 % for stayed cable near the overlapping section, respectively. Also, the error of deck's displacement is about 3.3 %. Although the error of analysis results by two models is taken place, the error is small enough to apply to a concept design in the preliminary design stage.

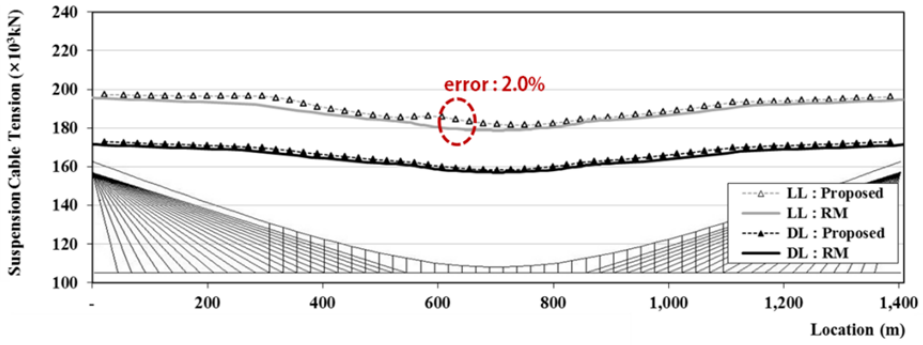

(a) Tension of suspension cable

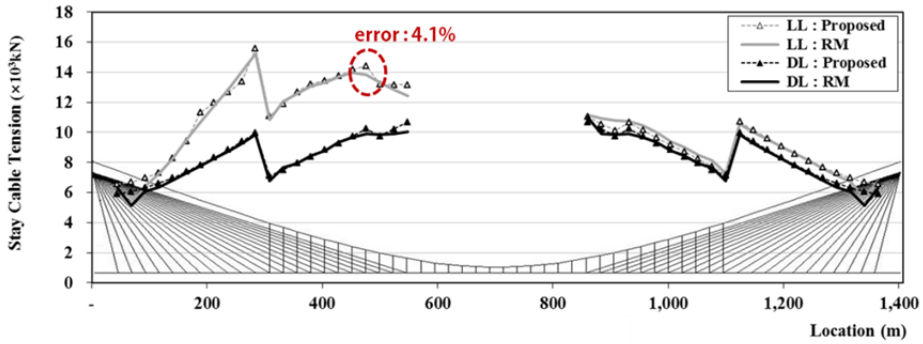

(b) Tension of stayed cable

Figure 2.29 Results of tension under live loads of 3rd Bosphorus Bridge

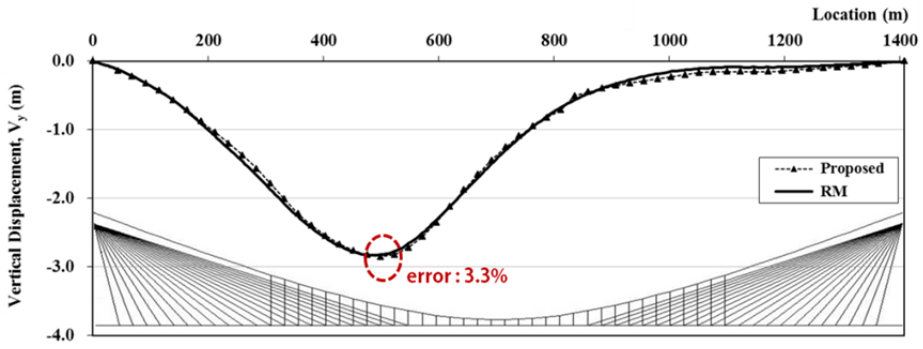

Figure 2.30 Results of displacement under live loads of 3rd Bosphorus Bridge

2.4.3 Summary of the verification

To verify and confirm the accuracy and adequacy of the proposed simplified analysis model, the suspension bridge with a main span length of 850 m and the 3rd Bosphorus Bridge with a main span length of 1,408 m are analyzed. The initial equilibrium state simulated by the simplified analysis model has the insignificant discrepancy in results, and the error of cable tension in both bridges is about 1.0 %. The time efficiency is remarkably improved as the time consumption for assembling and analyzing the analysis model takes several seconds in case of the proposed model, but it takes several working days when a skilled engineer uses the commercial FEM program. Also, the structural behaviors of the example bridges under live load are compared with the results obtained by the commercial FEM program, and the results correspond with each other well. When the railway loads are loaded, some discrepancies in cable tension are taken place, and the error may come from the ignorance of the flexibility in deck. However, all of the results represent the features of the structural behavior for a combined system, and the accuracy is enough reliable. Consequently, the structural analysis using the proposed simplified analysis model is able to apply to this study and the preliminary design of a cable-stayed suspension bridge.

3. PARAMETRIC INVESTIGATION OF EFFECTS OF DESIGN VARIATIONS ON A STRUCTURAL BEHAVIOR UNDER LIVE LOADS

In this chapter, the effects of design variations including the change of a side span length, a composition of a suspension section and an overlapping section, a cable sag, and a dead load distribution factor on a structural behavior are investigated by the proposed structural analysis model. The 3rd Bosphorus Bridge applied to the verification of the proposed model in the previous chapter is employed to this parametric investigation. Basically, the origin value of the design variable is the same as Table 2.4. The live loads for the parametric investigation consist of two cases including a road loading case and a rail loading case as shown in Figure 3.1. The road loading case is a uniformly distributed load of 48 *kN/m* for 8 lanes on the deck, and the rail loading case uses the rail load model, LM71, in Eurocode as described in the sub-chapter 2.4.2 of this dissertation. The rail load assumes that a length of a train is 270 m and two trains in both directions are located in the same position on the deck, as illustrated in Figure 3.1(b). Particularly, the rail load model is loaded along the span length sequentially, and then the envelope curves for stress and deformation are plotted and analyzed.

The variations of each design variable are discretely changed, and are listed in Figure 3.2 and Table 3.1. For this parametric investigation, the area of the suspension cable, stay cables and hangers are re-calculated with respect to the dead load condition as the cable system is changed.

The structural behavior including a tension, stress and deformation of each cable and deck is investigated. The variation of design variables leads the change of the cable configurations, and the effects of the variation on the structural behavior are calculated for two load cases, respectively.

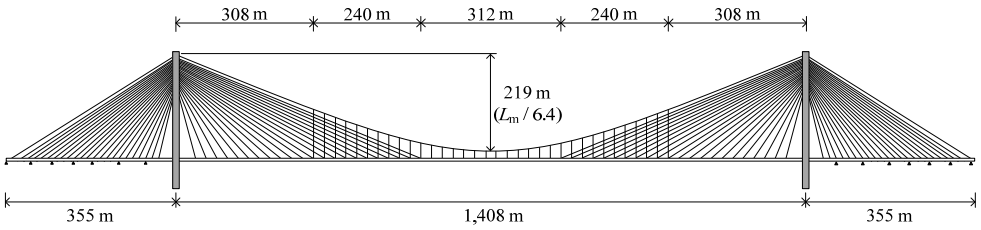

(a) Original cable system of the 3rd Bosphorus Bridge

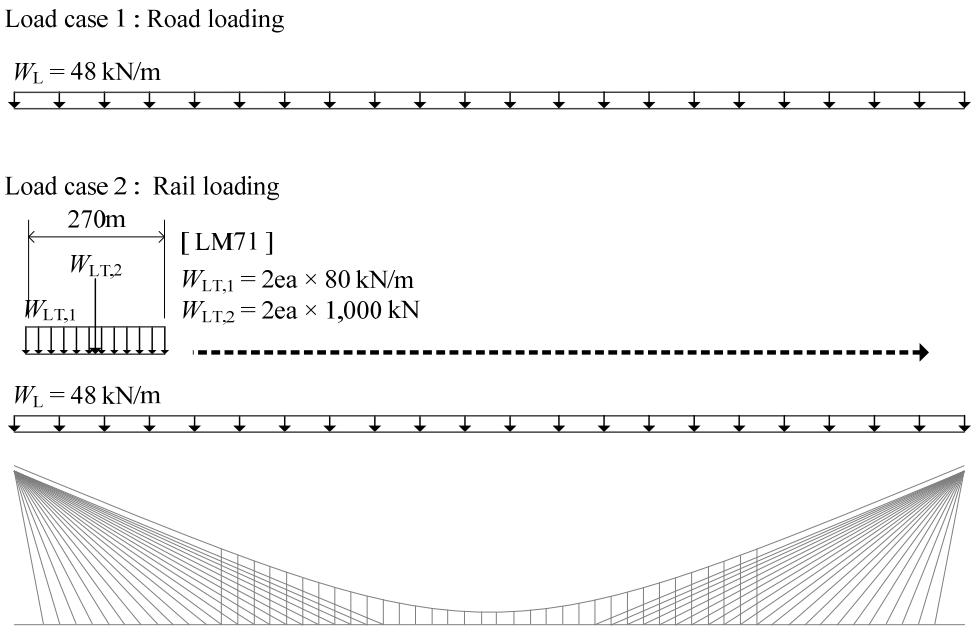

(b) Live loads for the parametric investigation

Figure 3.1 Example bridge for the parametric investigation

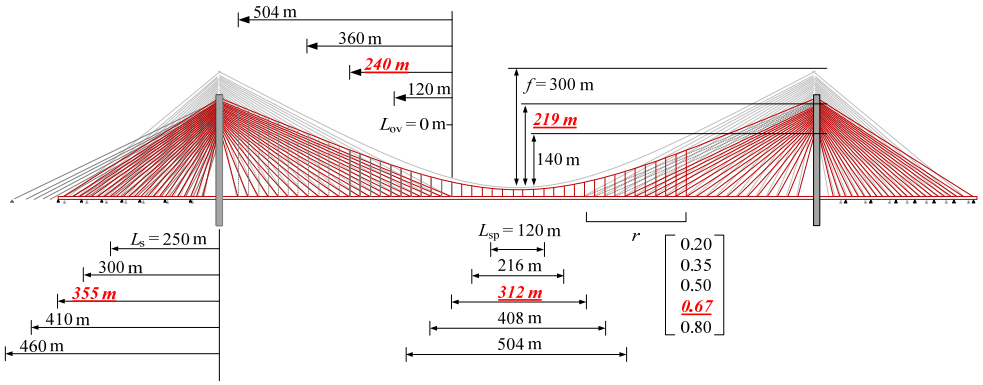

Figure 3.2 Geometric configurations according to the variation of design variables

Table 3.1 Variation of design variables for the parametric investigations

Variables	Origin value	Variation	Remarks
β_s	$\frac{355}{1{,}408} = 0.25$	0.17 ~ 0.33	L_s = 250 ~ 460 m
β_{sp}	$\frac{312}{1{,}408} = 0.22$	0.09 ~ 0.36	L_{sp} = 120 ~ 504 m
β_{ov}	$\frac{2 \times 240}{1{,}408 - 312} = 0.44$	0.00 ~ 1.00	L_{ov} = 0 ~ 504 m
β_f	$\frac{219}{1{,}408} = 0.16$	0.10 ~ 0.20	f = 140 ~ 300 m
r	0.63	0.20 ~ 0.80	

3.1 Effects of the Side Span Length

In this sub-chapter, the effect of the variation of the side span length, L_s, for the 3rd Bosphorus Bridge on the structural behavior is investigated. The origin value of the side span length is 355 m, and the variation is { 250 m, 300 m, 355 m, 410 m, 460 m } while keeping the other design variables including the length of suspension section (L_{sp}), the length of overlapping section (L_{ov}), the cable sag (f), and the dead load distribution factor (r).

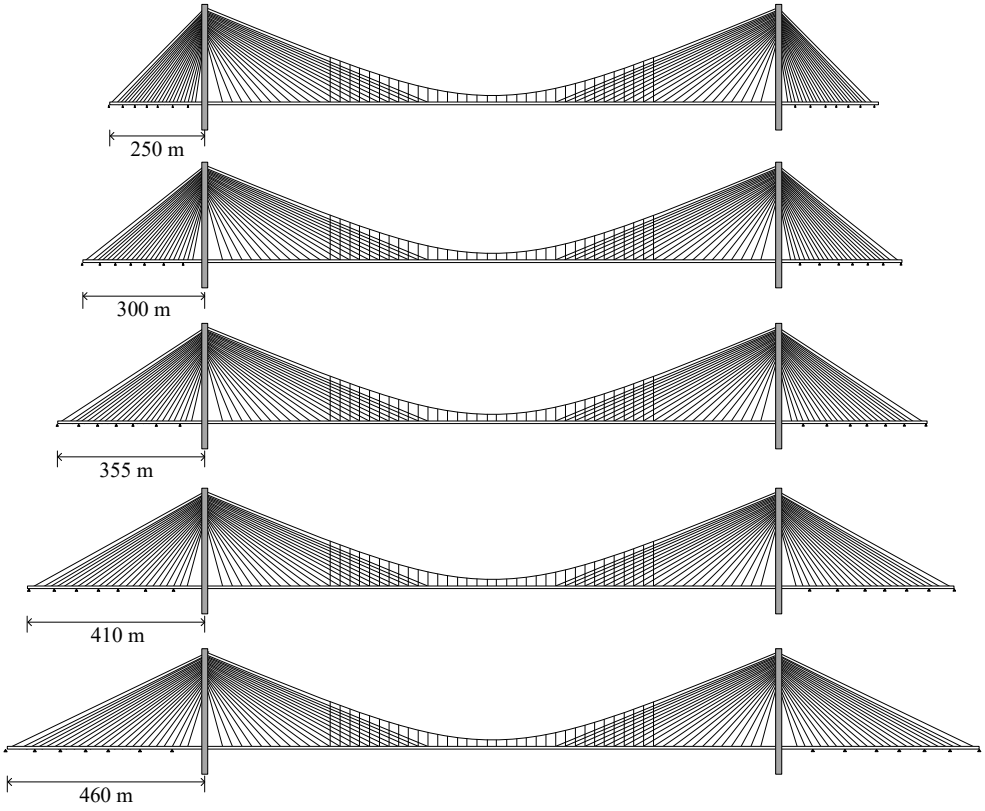

Figure 3.3 Variation of the side span length, L_s

As a result of an initial equilibrium configuration analysis, the suspension cable's area in the center span is not affected by the variation of L_s because the dead load supported by the suspension cable is not changed as summarized in Table 3.2. The total quantity of cables including suspension, stay and hangers with various side span lengths is plotted as the ratio normalized by the original quantity, Q_0, in Figure 3.4. As L_s increases, the cable quantity is slightly increased.

Table 3.2 Calculation of the area of suspension cable with various L_s

L_s	250 m	300 m	355 m	410 m	460 m
β_s	0.17	0.21	0.25	0.29	0.33
A_{sp}	0.3287	0.3287	0.3287	0.3287	0.3287
A_{sp}/A_{origin}	1.00	1.00	1.00	1.00	1.00

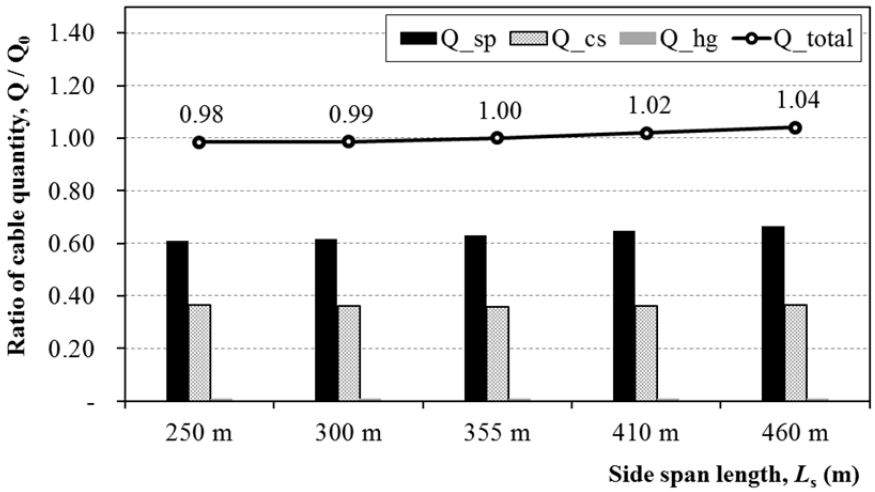

Figure 3.4 Cable quantities with various L_s

3.1.1 Effects on the cables

(1) Road loading case

Figure 3.5 shows the axial stress and angular change of the suspension cable according to the variation of the side span length, L_s. The axial stress has the minimum value at the center of span and the maximum value at the top of pylon. The angular change is defined as the discrepancy between the cable angle at a cable band under live load and the angle under self-weight. Under the road load, the maximum angular change is about 1.0 degree in the suspension section.

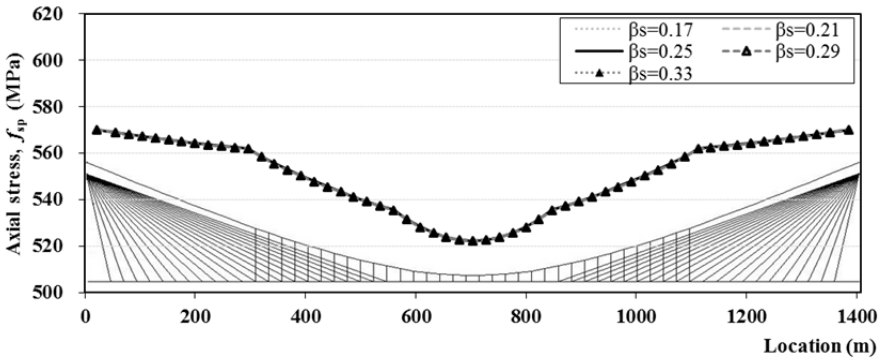

(a) Axial stress of suspension cable

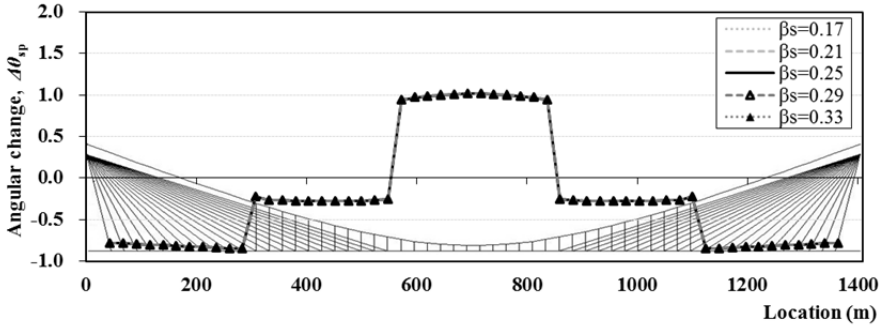

(b) Angular change of suspension cable

Figure 3.5 Stress and deformation of cable under road load with various L_s

The tension increment of hanger ropes and stay cables under live load are not affected by the variation of L_s, too. The tension increment of hanger in the overlapping section tends to increase as the length of the hanger rope is getting longer. Also, the increment of the hanger rope tension in the overlapping section is about 36 ~ 40% of the live load excepting the longest one, which is obviously related to the dead load distribution factor, *r,* defined as 0.63 in this bridge. Therefore, the area of the longest hanger rope should be designed larger than others. The tension increment of stay cables is increased as the stay cable's length increases, and the increment in the overlapping section is reduced due to the load distribution factor.

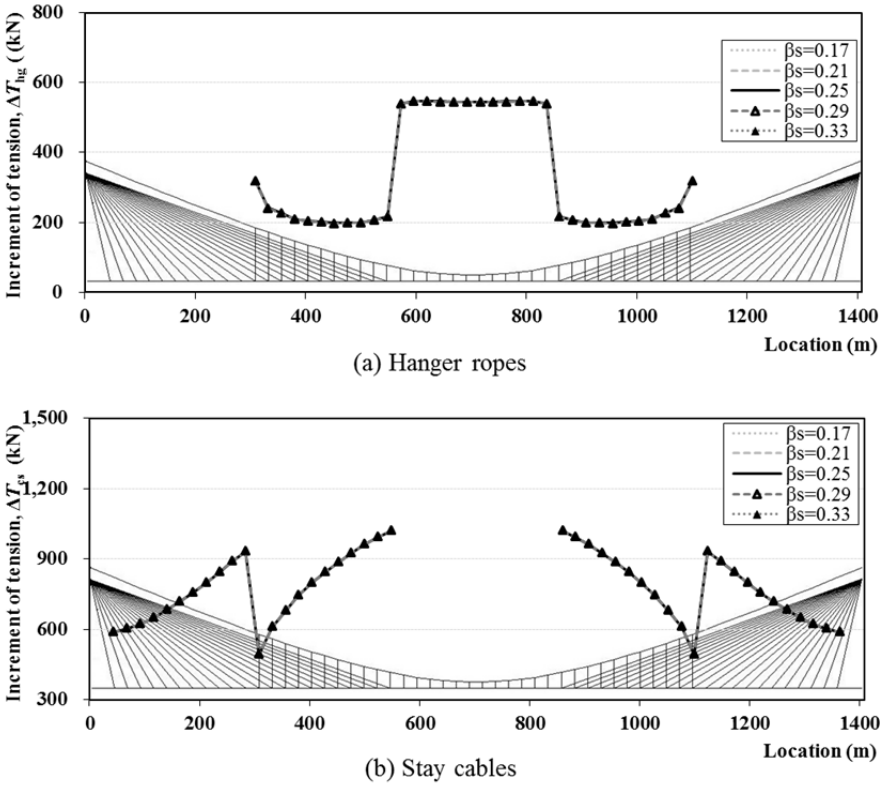

Figure 3.6 Increment of tension under road load with various L_s

(2) Rail loading case

The envelope for the axial stress and deformation of the suspension cable under rail load is illustrated in Figure 3.7, which is noted that there is no effect of the variation of L_s on the stress and deformation. The maximum axial stress under rail load is 20% larger than the stress under road load, and the maximum angular change is 40% larger than the one under road load because the rail load is bigger and partially loaded on the deck. However, the discrepancy of the axial stress may be larger because the angular change leads to a large secondary stress on the cross section of suspension cable.

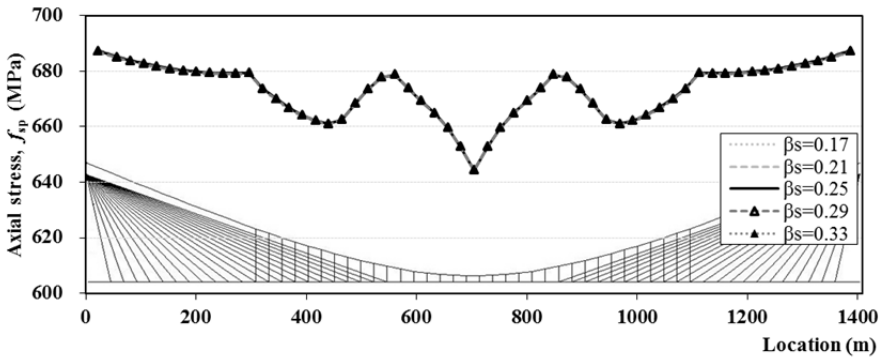

(a) Axial stress of suspension cable

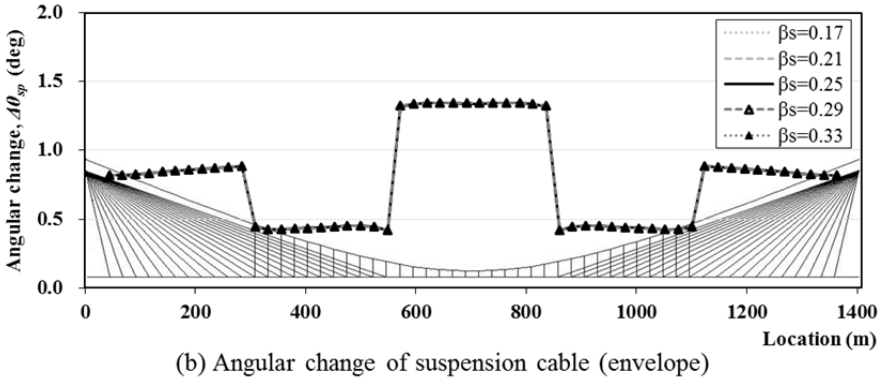

(b) Angular change of suspension cable (envelope)

Figure 3.7 Stress and deformation of suspension cable under rail load with various L_s

For hanger ropes and stay cables, it is important to investigate the increment of stress under rail load because the fatigue is critical to design the railway cable supported bridge and the fatigue performance depends on the increment of stress. The stress increment of hanger ropes is about 200 MPa which is the same as one third of the axial stress under dead load, and it is very uniform along the bridge's longitudinal direction regardless of the suspension section and overlapping section. In case of stay cables, the increment of stress in the overlapping section is obviously decreased when the stay cable length is increased, and the amplitude of the stress is larger than one of hanger ropes as shown in Figure 3.8.

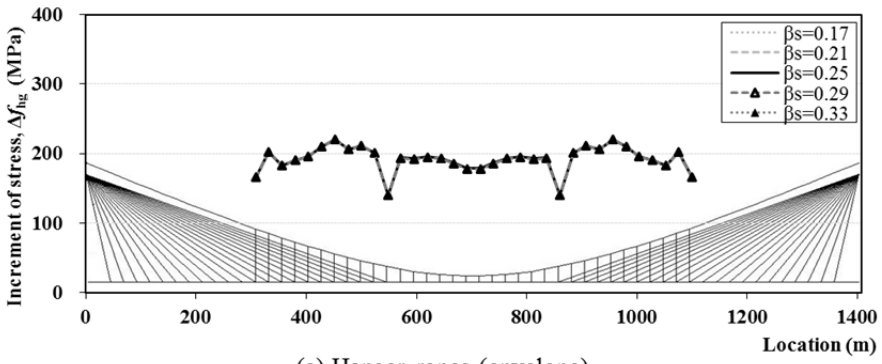

(a) Hanger ropes (envelope)

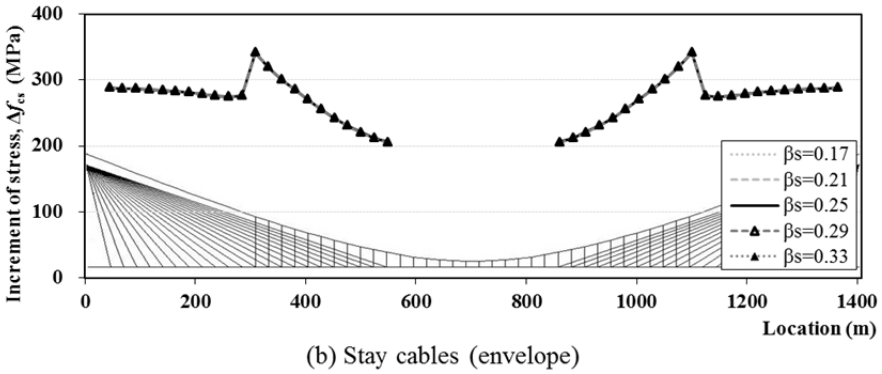

(b) Stay cables (envelope)

Figure 3.8 Increment of stress under rail load with various L_s

3.1.2 Effects on the deck

(1) Road loading case

The deformation of the deck including a vertical displacement and a curvature is affected by the variation of L_s as plotted in Figure 3.9. As L_s increases, the maximum vertical displacement and curvature is slightly increased because the cable horizontal stiffness at the top of pylon decreases and the horizontal displacement at the top of pylon is increased. However, the increment of the maximum curvature in the center is so small that the effect on the structural behavior can be negligible.

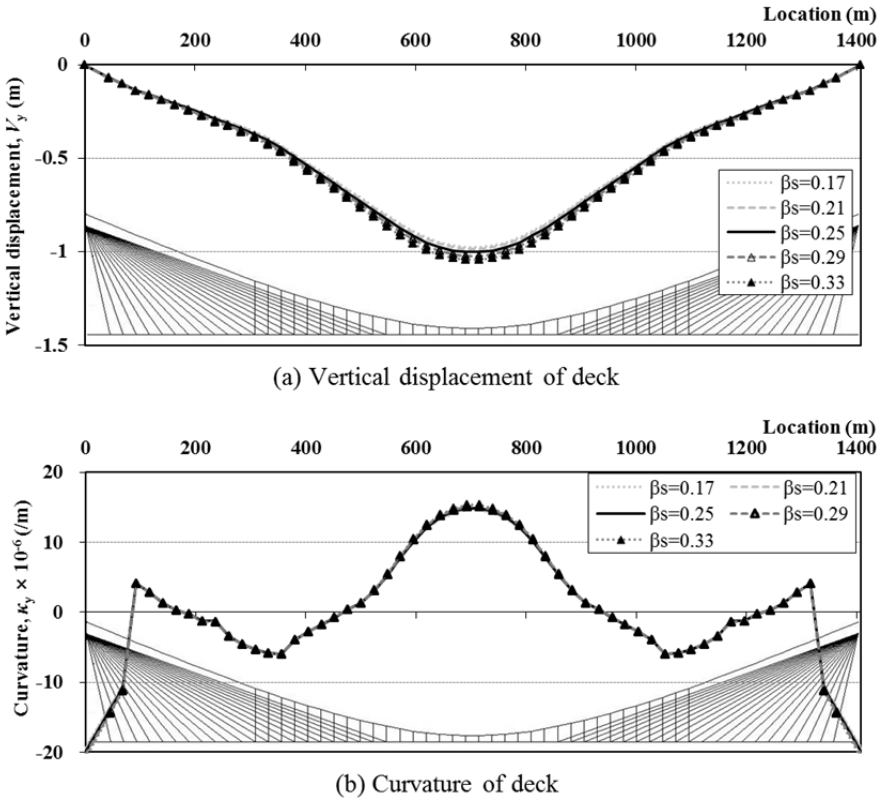

Figure 3.9 Deformation of deck under road load with various L_s

(2) Rail loading case

For analyzing the deformation of the deck under rail load, the envelope curves for the vertical displacement and the curvature are plotted in Figure 3.10. The maximum vertical displacement is appeared in the suspension section of the bridge's center, and it is over 3 times the result under road load. Also, in case of the curvature, the maximum curvature under rail load is about 17 times the result under road load. Although both deformations are slightly increased as L_s increases, the amplitude is so insignificant that the effect on the structural behavior can be negligible.

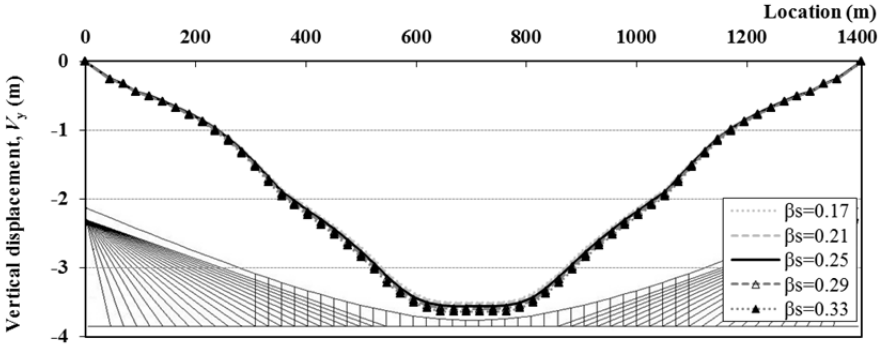

(a) Vertical displacement of deck (envelope)

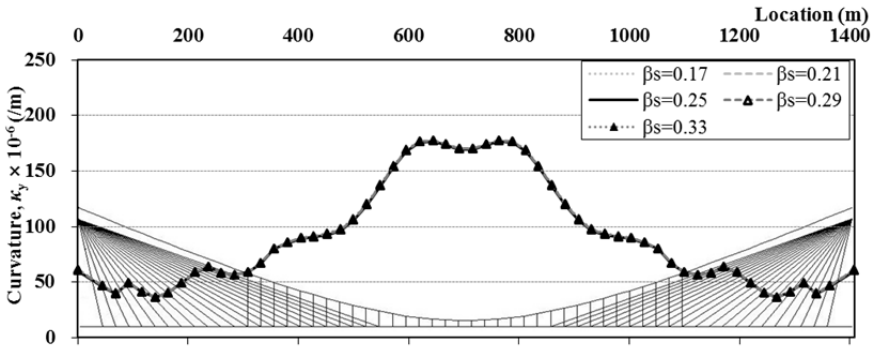

(b) Curvature of deck (envelope)

Figure 3.10 Deformation of deck under rail load with various L_s

3.1.3 Effects on the pylon

Generally, when L_s increases, the horizontal stiffness of the cable in the side span which is defined as k_c in sub-chapter 2.3 is decreased because the cable sag effect increases. Therefore, the horizontal displacement at the top of pylon is increased as L_s increases as plotted in Figure 3.11. The displacement under rail load is double as large as that under road load. On the contrary, as L_s increases, the vertical reaction on the top is decreased since the side span's angle is decreased and the vertical portion of the cable tension is decreased.

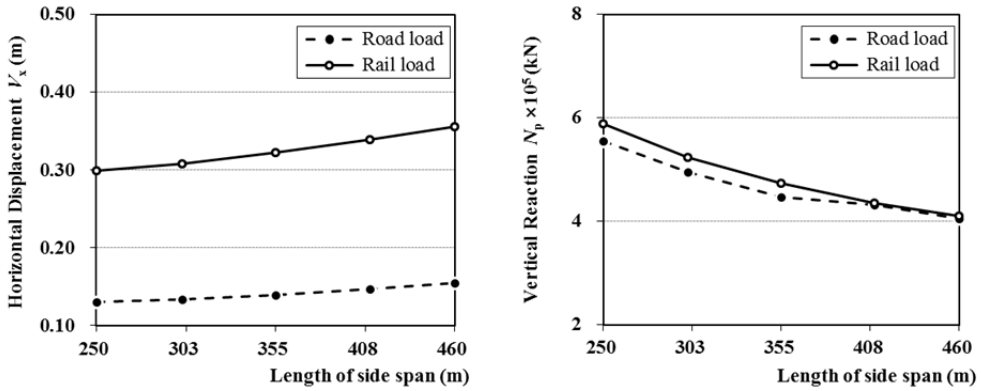

(a) Horizontal displacement at the top (b) Vertical reaction at the top

Figure 3.11 Pylon's behavior with various L_s

3.2 Effects of the Suspension Section Length

In this sub-chapter, the effect of the variation of the suspension section length, L_{sp}, for the 3rd Bosphorus Bridge on the structural behavior is investigated. The origin value of L_{sp} is 312 m, and the variation is { 120 m, 216 m, 312 m, 408 m, 504 m } while keeping the other design variables. Figure 3.12 shows the change of a configuration according to the variation of L_{sp}.

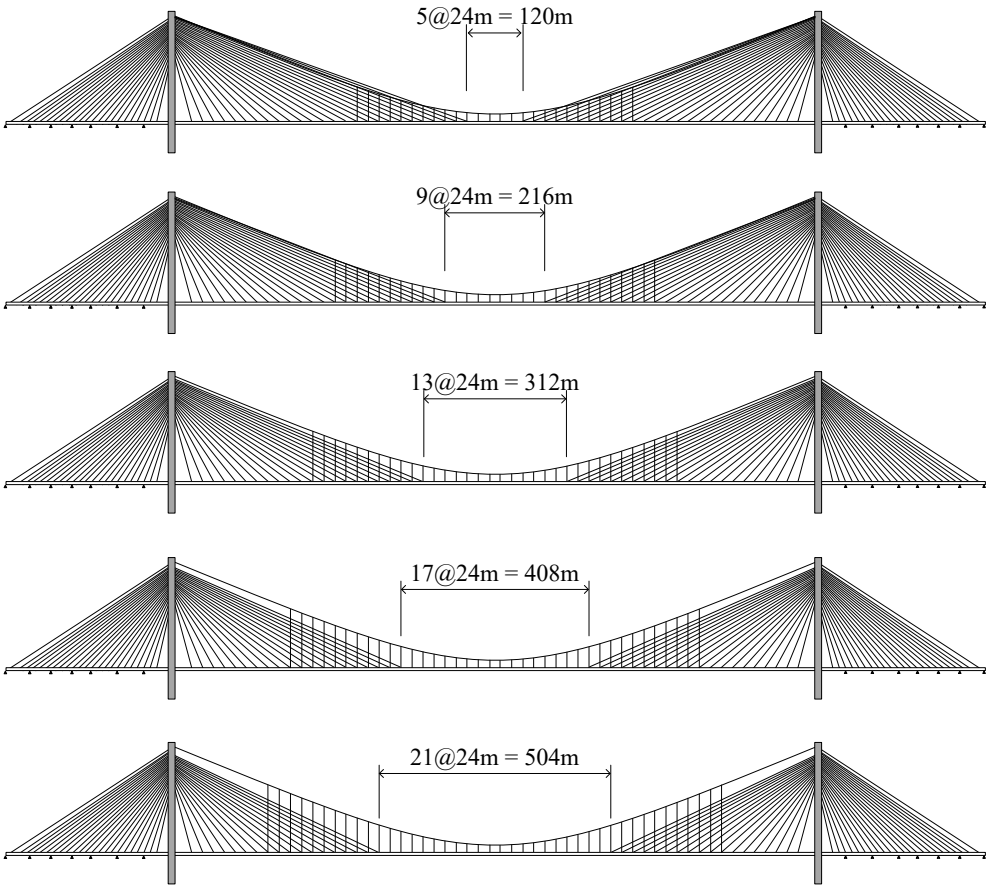

Figure 3.12 Variation of the suspension section length, L_{sp}

As a result of an initial equilibrium configuration analysis, the suspension cable's area in the center span is increased as L_{sp} increases because the dead load supported by the suspension cable is increased as summarized in Table 3.3. As L_{sp} increases, the total quantity of cables including a suspension, stays and hangers is increased while the quantity of suspension cable, Q_{sp}, is increased and the quantity of stay cables Q_{cs}, is decreased as plotted in Figure 3.13.

Table 3.3 Calculation of the area of suspension cable with various L_{sp}

L_{sp}	120 m	216 m	355 m	408 m	504 m
β_{sp}	0.09	0.15	0.22	0.29	0.36
A_{sp}	0.2025	0.2681	0.3287	0.3863	0.4385
A_{sp}/A_{origin}	0.62	0.82	1.00	1.18	1.33

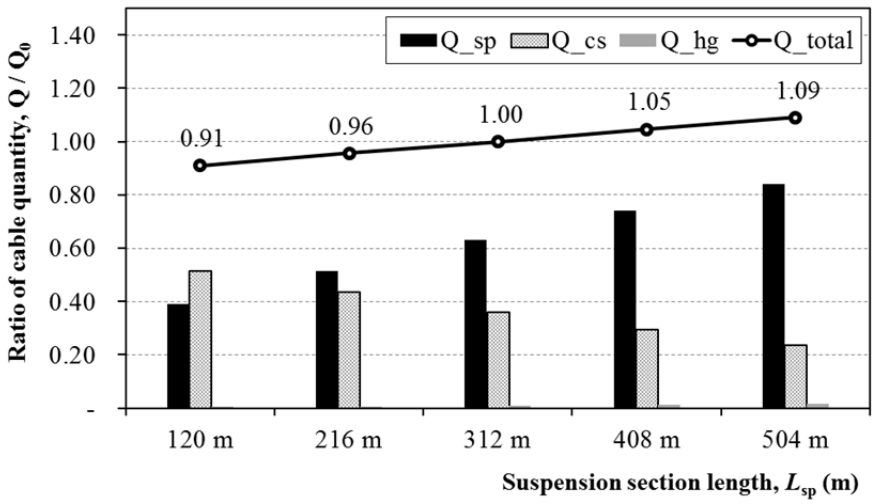

Figure 3.13 Cable quantities with various L_{sp}

3.2.1 Effects on the cables

(1) Road loading case

The maximum axial stress of the suspension cable at the top of pylon is not affected by the variation of L_{sp}, while the minimum axial stress at the center of span is decreased as the suspension section is expanded. Similarly, the angular change of the suspension cable is remarkably reduced as the L_{sp} increases as shown in Figure 3.14. Because this angular change causes a large secondary stress in the cross section of the cable under live loads, it is very important to design the suspension section length.

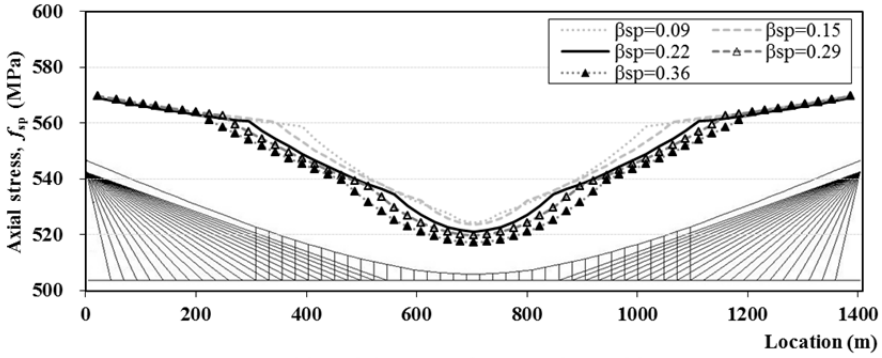

(a) Axial stress of suspension cable

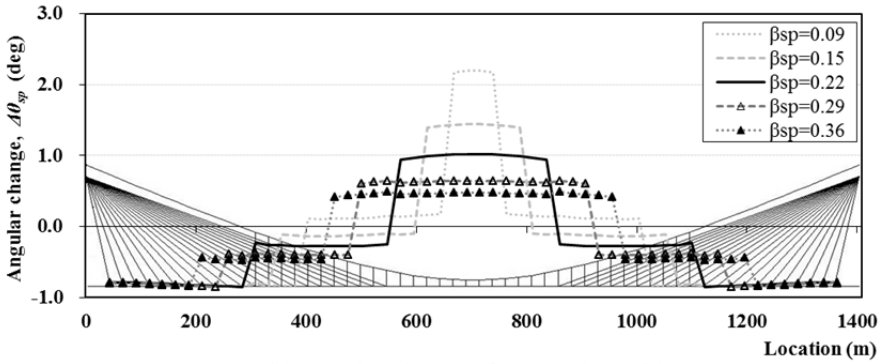

(b) Angular change of suspension cable

Figure 3.14 Stress and deformation of suspension cable under road load with various L_{sp}

The increment of tension for hanger ropes is nearly uniform in the overlapping section and the suspension section, respectively, regardless of the variation of L_{sp}. The ratio of the increment of tension in the overlapping section to the increment in the suspension section is about 0.37 which is related to the dead load distribution factor of 0.63 for this bridge. However, in case of the longest hanger rope, the increment of tension is over 50 % of the increment in the suspension section, and it is increased as the suspension section is expanded. Also, the increment of tension for stay cables at both the stayed section and the overlapping section is clearly decreased as L_{sp} increases as shown in Figure 3.15.

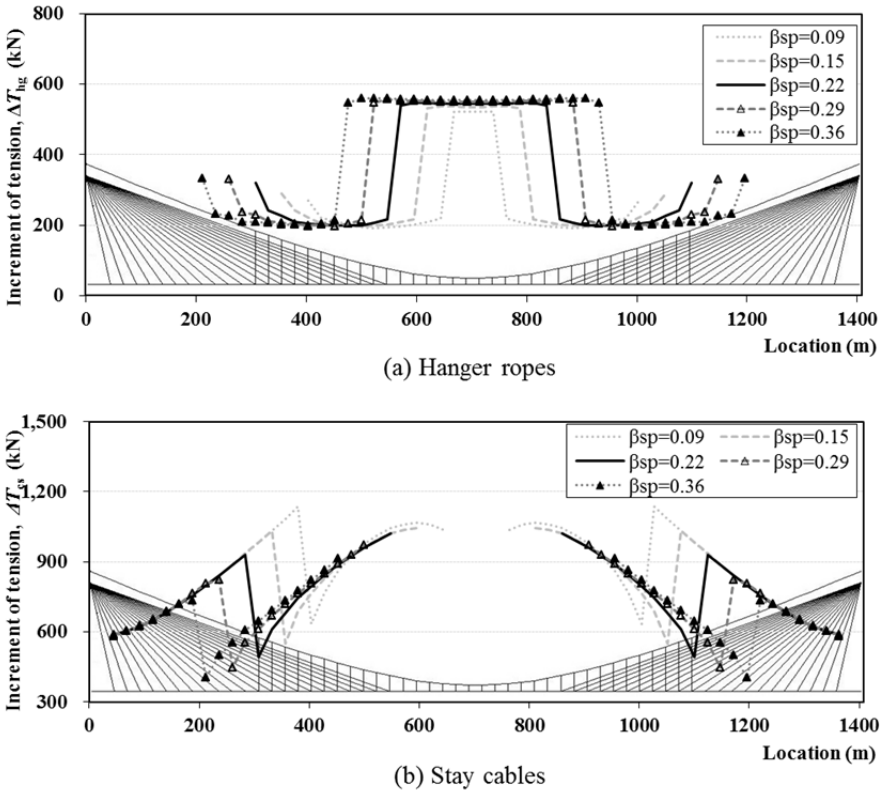

Figure 3.15 Tension increment under road load with various L_{sp}

(2) Rail loading case

The envelope for the axial stress and deformation of the suspension cable under rail load is illustrated in Figure 3.16, which is noted that the stress is increased and the angular change is decreased as the suspension section is expanded. Particularly, the axial stress of suspension cable tends to be maximized at the border between the suspension section and the overlapping section. The angular change under rail load is about 40% larger than the result under road load, which develops the large secondary stress in the cross section of suspension cable.

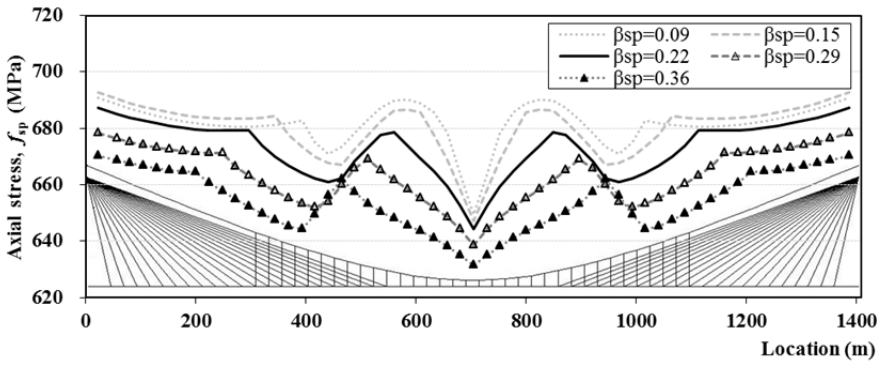

(a) Axial stress of suspension cable

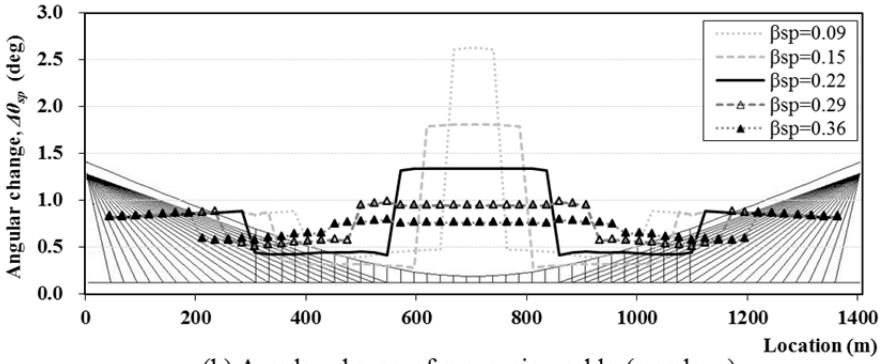

(b) Angular change of suspension cable (envelope)

Figure 3.16 Stress and deformation of suspension cable under rail load with various L_{sp}

As the suspension section is expanded, the increment of the stress for hanger ropes under rail load is increased in the suspension section and decreased in the overlapping section, as well as the increment of stay cables in the overlapping section is slightly increased as shown in Figure 3.17.

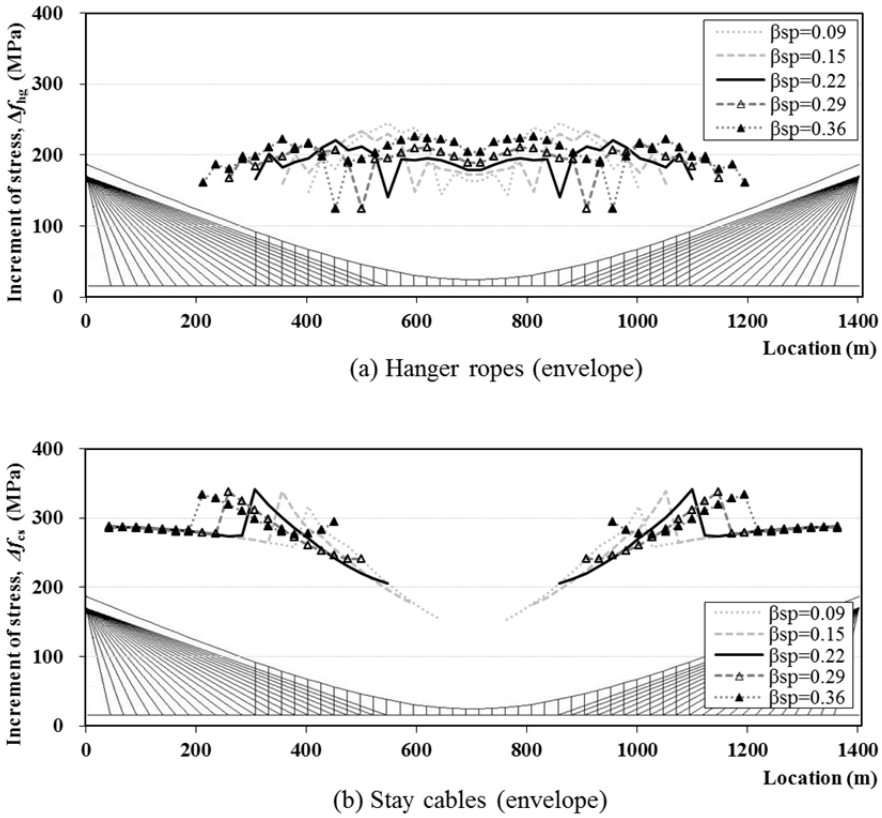

Figure 3.17 Increment of stress under rail load with various L_{sp}

3.2.2 Effects on the deck

(1) Road loading case

As the suspension section is expanded, the deformations including the maximum vertical displacement and the curvature of deck under rail load are decreased as shown in Figure 3.18. The reduction rate of the curvature according to the variation of L_{sp} is larger than the reduction rate of the vertical displacement. The ratio of decline for the vertical displacement is about 20 % from β_{sp} = 0.09 to β_{sp} = 0.36, and the reduction rate of the curvature is about 50%.

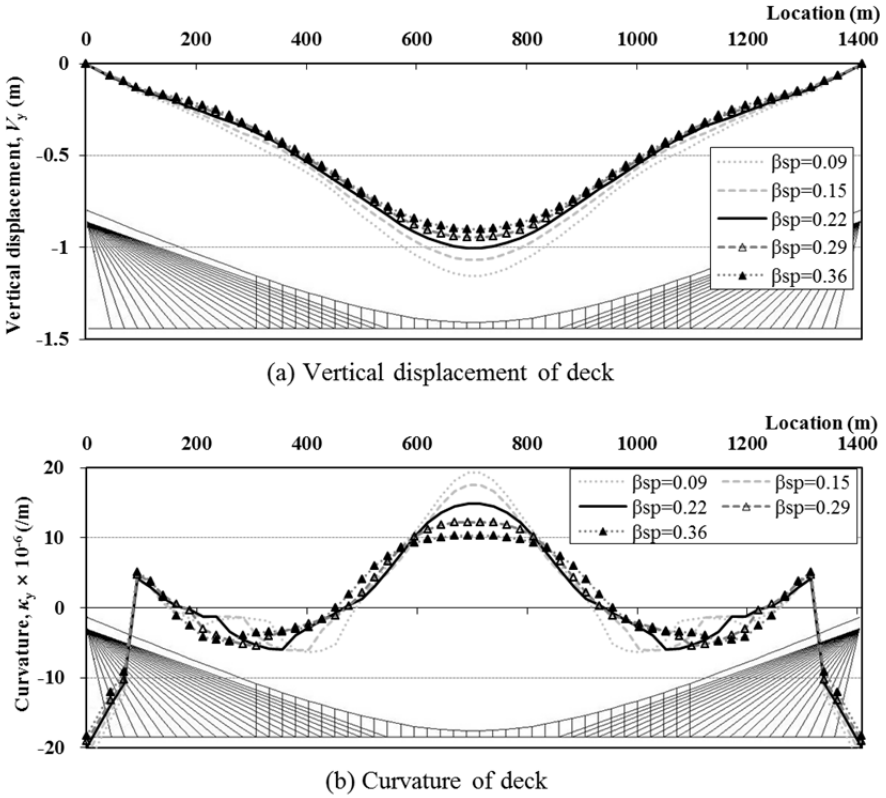

Figure 3.18 Deformation of deck under road load with various L_{sp}

(2) Rail loading case

The envelopes of the vertical displacement and the curvature of deck at the center under rail load shows that the deformations in the suspension and overlapping section are clearly decreased as the suspension section is expanded as plotted in Figure 3.19. However, when the ratio, β_{sp}, is over 0.22, the reduction of the deformation can be negligible. On the other hand, both deformations of the deck have a small amplitude in the envelopes in the stayed section.

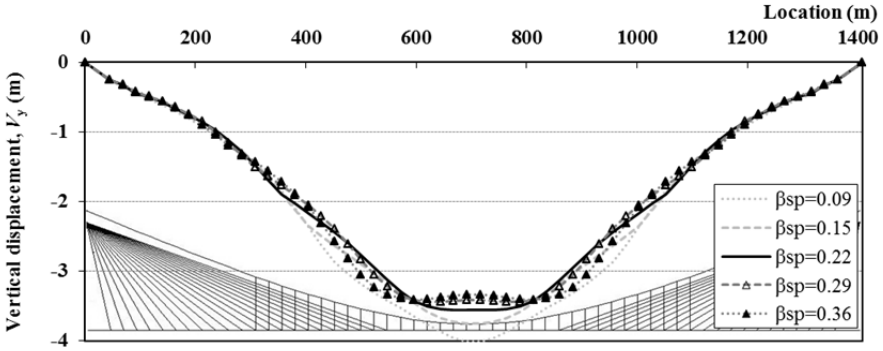

(a) Vertical displacement of deck (envelope)

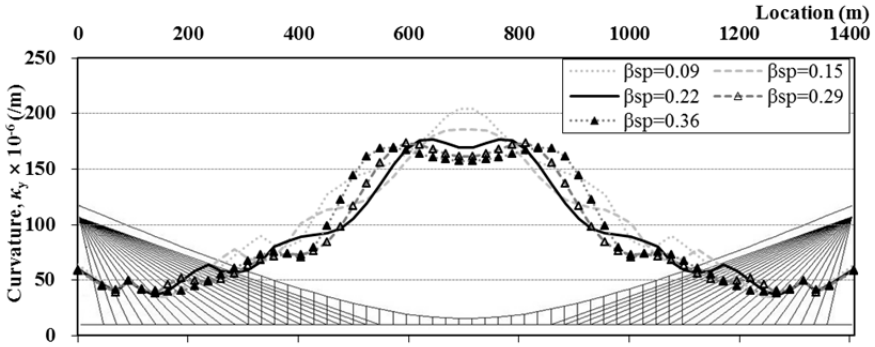

(b) Curvature of deck (envelope)

Figure 3.19 Deformation of deck under rail load with various L_{sp}

3.2.3 Effects on the pylon

Since the area of suspension cable is increased as the suspension section is expanded, the horizontal stiffness of cables at the top of pylon is increased. Therefore, the horizontal displacement at the top is clearly decreased according to the growth of the length of suspension section as shown in Figure 3.20. The displacement under rail load is over double as large as that under road load. On the other hand, the vertical reaction on the top is slightly decreased as the length of the suspension section is increased.

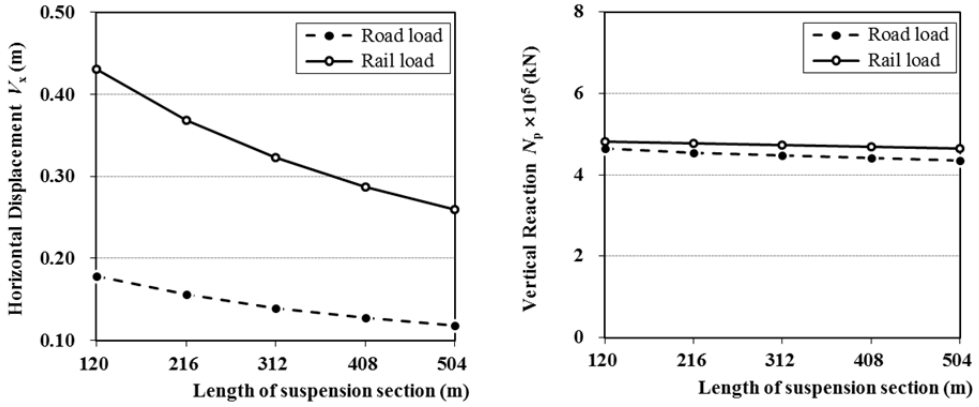

(a) Horizontal displacement at the top (b) Vertical reaction at the top

Figure 3.20 Pylon's behavior with various L_{sp}

3.3 Effects of the Overlapping Length

In this sub-chapter, the effect of the variation of the overlapping length, L_{ov}, for the 3rd Bosphorus Bridge on the structural behavior is investigated. The origin value of L_{ov} is 240 m, and the variation is { 0 m, 120 m, 240 m, 360 m, 504 m } while keeping the other design variables including the side span length (L_s), the suspension section length (L_{sp}), the cable sag (f), and the dead load distribution factor (r). as illustrated in Figure 3.21.

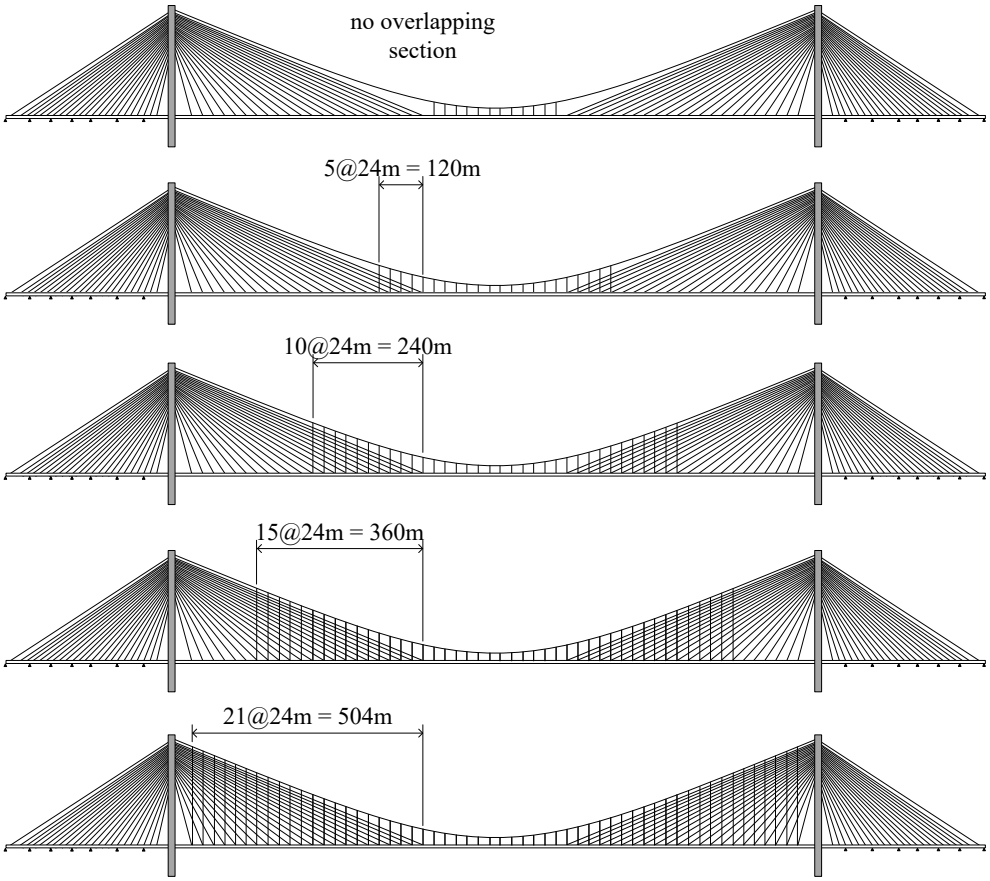

Figure 3.21 Variation of the length of overlapping section

As a result of an initial equilibrium configuration analysis, the suspension cable's area in the center span is increased as L_{ov} increases because the dead load supported by the suspension cable is increased as summarized in Table 3.4. In case of the total quantity of cables, as the overlapping length increases, the total quantity is slightly increased while the quantity of suspension cable, Q_{sp}, is increased and the quantity of stay cables Q_{cs}, is decreased as plotted in Figure 3.22.

Table 3.4 Calculation of the area of suspension cable with various L_{ov}

L_{ov}	0 m	120 m	240 m	360 m	504 m
β_{ov}	0.00	0.22	0.45	0.66	1.00
A_{sp}	0.2292	0.2899	0.3287	0.3562	0.3768
A_{sp}/A_{origin}	0.70	0.88	1.00	1.08	1.15

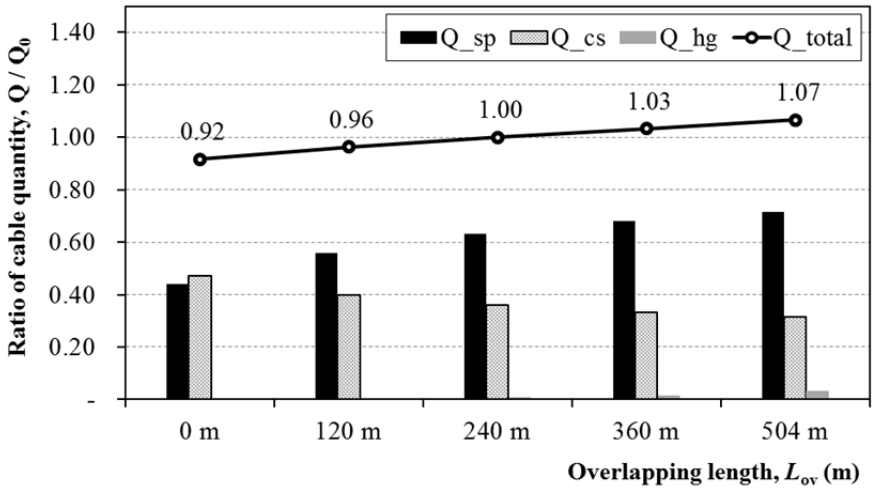

Figure 3.22 Cable quantities with various L_{ov}

3.3.1 Effects on the cables

(1) Road loading case

The maximum axial stress of the suspension cable at the top of pylon is not affected by the variation of L_{ov}, while the minimum axial stress at the center of span is decreased as the overlapping section is expanded. Similarly, the angular change of the suspension cable is remarkably reduced as the L_{ov} increases as shown in Figure 3.23. When the ratio of the overlapping length to the stayed section is over 0.66, the reduction of the angular change by the expansion of the overlapping length is small.

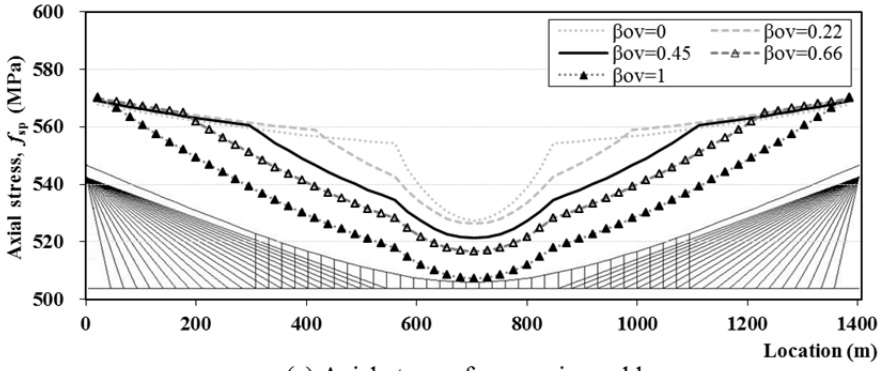

(a) Axial stress of suspension cable

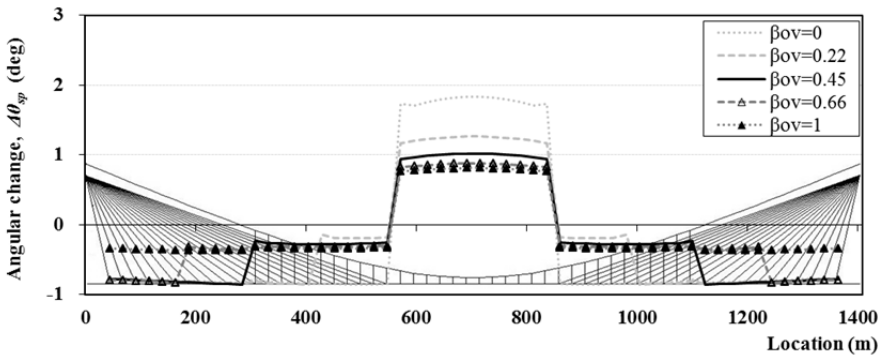

(b) Secondary stress of suspension cable

Figure 3.23 Stress and deformation of suspension cable under road load with various L_{ov}

The increment of tension for hanger ropes is nearly uniform in the overlapping section and the suspension section, respectively, regardless of the variation of L_{ov}. However, the increment in the longest hanger rope is considerably enlarged, and the enlarged amount is decreased as L_{ov} increases. The amount is 200 kN for Dischinger system (β_{ov}=0) and 100 kN for Roebling system (β_{ov}=1). In case of stay cables, the increment of tension under live loads is clearly decreased as L_{ov} is expanded as shown in Figure 3.24. Therefore, it is clarified that the expansion of the overlapping length leads to reduce the stress, tension and deformation of cables although the quantities of cables increases. It makes a trade-off problem in the design stage.

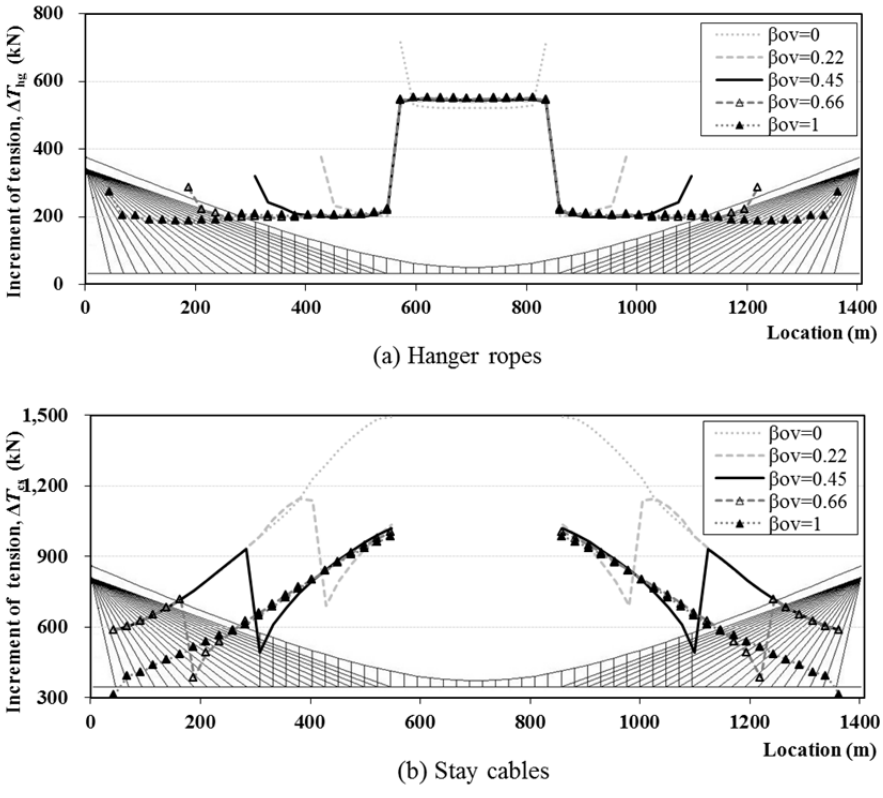

Figure 3.24 Increment of tension under road load with various L_{ov}

(2) Rail loading case

The envelope for the axial stress and deformation of the suspension cable under rail load is illustrated in Figure 3.25, which is noted that the stress and the angular change of suspension cable are significantly decreased as L_{ov} is expanded. Particularly, the axial stress of suspension cable tends to be maximized at the border between the suspension section and the overlapping section. The angular change under rail load is about 40% larger than the result under road load, which develops the large secondary stress in the cross section of suspension cable.

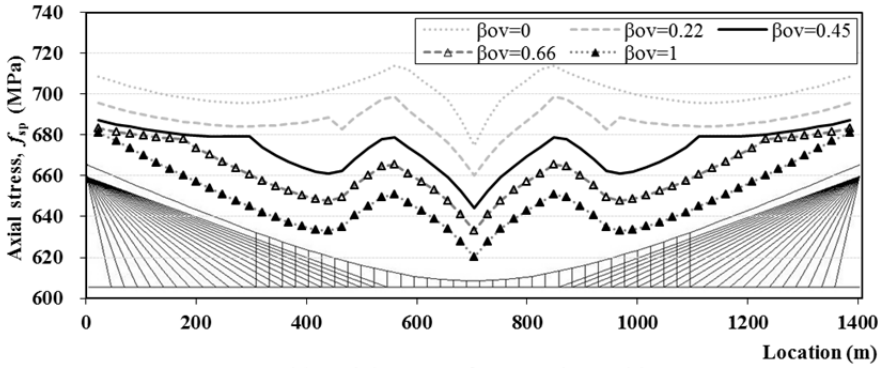

(a) Axial stress of suspension cable

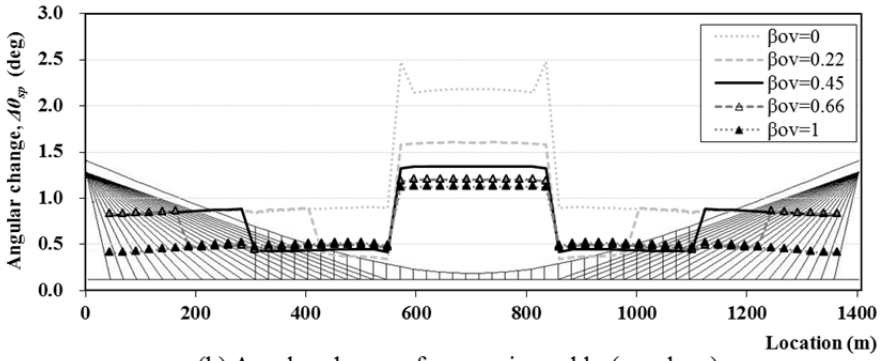

(b) Angular change of suspension cable (envelope)

Figure 3.25 Stress and deformation of suspension cable under rail load with various L_{ov}

As L_{ov} expands, the increment of the stress for hanger ropes is decreased in the suspension section and slightly increased in the overlapping section. The increment for the longest hanger rope is the largest one among them. In case of stay cables, the increment of stress is increased as L_{ov} expands as shown in Figure 3.26.

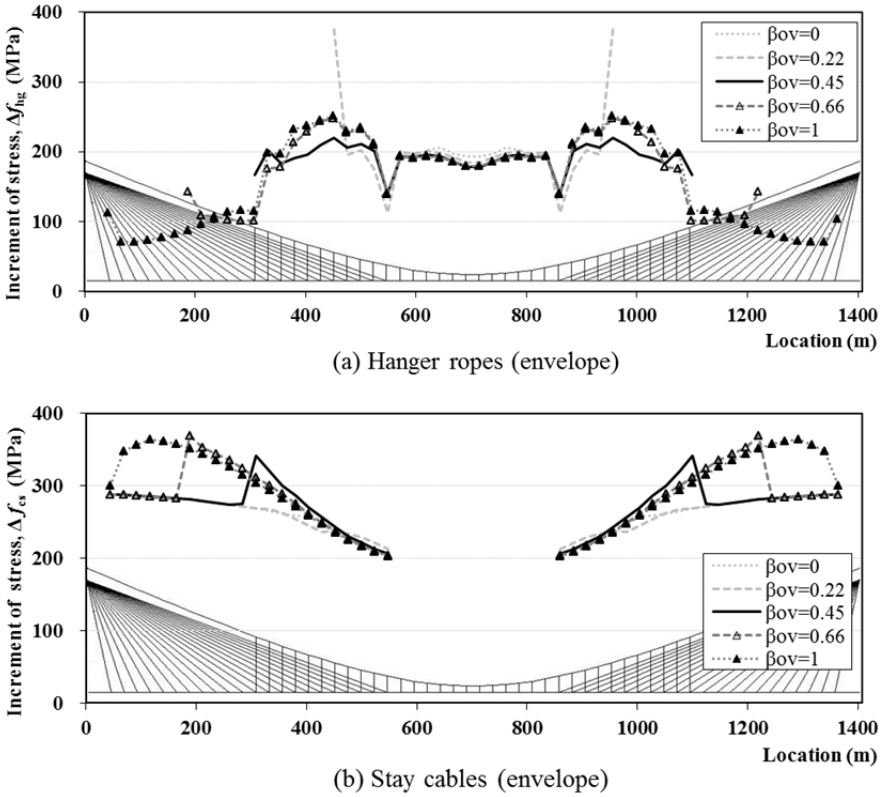

Figure 3.26 Increment of stress under rail load with various L_{ov}

3.3.2 Effects on the deck

(1) Road loading case

As L_{ov} expands, the maximum vertical displacement and the curvature of deck at the center under rail load decrease as shown in Figure 3.27. The reduction rate of the curvature according to the variation of L_{ov} is larger than the reduction rate of the vertical displacement. The ratio of decline for the vertical displacement is about 25 % from Dischinger system (β_{ov}=0) to Roebling system (β_{ov}=1), and the reduction rate of the curvature is about 50%.

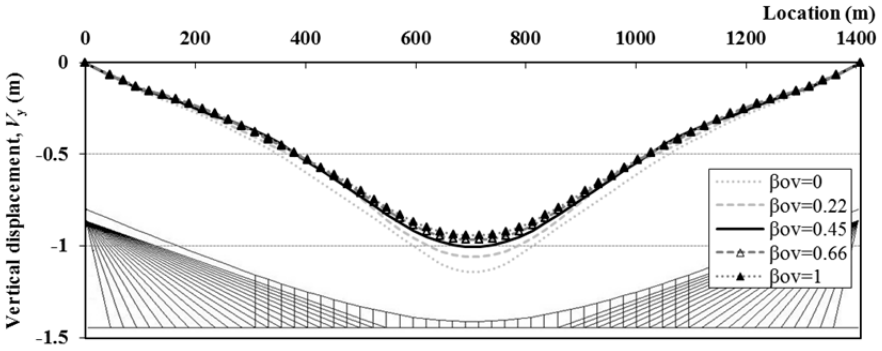

(a) Vertical displacement of deck

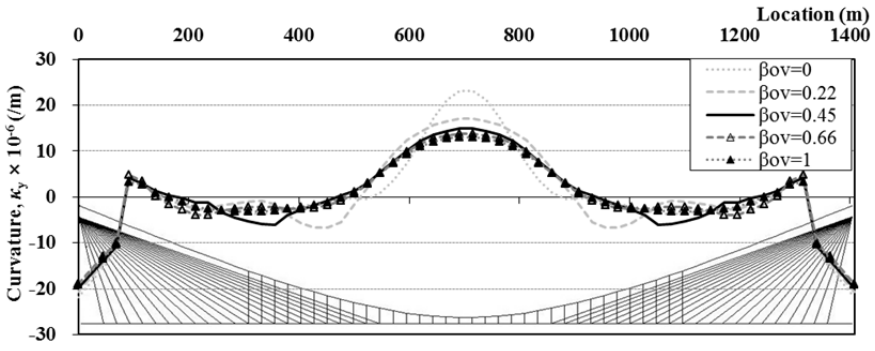

(b) Curvature of deck

Figure 3.27 Deformation of deck under road load with various L_{ov}

(2) Rail loading case

The envelopes of the vertical displacement and the curvature of deck at the center under rail load shows that the deformations in the suspension and overlapping section are slightly decreased as L_{ov} is expanded as plotted in Figure 3.28. However, when the ratio, β_{ov}, is over 0.45, the reduction of the deformation can be insignificant. On the other hand, both deformations of the deck in the envelopes in the stayed section are not significantly affected by the variation of L_{ov}.

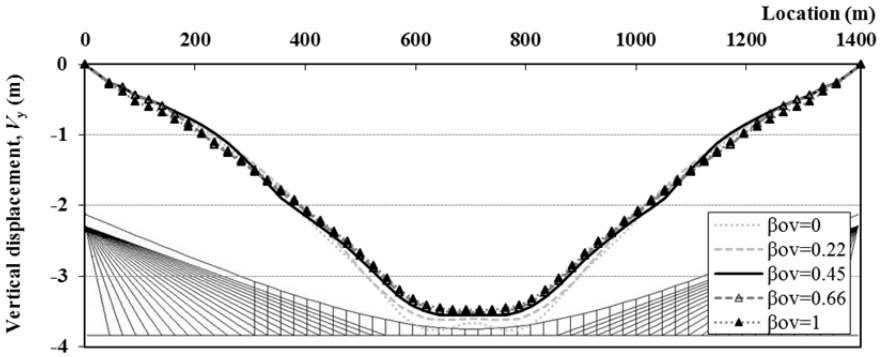

(a) Vertical displacement of deck (envelope)

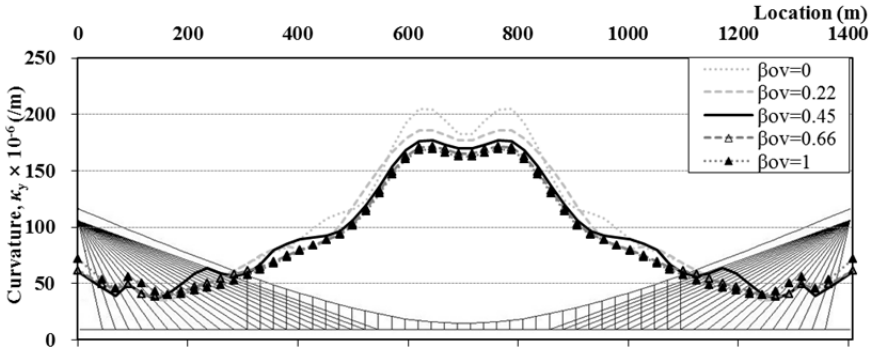

(b) Curvature of deck (envelope)

Figure 3.28 Deformation of deck under rail load with various L_{ov}

3.3.3 Effects on the pylon

Since the area of suspension cable is increased as L_{ov} expands as summarized in Table 3.4, the stiffness of the equivalent horizontal cable spring in the side span is increased. Therefore, the horizontal displacement at the top decreases clearly according to the expansion of the overlapping section length as illustrated in Figure 3.29. The displacement under rail load is over double as large as that under road load. On the other hand, although the vertical reaction on the top decreases slightly as L_{ov} is increased, the change is insignificant.

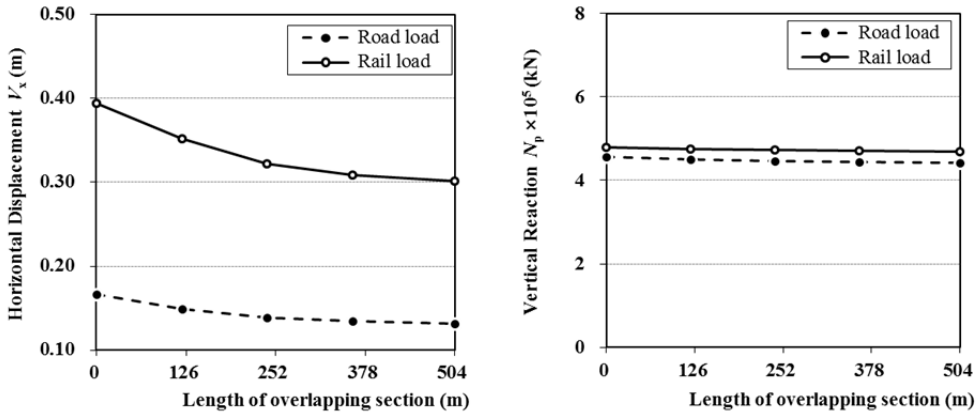

(a) Horizontal displacement at the top (b) Vertical reaction at the top

Figure 3.29 Pylon's behavior with various L_{ov}

3.4 Effects of the Cable Sag

In this sub-chapter, the effect of the variation of the cable sag for suspension cables in the main span, *f*, for the 3rd Bosphorus Bridge on the structural behavior is investigated. The origin value of the sag is 219 m, and the variation is { 140 m, 180 m, 219 m, 260 m, 300 m } while keeping the other design variables. This variation represents the sag ratio from 1/10 to 1/4.7. Figure 3.30 shows the change of a configuration according to the variation of the cable sag.

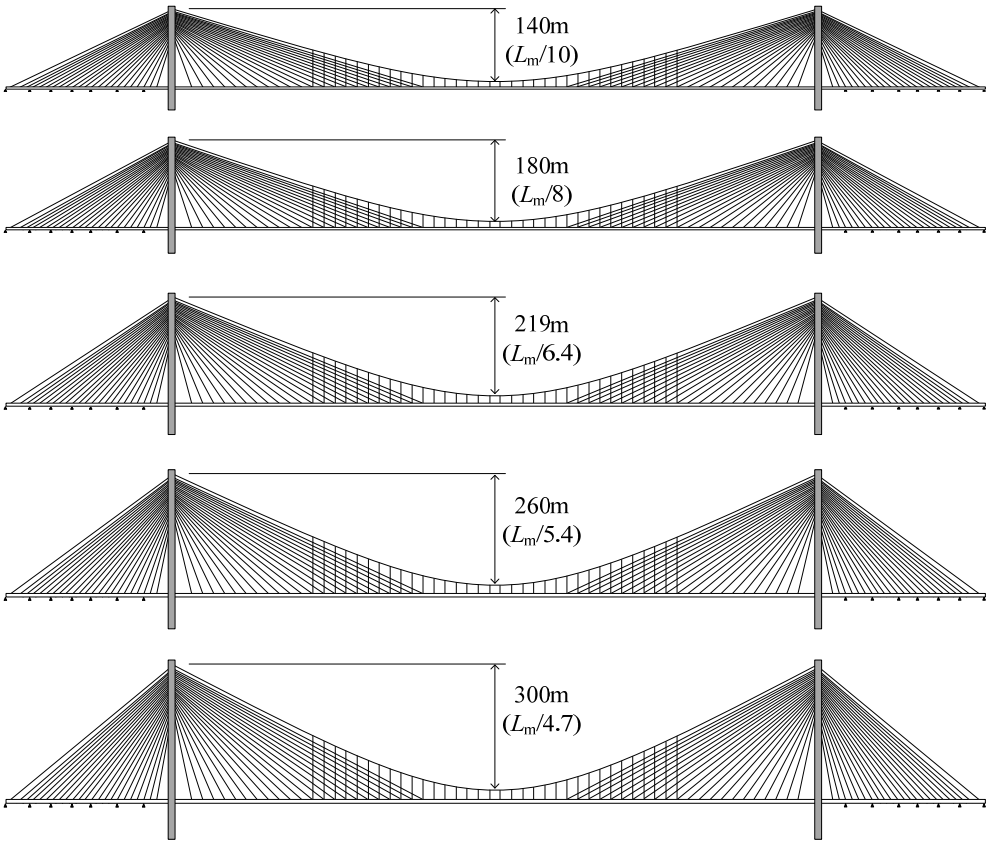

Figure 3.30 Variation of the cable sag

As a result of an initial equilibrium configuration analysis, the suspension cable's area in the center span is decreased as the cable sag increases as summarized in Table 3.5. In case of the total quantity of cables, as the cable sag increases, the total quantity is remarkably decreased with the reduction of the quantity of suspension cable, Q_{sp} and the quantity of stay cables Q_{cs} as plotted in Figure 3.31.

Table 3.5 Calculation of the area of suspension cable with various sag

f	140m	180m	219m	260m	300m
β_f	$\frac{1}{10}$	$\frac{1}{8}$	$\frac{1}{6.4}$	$\frac{1}{5.4}$	$\frac{1}{4.7}$
A_{sp}	0.5471	0.4047	0.3287	0.2763	0.243
A_{sp}/A_{origin}	1.66	1.23	1.00	0.84	0.74

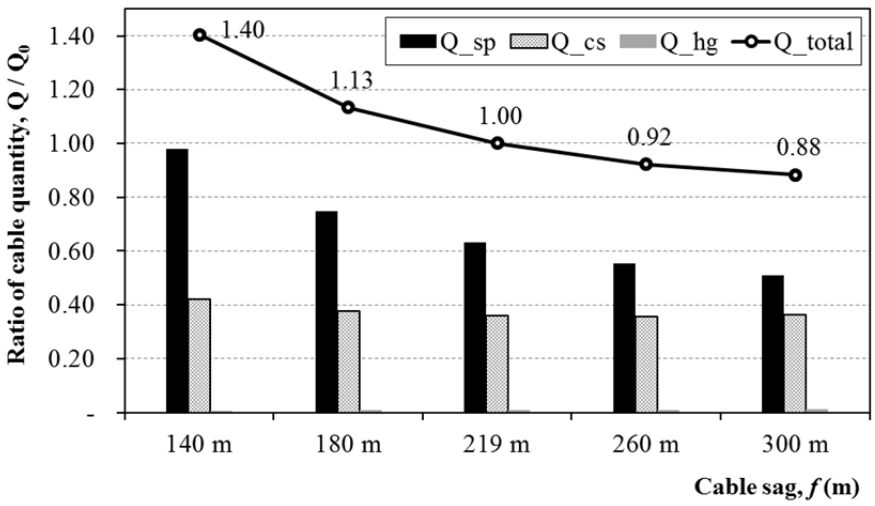

Figure 3.31 Cable quantities with various sag

3.4.1 Effect on the cables

(1) Road loading case

As the cable sag is getting higher, the axial stress of suspension cable in the center of the span is clearly decreased, but the angular change of suspension cable is remarkably increased. The angular change of suspension cable in the suspension section when β_f=1/10 is three times larger than the change when β_f=1/4.7.Therefore, it is necessary to examine the axial stress considering the secondary stress in the cross section of suspension cable for the design of cable sag.

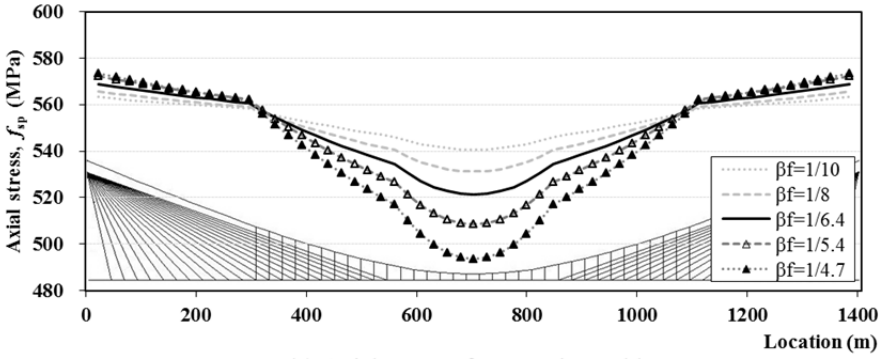

(a) Axial stress of suspension cable

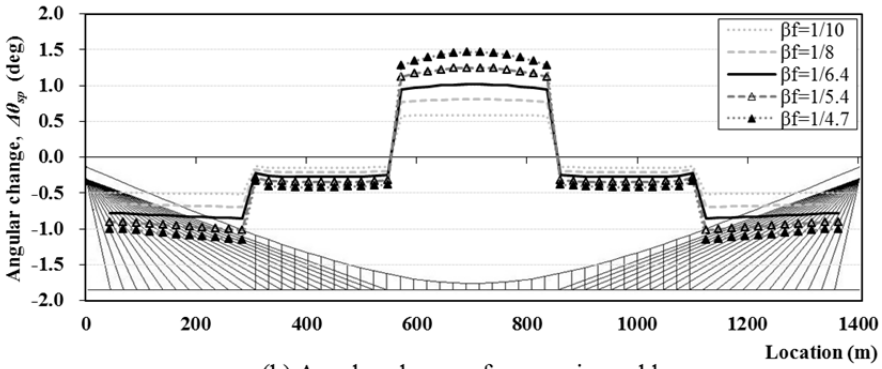

(b) Angular change of suspension cable

Figure 3.32 Stress and deformation of suspension cable under road load with various sag

The increment of tension for hanger ropes is not nearly changed as the variation of the sag. However, the increment in the longest hanger rope is considerably decreased as the sag decreases. The increment at the longest hanger is about 360 kN and 230 kN in case of f = 300 m and 140 m, respectively. Also, the increment of tension for stay cables is clearly decreased as the sag is increased shown in Figure 3.33. Consequently, the effect of the variation of the cable sag on the cable tension and stress under road load is very remarkable to the amplitude of the tension for the stay cable.

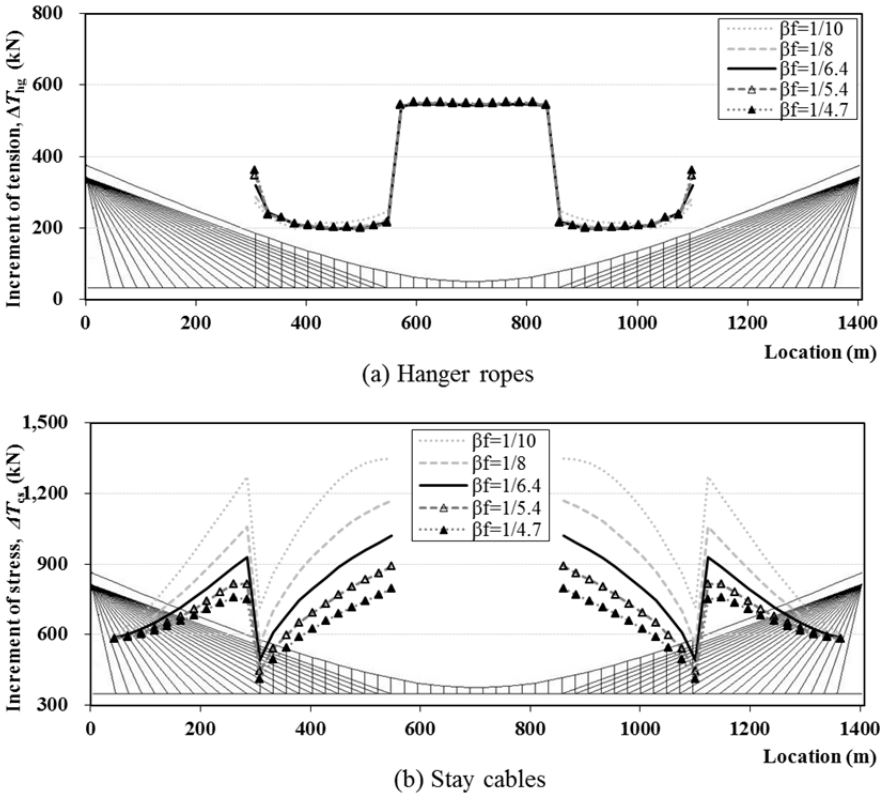

Figure 3.33 Increment of stay tension with various sag

(2) Rail loading case

The envelope for the axial stress and deformation of the suspension cable under rail load is illustrated in Figure 3.34, which is noted that the maximum stress and the angular change of suspension cable are significantly increased as the sag increases. However, the axial stress of suspension cable at the center of span is decreased as the sag increases. The angular change under rail load is about 30% larger than the result under road load, which develops the large secondary stress in the cross section of suspension cable.

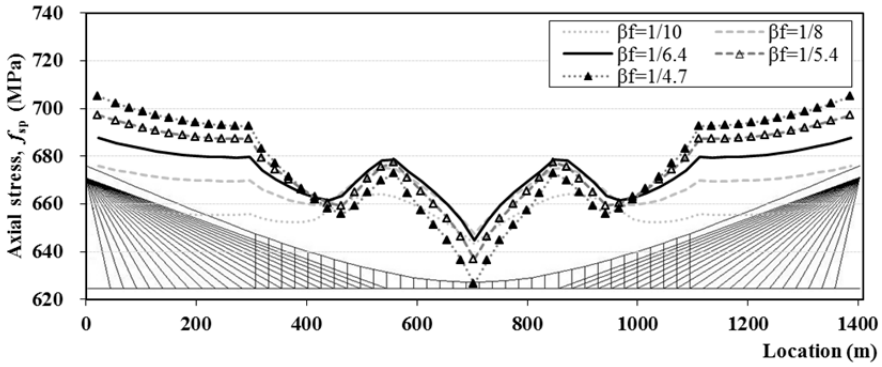

(a) Axial stress of suspension cable

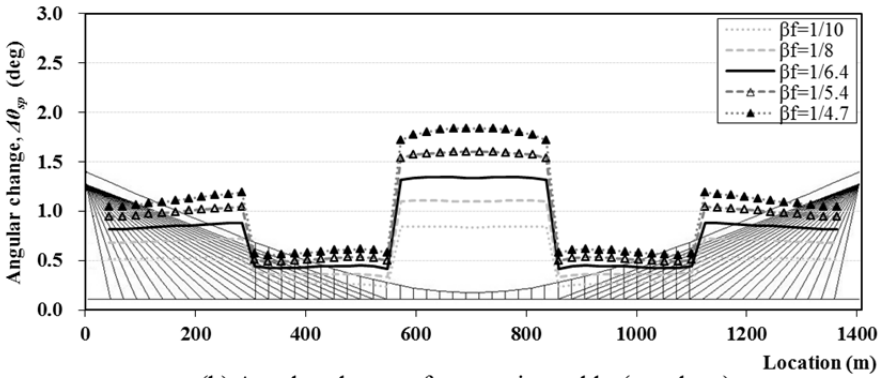

(b) Angular change of suspension cable (envelope)

Figure 3.34 Stress and deformation of suspension cable under rail load with various sag

As the cable sag is getting higher, the increment of the stress for hanger ropes is clearly decreased in the overlapping section but the increment in the suspension section is not nearly affected as shown in Figure 3.35. Also, the increment of the stress for stay cables is obviously decreased as the cable sag increases. Therefore, it can be noted that the high sag is effective to reduce the fatigue problem in hangers and stay cable under rail load.

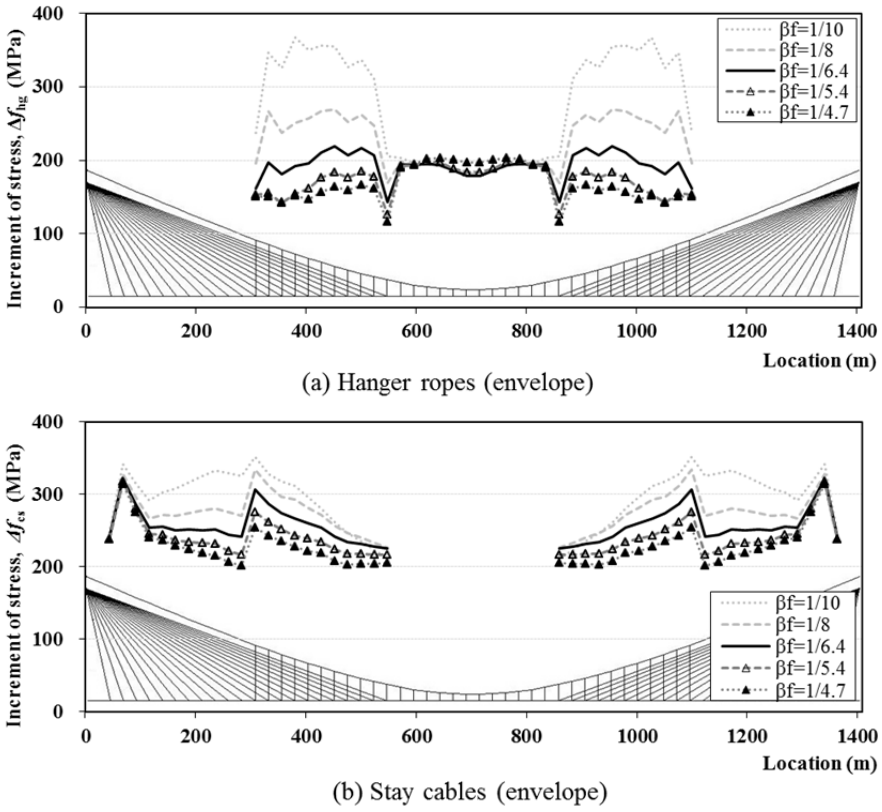

Figure 3.35 Increment of stress under rail load with various sag

3.4.2 Effects on the deck

(1) Road loading case

As the sag is getting higher, the maximum vertical displacement and the curvature of deck at the center under rail load decrease as shown in Figure 3.36. The reduction rate of the vertical displacement according to the variation of the cable sag is larger than the reduction rate of the curvature. The ratio of decline for the vertical displacement is about 40 % from the sag of 140 m to the sag of 300 m, and the reduction rate of the curvature is about 25% in the same variation of the sag.

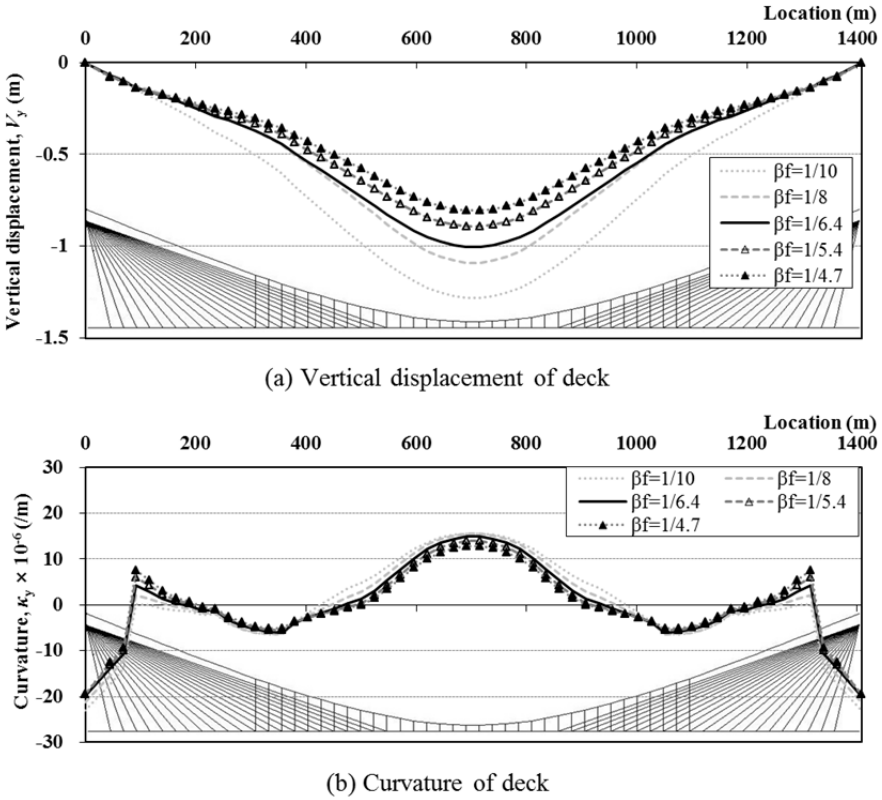

(a) Vertical displacement of deck

(b) Curvature of deck

Figure 3.36 Deformation of deck under road load with various sag

(2) Rail loading case

The envelope of the vertical displacement at the center under rail load is decreased as the sag is getting higher as shown in Figure 3.37. On the contrary, the envelope of the curvature is increased as the sag increases. The maximum value of the vertical displacement is decreased by 20 %, and the curvature is increased by 35% as the sag varies from 140 m to 300 m.

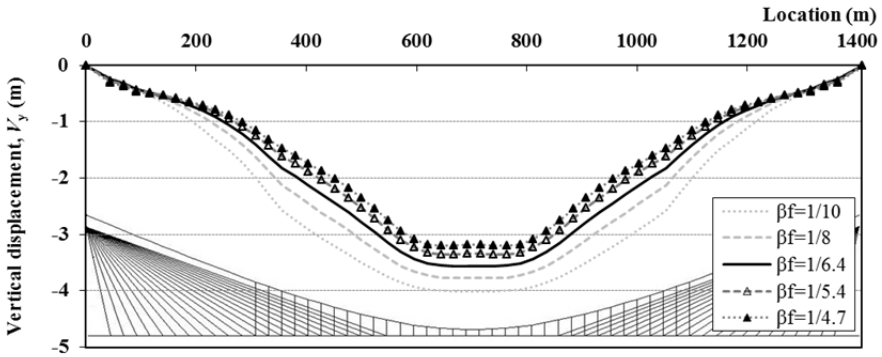

(a) Vertical displacement of deck (envelope)

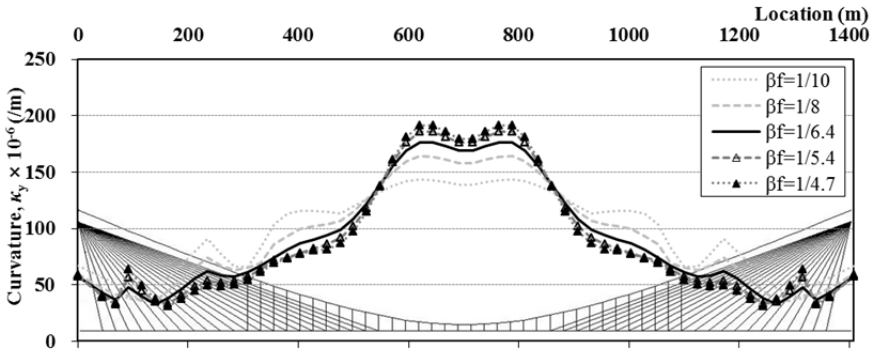

(b) Curvature of deck (envelope)

Figure 3.37 Deformation of deck under rail road with various sag

3.4.3 Effects on the pylon

Since the area of suspension cable is decreased as the sag is getting higher as summarized in Table 3.5, the stiffness of the equivalent horizontal cable spring at the top of pylon is decreased. Therefore, the horizontal displacement at the top increases clearly according to the growth of the sag as illustrated in Figure 3.38. The displacement under rail load is over double as large as that under road load. On the other hand, the vertical reaction on the top decreases slightly as the sag is increased, but the change is insignificant.

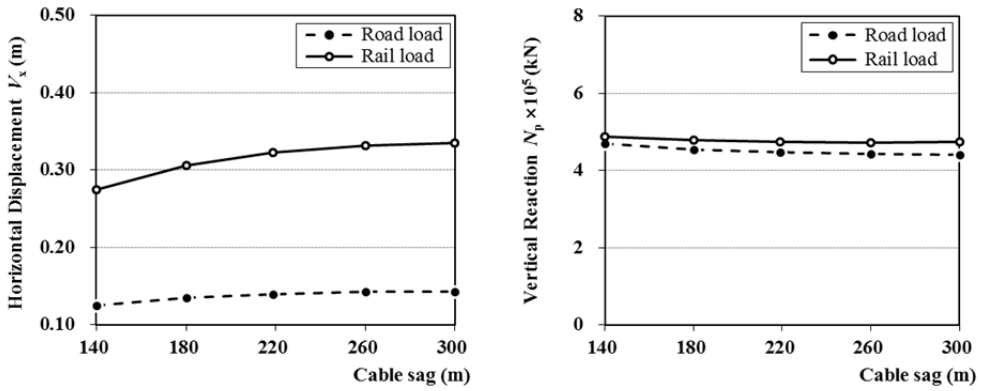

(a) Horizontal displacement at the top (b) Vertical reaction at the top

Figure 3.38 Pylon's behavior with various sag

3.5 Effects of the Dead Load Distribution Factor

In this sub-chapter, the effect of the variation of the dead load distribution factor, r, for the 3rd Bosphorus Bridge on the structural behavior is investigated. The origin value of the factor is 0.67, and the variation is { 0.20, 0.35, 0.50, 0.67, 0.80 } while keeping the other design variables. The dead load distribution factor can be expressed by a function, $r(x)$ as illustrated in Figure 3.39. $r(x)$ is a constant function in the suspension section and the stayed section, and it is a linear function in the overlapping section. Surely, although $r(x)$ may be a polynomial function, a linear function is assumed for the convenience of calculation in this study. Therefore, the dead load distribution factor has two variables, r_1 and r_2. However, this investigation uses a constant function, $r = r_1 = r_2$, for the distribution factor along the location.

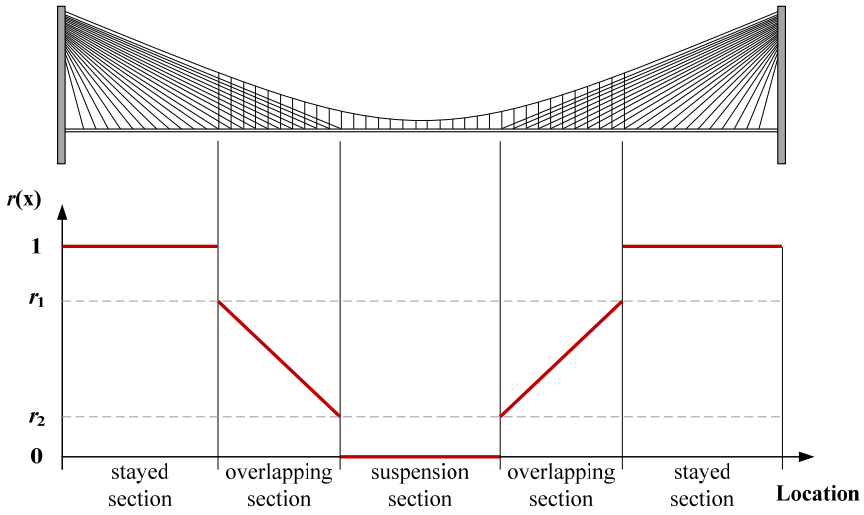

Figure 3.39 A function for a dead load distribution factor, $r(x)$

As a result of an initial equilibrium configuration analysis, the suspension cable's area in the center span is decreased as the dead load distribution factor increases because the dead load supported by the suspension cable is decreased as summarized in Table 3.6. In case of the total quantity of cables, as the distribution factor increases, the total quantity is gradually while the quantity of suspension cable, Q_{sp}, is decreased and the quantity of stay cables Q_{cs}, is increased as plotted in Figure 3.40.

Table 3.6 Calculation of the area of suspension cable with various *r*

r	0.20	0.35	0.50	0.67	0.8
A_{sp}	0.4728	0.4271	0.3812	0.3287	0.2901
A_{sp}/A_{origin}	1.44	1.30	1.16	1.00	0.88

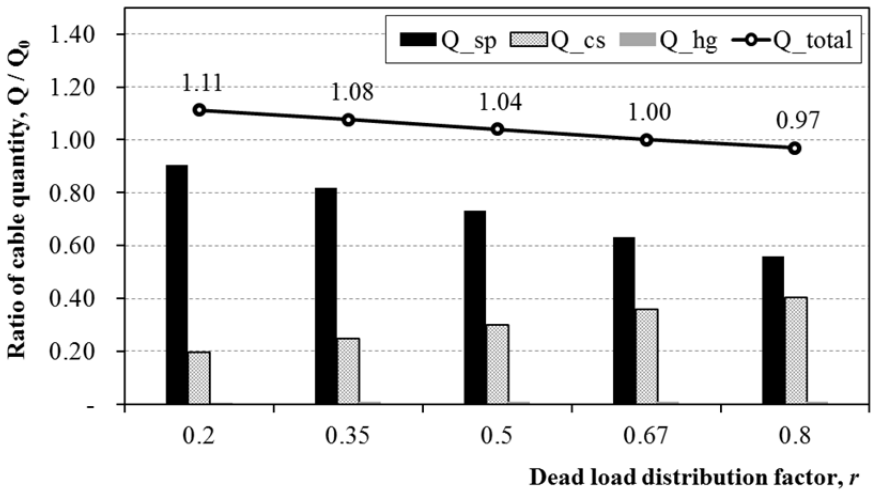

Figure 3.40 Cable quantities with various distribution factors

3.5.1 Effects on the cables

(1) Road loading case

As the dead load distribution factor increases, the maximum axial stress of suspension cable is not changed, but the stress in the suspension section and the overlapping section is slightly increased. Also, the angular change of suspension cable is significantly increased as shown in Figure 3.41, and the change of the distribution factor may develop the secondary stress in the cross section of suspension cable.

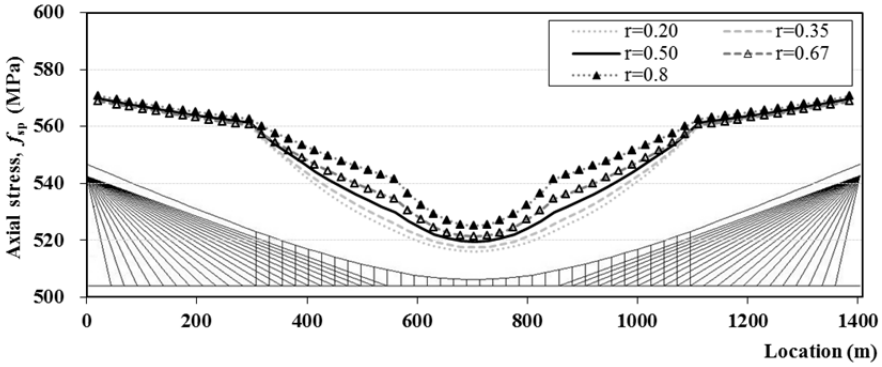

(a) Axial stress of suspension cable

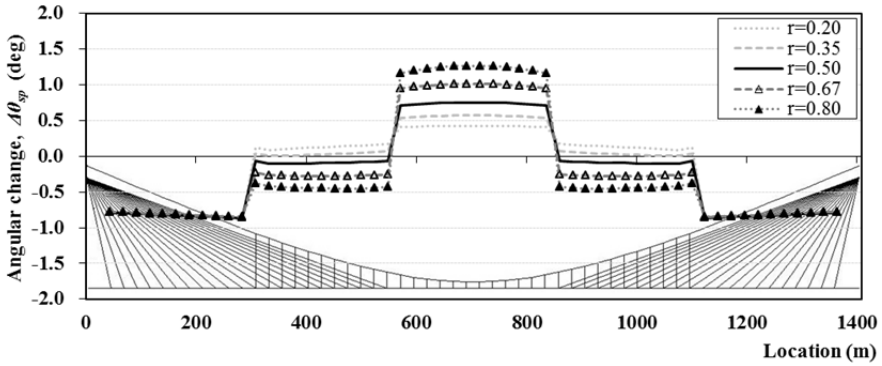

(b) Secondary stress of suspension cable

Figure 3.41 Stress of suspension cable under road load with various factors, *r*

The increment of tension for hanger ropes is clearly changed as the variation of the dead load distribution factor. Also, the increment of tension in the longest hanger rope is taken place equally. The increment of tension for stay cables is clearly increased as the dead load distribution factor is increased shown in Figure 3.42. Therefore, it is clarified that the low dead load distribution factor leads to reduce the stress, tension and deformation of suspension and stay cables although the quantities of cables increases. It makes a trade-off problem in the design stage.

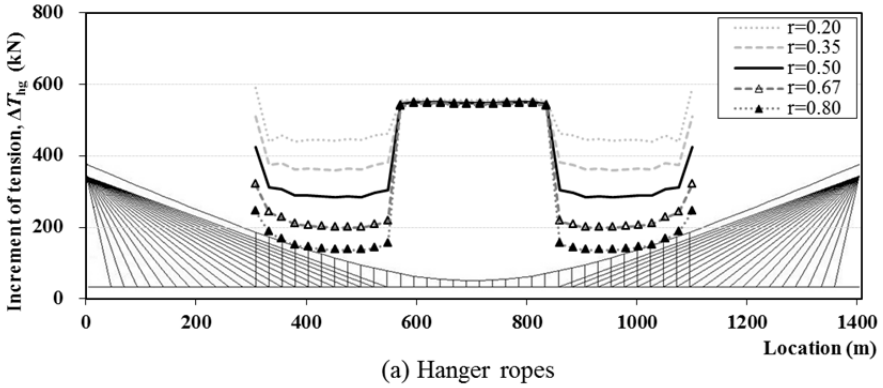

(a) Hanger ropes

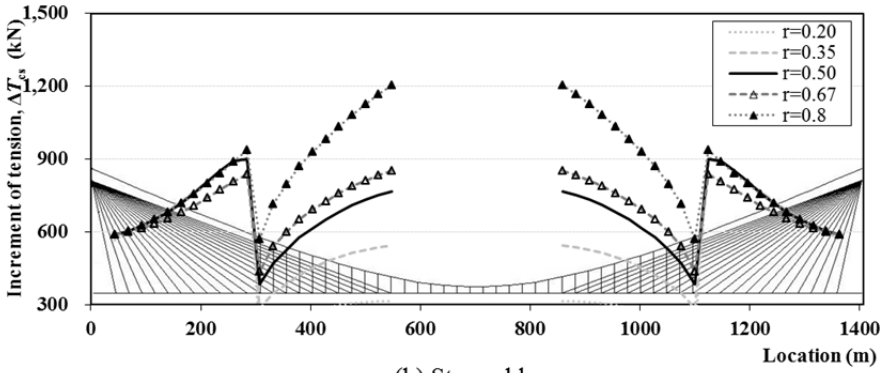

(b) Stay cables

Figure 3.42 Increment of tension under road load with various factors, *r*

(2) Rail loading case

The envelope for the axial stress and deformation of the suspension cable under rail load is illustrated in Figure 3.43, which is noted that the stress and the angular change is increased as the dead load distribution factor increases. Particularly, the axial stress of suspension cable tends to be maximized at the border between the suspension section and the overlapping section. The angular change under rail load is about 25% larger than the result under road load, which develops the large secondary stress in the cross section of suspension cable.

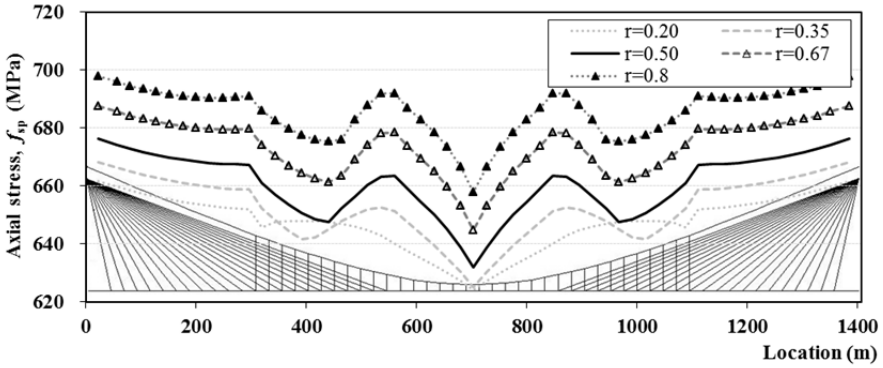

(a) Axial stress of suspension cable

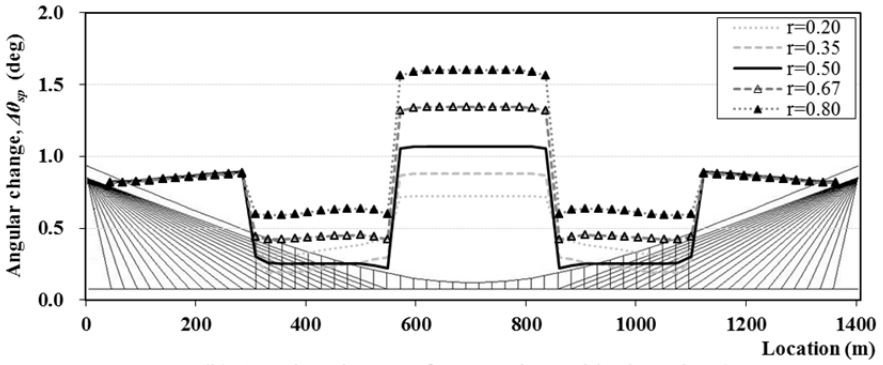

(b) Angular change of suspension cable (envelope)

Figure 3.43 Stress of suspension cable under rail load with various factors, *r*

As the load distribution factor increases, the increment of the stress for hanger ropes is clearly decreased in the overlapping section, but the increment in stay cables is obviously increased as *r* increases. Because the amplitude of the axial stress in cables leads a fatigue problem under live loads, it is necessary to examine the amplitude of both cables for designing the distribution factor.

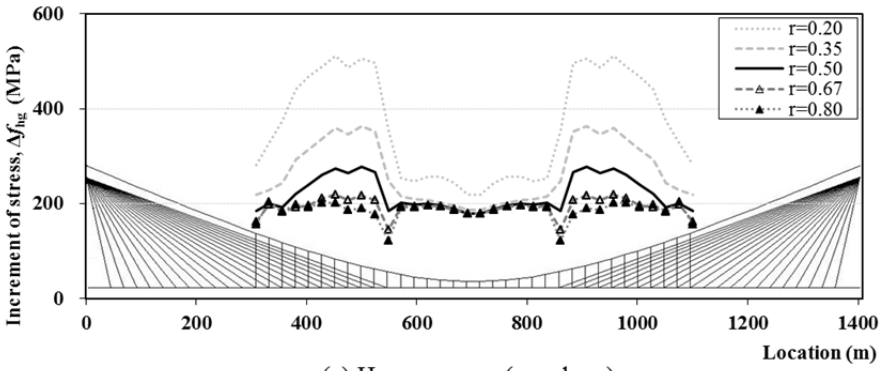

(a) Hanger ropes (envelope)

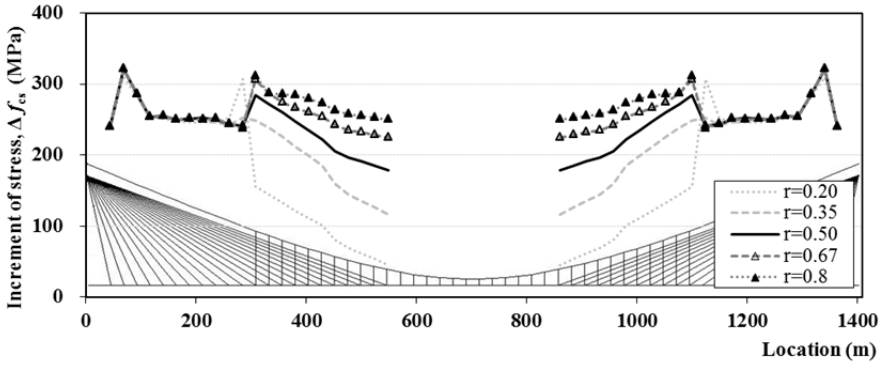

(b) Stay cables (envelope)

Figure 3.44 Increment of tension under rail load with various factors, *r*

3.5.2 Effects on the deck

(1) Road loading case

As the dead load distribution factor, *r*, increases, the maximum vertical displacement and the curvature of deck at the center under rail load is increased as shown in Figure 3.45. The increment rate of the curvature according to the variation of the distribution factor is larger than the increment rate of the vertical displacement.

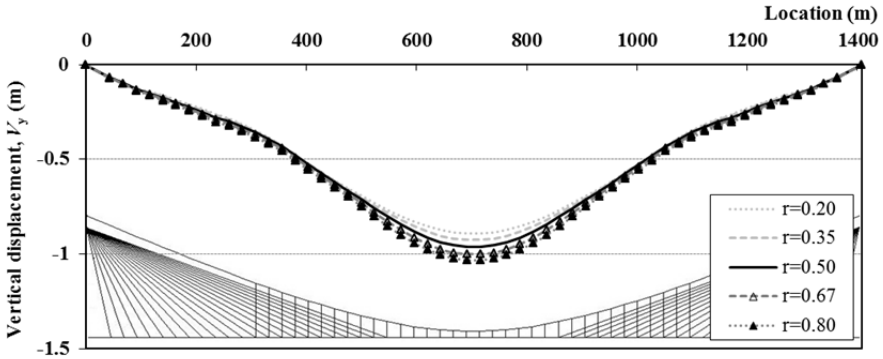

(a) Vertical displacement of deck

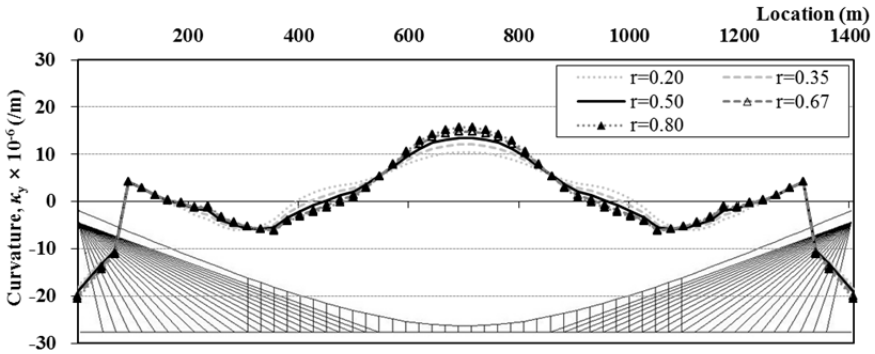

(b) Curvature of deck

Figure 3.45 Deformation of deck under road load with various factors, *r*

(2) Rail loading case

The envelope of the vertical displacement under rail load is decreased as the dead load distribution factor increases as shown in Figure 3.46. Particularly, when the factor is 0.20, the discrepancy of the vertical displacement in the overlapping section between r=0.20 and other cases is remarkably small, but the change of the envelope is not significantly decreased when the factor is over 0.35. This situation is applied to the envelope of the curvature, too. Therefore, for the deformation of deck, the dead load distribution factor may be considered over 0.35.

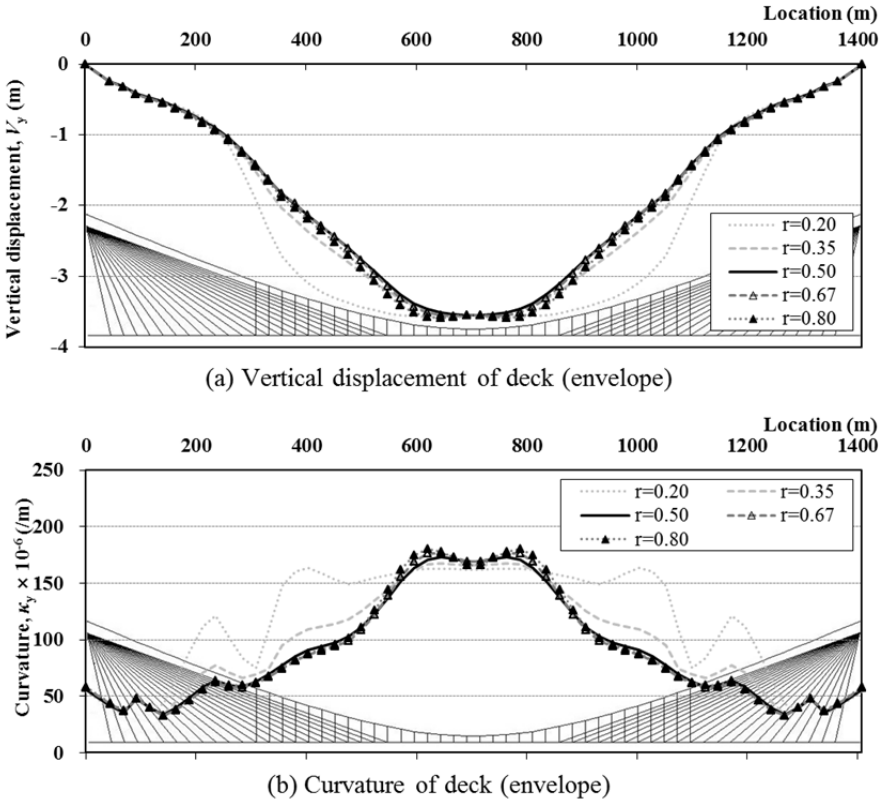

Figure 3.46 Deformation of deck under rail load with various factors, r

3.5.3 Effect on the pylon

Since the area of suspension cable is decreased as the dead load distribution factor increases as summarized in Table 3.6, the equivalent horizontal stiffness of the suspension cable in the side span is decreased. Therefore, the horizontal displacement at the top clearly increases according to the increase of the deal load distribution factor as illustrated in Figure 3.47. The displacement under rail load is over double as large as that under road load. On the other hand, the vertical reaction on the top is not affected by the variation of the dead load distribution factor.

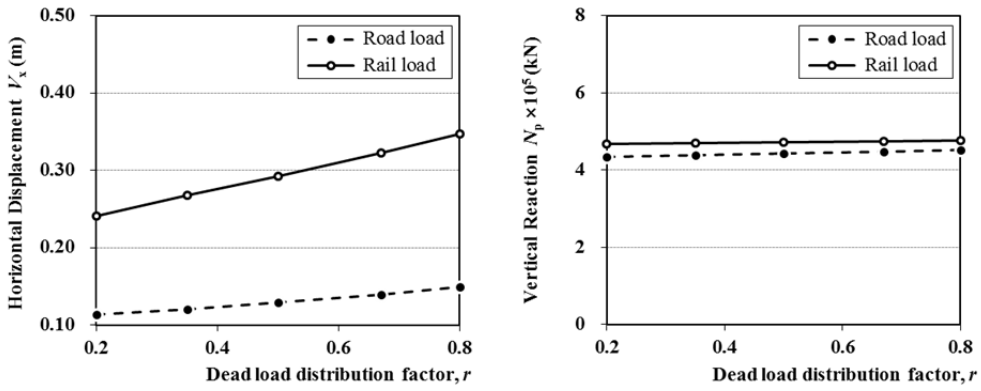

(a) Horizontal displacement at the top (b) Vertical reaction at the top

Figure 3.47 Pylon's behavior with various factors, *r*

3.6 Summary of Parametric Investigations

In this sub-chapter, the effects of the variation of the design variables on the structural behaviors are summarized. For comparing the results due to different variables, a sensitivity analysis is performed. The variations of design variables are normalized by the main span length, and the results are normalized by the structural behavior under the original design value as expressed in Equation 3.1. Then, the relationship between the normalized variation of each variable and the normalized behavior is plotted.

$$\overline{V} = \frac{V_i - V_o}{L_m} \tag{3.1a}$$

$$\overline{R} = \frac{R_i}{R_o} \tag{3.1b}$$

where, $\overline{V}$ is the normalized variation, V_i is the various value for L_s, L_{sp}, L_{ov}, f, and r, V_o is the origin value for each variable of the example bridge, and L_m is the main span length of 1,408 m. Also, $\overline{R}$ is the normalized result for structural behaviors, R_i is the structural analysis result by various value of design variables, and R_o is the result by the origin value of each design variable.

Briefly, since the effects of the variation of the design variables on the structural behaviors conflict each other, it is clarified that the increment of a specific design variable may lead to reduce the stress, tension and deformation although the other design variable could give the opposite result. Therefore, it is necessary to assemble and analyze numerous combinations of the design variables in the design stage for finding a best solution of cable system for a cable-stayed suspension bridge.

3.6.1 Effects of the variation of L_s

Figure 3.48 summarizes the results of structural behaviors according to the variation of L_s. The horizontal axis means the normalized variation of the side span length by the main span length, L_m. The vertical axis means the normalized result of a suspension cable's stress (f_{sp}), an increment of stress in hangers (Δf_{hg}) and stay cables (Δf_{cs}), an angular change of suspension cable ($\Delta\theta_{sp}$), a vertical displacement of deck (V_y), a curvature of deck (κ_y), and a horizontal displacement at the pylon top (V_x).

Basically, most results excluding Δf_{hg} are increased as L_s increases, and this situation is equally applied to both loading cases. The very sensitive behavior by the variation of L_s is V_x, and the deformation of deck including the vertical displacement and curvature is clearly affected, too. However, the structural behavior related to cables is not significantly affected by the variation of L_s.

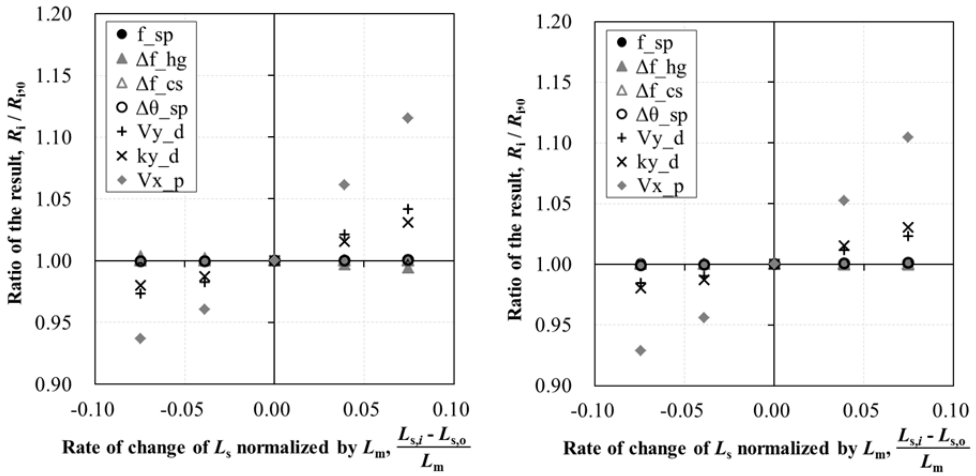

(a) Load case 1 : road load (b) Load case 2 : rail load

Figure 3.48 Summarized behavior with various L_s

3.6.2 Effects of the variation of L_{sp}

In Figure 3.49, the horizontal axis means the normalized variation of the suspension section length, L_{sp}, by the main span length, L_m. As L_{sp} increases, most behaviors are decreased in both loading cases, but the increment of hanger's stress is slightly increased. Each sensitivity for all behaviors is very similar between both loading cases. Particularly, the angular change of suspension cable is very sensitive to the variation of L_{sp}, and the angular change leads a large secondary stress in the cross section. It may be a key to design a suspension section of a cable-stayed suspension bridge. Also, the deformation of deck including the vertical displacement and curvature is clearly affected, too. However, the structural behavior related to cables is not significantly affected by the variation of L_{sp} likewise the case for a variation of L_s.

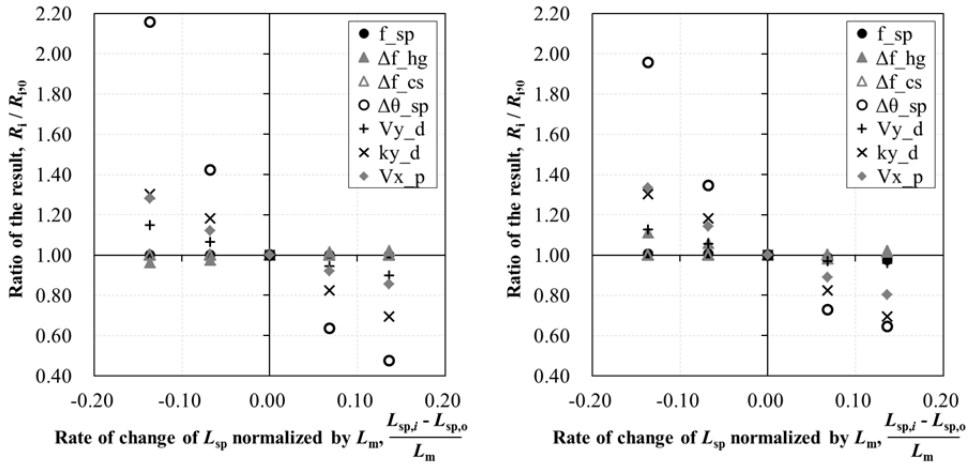

(a) Load case 1 : road load (b) Load case 2 : rail load

Figure 3.49 Summarized behavior with various L_{sp}

3.6.3 Effects of the variation of L_{ov}

In Figure 3.50, the horizontal axis means the normalized variation of the overlapping length, L_{ov}, by the main span length, L_m. As L_{ov} increases, most behaviors under both loading cases are decreased, but the stress increment of hangers and stay cables is increased in the rail load case. Each sensitivity for all behaviors excluding the stress increment of hangers and stay cables is very similar between both loading cases. Particularly, the angular change of suspension cable and the curvature of deck are very sensitive to the variation of L_{ov}, and the angular change leads a large secondary stress in the cross section. It may be a key to design a suspension section of a cable-stayed suspension bridge. Also, the vertical displacement of deck and the horizontal displacement of pylon are clearly affected, too. However, the stress of suspension cable is not significantly affected by the variation of L_{sp}.

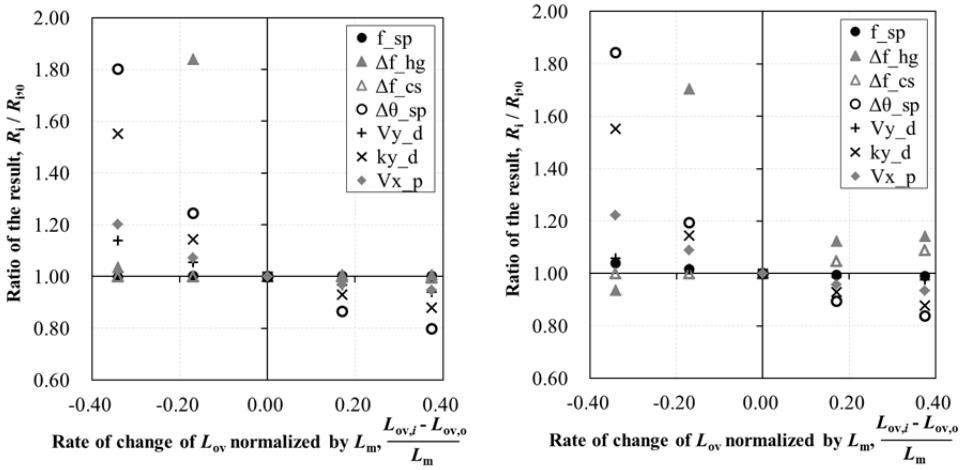

(a) Load case 1 : road load (b) Load case 2 : rail load

Figure 3.50 Summarized behavior with various L_{ov}

3.6.4 Effects of the variation of f

In Figure 3.51, the horizontal axis means the normalized variation of the cable sag, f, by the main span length, L_m. As f increases, V_x of pylon and the behavior of suspension cable including f_{sp} and $\Delta\theta_{sp}$ are increased under both loading cases. Contrarily, the deformation of deck and the stress increment of hangers and stay cables are decreased as f increases. Each sensitivity for all behaviors excluding the stress increment of hangers and stay cables is very similar between both loading cases. Particularly, the angular change of suspension cable and the curvature of deck are very sensitive under a road load, but the increment of stress of hangers is very sensitive under a rail load. On the other hand, the sensitivity for the vertical displacement of deck under a rail load is lower than the sensitivity under a road load. The stress of suspension cable is slightly increased as f increases, but it is not significant.

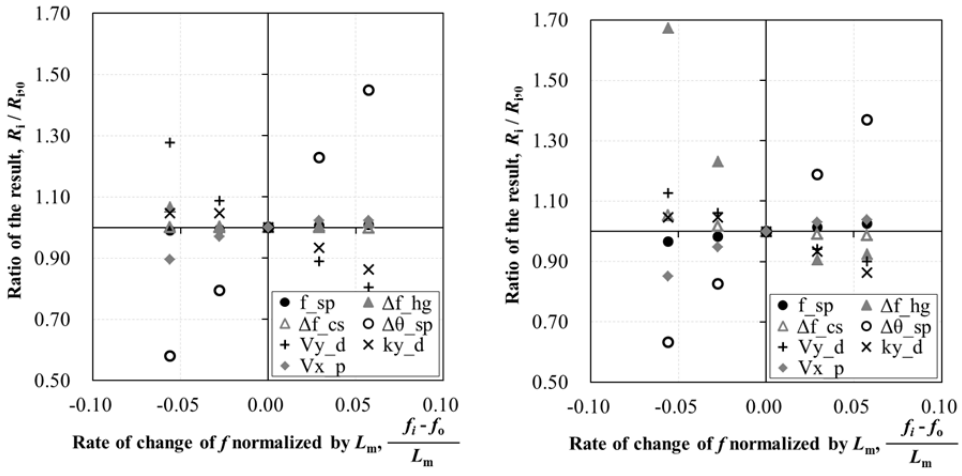

Figure 3.51 Summarized behavior with various f

3.6.5 Effects of the variation of *r*

In Figure 3.52, the horizontal axis means the normalized variation of the dead load distribution factor, *r*, by the origin value of the example bridge. As *r* increases, all behaviors under both loading cases are clearly increased, but the stress increment of hangers is remarkably decreased in the rail load case. Particularly, the angular change of suspension cable and the curvature of deck are very sensitive to the variation of *r* under a road load, and the increment of stress of hangers is very sensitive under a rail load.

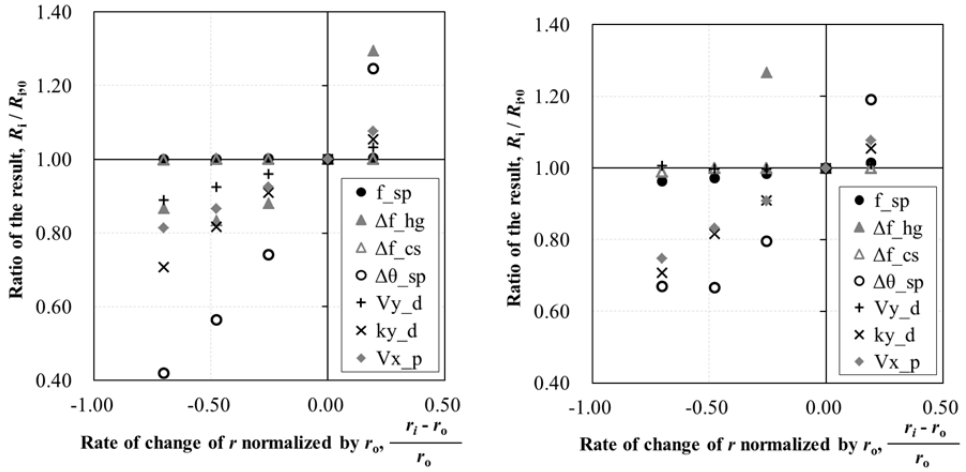

(a) Load case 1 : road load (b) Load case 2 : rail load

Figure 3.52 Summarized behavior with various *r*

In sum, through the sensitivity analysis, the results of $\Delta\theta_{sp}$, Δf_{hg}, V_y, and κ_y are sensitive to the variation of the design variables, but the f_{sp} and f_{cs} are not relatively affected.

4. OPTIMIZATION OF CABLE SYSTEM USING THE PROPOSED SIMPLIFIED MODEL AND GENETIC ALGORITHM

4.1 Optimization Problem of Cable System

4.1.1 Definition of an optimization problem

Finding the optimal design of cable supported bridges is a challenging task because the design is influenced by a large number of design variables including an arrangement of cables, a length of span, a height of pylon, material and section properties (Olfat, 2012). In particular, it is much complicated to optimize a design of a cable-stayed suspension bridge which has all variables for a suspension system and a stayed system as well as several variables to define an overlapping section of two cable systems. Also, as described in the previous chapter, the effects of the variation of such design variables on the structural behavior of a cable-stayed suspension bridge are in a trade-off situation between the quantity and the performance. In this research, therefore, an optimization procedure to solve the trade-off problem for the cable system of a cable-stayed suspension bridge including cable areas, composition of spans, sag and arrangement of overlapping section is proposed with assuming the material and section properties given from the existing cable supported bridges at present.

However, because the suspension system and the stay system have several structural types and each type has different features of the structural behavior under loads, it is necessary to restrict the structural type. The suspension cable employed in this

research is anchored at the anchorage in both ends of a bridge, and the anchorage is a gravity type. Also, the stay cable is a fan type, and the overlapping section is located in the center span as illustrated in Figure 4.1.

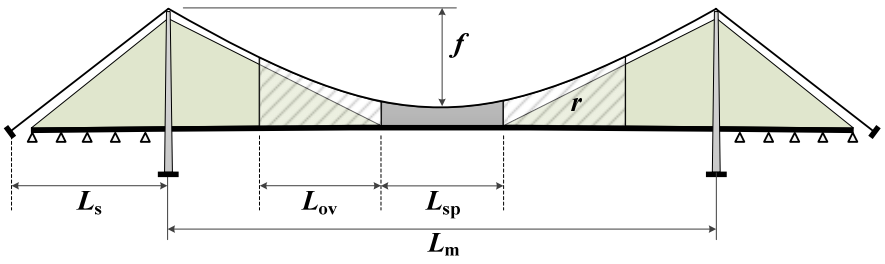

Figure 4.1 Scheme of a cable system for the optimization problem

In the previous chapter, the design variables including a side span length (L_s), a suspension section length (L_{sp}), an overlapping length (L_{ov}), a cable sag (f), and a dead load distribution factor (r) show that they affect directly the performance of bridge and the quantities of materials. As a consequence, the optimization procedure for cable system of a cable-stayed suspension bridge can be defined as the minimizing process of a construction cost with satisfying the specific design criteria under live loads.

4.1.2 Objective function for cost optimization

In the previous sub-chapter, the optimization problem is defined as the minimization of a construction cost. Therefore, the objective function which is denoted by C(**x**) is a total construction cost for the superstructures including suspension cables, hanger

cables, stay cables, structural steel for deck and concrete for pylons and anchorages. In this research, costs for substructures including excavation works, soil improvements, and pile works are excluded because the costs considerably depend on the geological condition. The objective function, C(**x**) is defined as a product of each material's unit construction price and a quantity as expressed in Equation 4.1.

$$C(\mathbf{x}) = \Sigma\, C_i \times Q_i(\mathbf{x}) = C_{cable} \times Q_{cable}(\mathbf{x}) + C_{steel} \times Q_{steel}(\mathbf{x}) + C_{concrete} \times Q_{concrete}(\mathbf{x}) \quad (4.1)$$

$$\mathbf{x} = \{ x_i \} = \{ L_s, \quad L_{sp}, \quad L_{ov}, \quad f, \quad r \} \quad (4.2)$$

where **x** is a set of design variables to define the configuration of a cable system, and C_i is a unit construction cost for each member per unit volume or unit weight. In general, C_i varies with the construction methods and the site conditions. Therefore, this study uses the unit cost suggested by Super Long Span Bridge R&D Center in 2011 as listed in Table 4.1. The cost includes a material cost and a labor cost.

Table 4.1 Unit construction cost for each material

Item		Cost, C_i	Applied Member
C_{cable}	C_{sp}	10 mil. KRW/Ton	suspension cable, hanger
	C_{cs}	13 mil. KRW/Ton	stay cable
C_{steel}	C_{st}	5.3 mil. KRW/Ton	deck
$C_{concrete}$	$C_{con,p}$	2.0 mil. KRW/m^3	pylon
	$C_{con,a}$	0.5 mil. KRW/m^3	anchorage

Ref) Final report of Super Long Span Bridge R&D Center (2011)

As shown in Table 4.1, the unit construction cost for each material is different in case of members using cable and concrete. The objective function expressed in Equation 4.1, C(**x**), can be revised by Equation 4.3.

$$C(\mathbf{x}) = C_{sp} \times \{ Q_{sp}(\mathbf{x}) + Q_{hg}(\mathbf{x}) \} + C_{cs} \times Q_{cs}(\mathbf{x}) + C_{st} \times Q_{d}(\mathbf{x}) + C_{con,p} \times Q_{py}(\mathbf{x}) + C_{con,a} \times Q_{an}(\mathbf{x}) \quad (4.3)$$

where Q_{sp} is a quantity of suspension cables, Q_{hg} is a quantity of hanger ropes and Q_{cs} is a quantity of stay cables. Also, the quantity of each member uses a unit of a weight (Ton) for cable and steel and a volume (m^3) for concrete in this research. First of all, a quantity of cable is simply calculated by Equation 4.4.

$$Q_{sp} = \gamma_{sp} \times L_{sp} A_{sp} \quad \text{for suspension cable} \quad (4.4a)$$

$$Q_{i} = \gamma_{i} \times \sum_{k=1}^{N_i} L_k^i A_k^i \quad \text{for hanger and stay cable } (i = hg, cs) \quad (4.4b)$$

where γ is a specific weight, L and A is a length and a cross section area, respectively. N_i is the number of cables for stay cables and hanger ropes. Q_d and Q_{py} is a quantity of deck and pylon, respectively, and it is calculated by Equation 4.5 and Equation 4.6.

$$Q_d = \gamma_{steel} \times A_d \times (L_m + 2 \times L_s) \quad (4.5)$$

$$Q_{PY} = N_p \times \left[\exp\left(\frac{\gamma_p}{0.7 f_d} h_p \right) - 1 \right] \quad (4.6)$$

where N_p is the axial force at the top of pylon including the dead and vertical live loads such as traffic and track loads, γ_p is the specific weight of concrete for pylon,

and h_p is the height of pylon. For the quantity of pylons, a correct quantity is of considerable complexity as the required dimensions of the pylons depend not only on the in-plane forces form the cable system but also on wind forces. However, the axial stress in the cross section of pylon under dead live loads can be assumed by the 60~80% value of a design stress of a material for pylon, f_d (Gimsing, 2012). The quantity of pylons is effectively evaluated by Equation 4.6. This research adopts the 70% of f_d.

Generally, an estimation of quantity for an anchorage is very complicated because there are a number of design variables due to the geological condition. In this research, the quantity is considered as a required weight to keep the sliding stability of an anchorage with a gravity type under live loads as described in Equation 4.7.

$$\mu \times \left(Q_{AN} - 2T_{SP,side} \times \sin\theta\right) > 1.5 \times 2T_{SP,side} \times \cos\theta \tag{4.7}$$

where μ is the coefficient of friction between the bottom of concrete anchorage and soil, $T_{sp,side}$ is the tension of suspension cable in the side span, and θ is the angle of suspension cable at the anchorage.

4.1.3 Genetic algorithm for optimization

Since a cable-stayed suspension bridge is a hybrid structural system that is a combination of a cable-stayed bridge and a suspension bridge, the bridge type has a high degree of statical indeterminacy with a number of design variables to define the cable system. In the previous chapter, it is clarified that variables largely affect the structural behavior as well as the cost, and the effects conflict each other. Therefore, the optimization of cable system for a cable-stayed suspension bridge necessarily

accompanies a lot of iteration works to calculate numerous combinations of the design variables. In this study, Genetic Algorithm (GA) is employed to find the optimal cable system efficiently, because GA based on the theory of biological evolution and adaptation has proved to be powerful, efficient, and capable of handling large number of variables (Olfat, 2012). The genetic operator for reproduction, mutation, and crossover in GA is employed to improve a fitness of the objective function during the optimization procedure. This study uses the genetic operator built in MATLAB, and input parameters for the operator are a population of 100, a generation of 1,000, a crossover of 0.8, and a mutation fraction of 0.2, respectively. In this study, the population means the structural analysis models assembled by the combinations of design variables defining cable system. Also, the tolerance for convergence is 10^{-6}.

4.2 Design Variables

4.2.1 Design variables of cable system

The cost optimization problem of a cable-stayed suspension bridge has several design variables to confirm the cable configuration. The variables expressed as a vector including a side span length (L_s), a suspension section length (L_{sp}), an overlapping length (L_{ov}), a cable sag (f), and a dead load distribution factor (r) in Equation 4.2 can be revised by design variables normalized by the main span length, L_m. The design variables are expressed in Equation 4.8 and Table 4.2.

$$\mathbf{x} = \{ x_i \} = \{ \quad \beta_s, \quad \beta_{sp}, \quad \beta_{ov}, \quad \beta_f, \quad r \quad \} \tag{4.8}$$

Table 4.2 Definition of design variables

x_i	Definition	Description
β_s	L_s / L_m	ratio of side span length to main span length
β_{sp}	L_{sp} / L_m	ratio of suspension section's length to main span length
β_{ov}	$2L_{ov} /(L_m - L_{sp})$	ratio of overlapping length to main span length excluded suspension section's length
β_f	f / L_m	ratio of suspension cable's sag to main span length
r	W_{cs} / W_g	dead load distribution factor

These design variables have a range based on the designer experiences, but this study refers to the design of existing suspension bridges and cable-stayed bridges. Figure 4.2 shows β_s and β_f for a number of completed suspension bridges and cable-stayed bridges in the world, and Figure 4.3 shows the general design of cable system for a cable-stayed bridge and a suspension bridge. Most cable supported bridges have a range from 0.2 to 0.5 for β_s, a range from $\frac{1}{6}$ to $\frac{1}{3.5}$ for β_f in case of cable-stayed bridges, and a range from $\frac{1}{11}$ to $\frac{1}{9}$ for β_f in case of suspension bridges regardless of the main span length. The variables of β_{sp} and β_{ov} to define the dimension of an overlapping section may have a range from 0 to 1, which can define a cable-stayed suspension bridge as Dischinger system, combined system, or Roebling system.

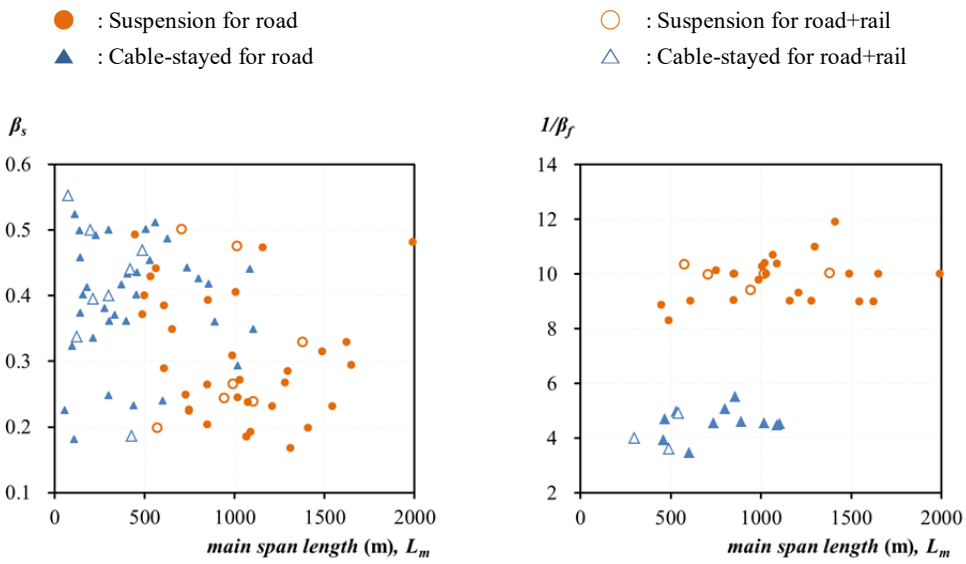

(a) Ratio of L_s to L_m (b) Ratio of f to L_m

Figure 4.2 β_s and β_f of suspension bridges and cable-stayed bridges

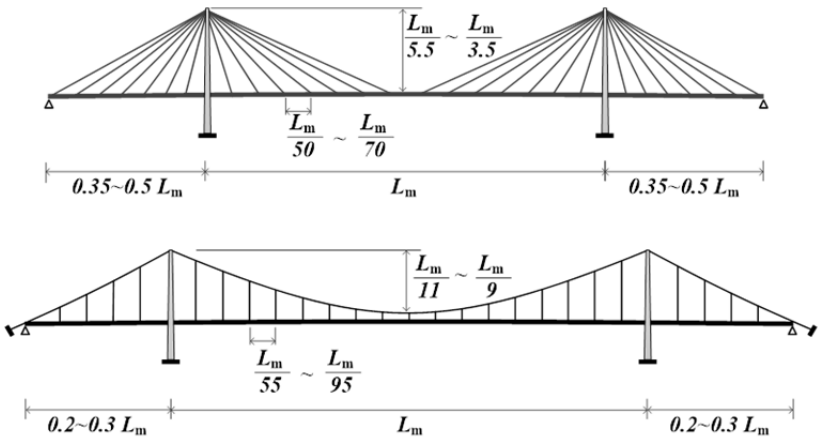

Figure 4.3 General design of cable system of cable-stayed and suspension system

The dead load distribution factor, r, is the ratio of a dead load carried by the stayed system, W_{cs}, to a total dead load of deck, W_g, as expressed in Equation 4.9. It can be expressed by a function, $r(x)$ as illustrated in Figure 4.4 and as described in Equation 4.10. $r(x)$ is a constant function in the suspension section and the stayed section, and it is a linear function in the overlapping section. Surely, although $r(x)$ may be a polynomial function, a linear function is assumed for the convenience of calculation in this study. Therefore, the dead load distribution factor has two variables, r_1 and r_2.

$$r = \frac{Dead\ load\ of\ deck\ supported\ by\ stay\ cables}{Dead\ load\ of\ deck} = \frac{W_{cs}}{W_g} \tag{4.9}$$

$$\begin{aligned} r &= 0 && \textit{for suspension section} \\ r &= r(x) && \textit{for overlapping section} \\ r &= 1 && \textit{for stayed section} \end{aligned} \tag{4.10}$$

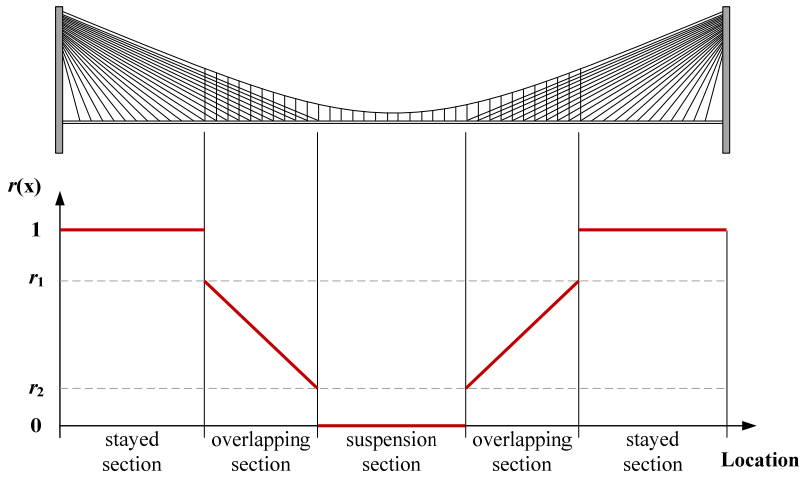

Figure 4.4 A function for a dead load distribution factor, $r(x)$

4.2.2 Live load

Generally, the live load may divide traffic loads and environmental loads. The traffic loads have a roadway load and railway load, and the environmental loads consist of a wind load, temperature load, and seismic load. In this research, the traffic loads of a roadway and a railway are considered as the live loads. For the traffic load of a roadway, the uniformly distributed load which is proposed in Korea Bridge Design Code (KBDC) is applied to this study. The loads can be calculated by Equation 4.11.

$$W_L = R \times N \times 12.7 \times \left(\frac{60}{L} \right)^{0.1} \quad \text{(kN/m)} \tag{4.11}$$

where R is the reduction factor according to the number of lanes as described in Table 4.3, N is the number of lanes, and L is the span length.

Table 4.3 Reduction factor of traffic loads by KBDC

Number of lanes	R
1	1.00
2	0.90
3	0.80
4	0.70
5~	0.65

For a rail load, a train load model, LM71, in Eurocode is applied. The load consists of uniformly distributed loads of 80 kN/m and four concentrated loads of 250 kN with an interval of 1.6m in the longitudinal direction of a bridge as illustrated in Figure 4.5. The rail load is loaded at the center and the quarter location of the span.

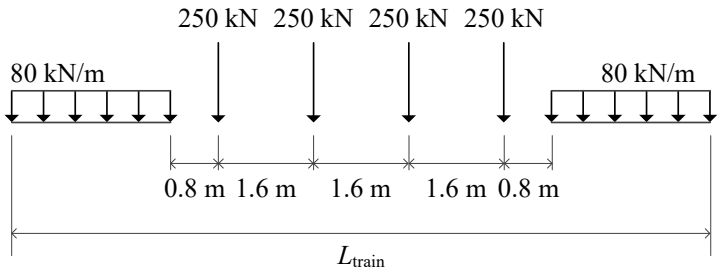

Figure 4.5 LM71 for train load in Eurocode

In this study, for checking the stress in the cross section and deformation at the preliminary design stage, the allowable stress design method is applied. Also, the two kinds of combination is considered as the traffic load and the traffic and rail load. Each combination is composed by Equation 4.12. D is the dead load, L_T is the roadway load, and L_R is the railway load.

$$1.0D + 1.0L_T \quad \text{for a roadway bridge} \tag{4.12a}$$

$$1.0D + 1.0L_T + 1.0L_R \quad \text{for a road-railway bridge} \tag{4.12b}$$

4.3 Design Constraints

In the optimization work with analyzing numerous combinations of design variables, it is necessary to examine whether every combination satisfies specific design constraints about stress and deformation under loads. The design constraints applied to this research are based on the provisions of bridge design codes such as KBDC, AASHTO and Eurocode, and include the stress and deformation of cables and deck as illustrated in Figure 4.6.

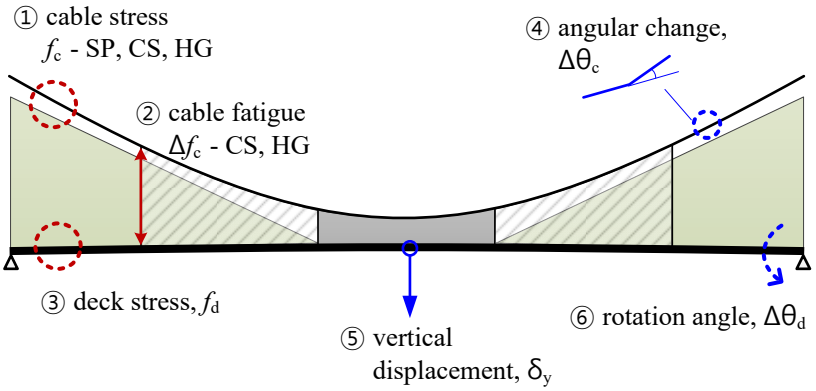

Figure 4.6 Scheme of design constraints for cable-stayed suspension bridge

4.3.1 Constraints on cables

(1) Axial stress of cable

For cable design, a limitation of an axial tensile stress under live loads is employed in this optimization procedure. The stress of cables under live loads should satisfy the allowable stress as expressed in Equation 4.13.

$$f_1 = \frac{T_{sp,liveload}}{A_{cable}} \le f_a = \frac{f_u}{SF} \tag{4.13}$$

where f_1 is the axial tensile stress under live loads, A_{cable} is the area of cross section of suspension cable, f_a is the allowable stress of cable, f_u is the tensile strength of wire, and SF is the safety factor defined in Table 4.4. as proposed in KBDC 2006. Particularly, SF is 2.0 when considering a secondary stress due to the angular change in the cross section of suspension cable.

Table 4.4 Safety factors of each cable for cable design criteria

Cables	Safety Factor	Remarks
Suspension cable	2.5	2.0 for considering secondary stress
Hanger rope	3.0	
Stay cable	2.2	

(2) Fatigue stress of cable

For hanger ropes and stay cables, the fatigue failure is one of the most important design criteria. In this research, the stress amplitude of stay cables and hangers between a dead load stage and a live load stage is examined whether it exceeds the allowable limit of the amplitude or not as expressed in Equation 4.14.

$$\Delta f_{E,2} = \lambda \Delta f_{71} = \lambda \left(f_{\max,rail\,load} - f_{\min,dead\,load} \right) \le \frac{\Delta f_c}{1.15} \tag{4.14}$$

where, $\Delta f_{E,2}$ is the equivalent stress amplitude, λ is the reduction factor, Δf_c is the stress amplitude associated to the load model 71, and Δf_c is the allowable limit of amplitude and it is suggested by 160 MPa for parallel wire strands with epoxy socketing, a bundle of parallel strands, and a bundle of parallel wires in Eurocode.

(3) Angular change of suspension cable

The angular change of suspension cable is defined as the rotated angle, $\Delta\Phi_{sp}$, due to the live loads from the hanging state under the only self-weight of cables as illustrated in Figure 4.7.

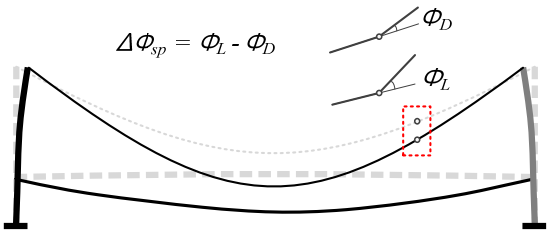

Figure 4.7 Angular change of suspension cable

In the parametric investigations, it is a key to solve the optimization problem because the angular change is very sensitive to the variation of design variables and leads a large secondary stress in the cross section. Unfortunately, the calculation of secondary stress of suspension cable is not significant, although Wyatt and Lee has proposed own formula in different ways as described in Equation 4.15 and Equation

4.16, respectively. Generally, it is known that Wyatt's equation tends to overestimate the secondary stress and Lee's equation tends to underestimate the secondary stress as well as has to assume the friction among parallel wires.

$$f_{sp,2} = 2\phi_{sp}\sqrt{Ef_t} \tag{4.15}$$

$$f_{sp,2} = 2\Delta\phi_1\sqrt{Ef_t\left(2\frac{\Delta\phi_0}{\Delta\phi_1}-1\right)} \qquad (here, \Delta\phi_1 = \frac{\mu_w p_0}{f_t}) \tag{4.16}$$

where, Φ_{sp} is the angular change, E is the elastic modulus of suspension cable, f_t is the tensile stress, $\Delta\Phi_1$ is the angular change of suspension cable near the cable band with considering the friction between wires, $\Delta\Phi_o$ is the angular change at the end of suspension cable, μ_w is the friction coefficient between wires, p_0 is the inner pressure applied to the cable by wrapping pressure. Therefore, the effect of the limitation for the angular change on the optimized result is investigated in this study, and the angular change has a range from 0.1 degree to 3.0 degree.

4.3.2 Constraints on decks

(1) Stress of deck

The deck of a combined system resists an axial force by stayed cables and a bending moment by vertical live loads simultaneously, and the combined stress should not exceed the yield stress of structural steel as expressed in Equation 4.17.

$$f_{deck} = \frac{N_d}{A_d} \pm E\kappa y \le f_a \tag{4.17}$$

Here, N_d is the compressive force in deck developed by the tension of stay cables, and A_d is the area of cross section of deck. E and f_a means the elastic modulus and allowable stress of steel, respectively. κ is the curvature of deck.

(2) Vertical displacement of deck

The criterion for the vertical displacement of deck under live loads for long span bridges is given in some design codes, and the limit of the displacement in Eurocode is as below. Here, δ_{max} is the maximum vertical displacement in the center span and L_m is the length of center span.

$$\delta_{\max} \leq \frac{L_m}{600} \tag{4.18}$$

(3) Rotation angle at the support

In case of a railway bridge, the angular rotation of deck at the ends or on the support is restricted to a specific value to secure the stability of trains when the train passes over the supports. When the rotation angle at the support under the railway load with the combination of SLS is $\Delta\theta$, the constraints can be expressed as Equation 4.19.

$$\Delta\theta \leq 0.0035 \ \ (rad) \tag{4.19}$$

Design criteria stated in the previous sub-chapter can be expressed the conditional functions. The conditions are summarized in Table 4.5.

Table 4.5 Summary of design criteria

ITEM		Equation for Constraints	Remarks
Cable	Axial stress	$g_1 \sim g_3 = \frac{T_c}{A_c} - \frac{f_u}{SF} \le 0$ $g_4 = \Delta\theta\,(\text{Angular change}) - \alpha\ (\text{deg}) \le 0$ $(0.1 \le \alpha \le 3.0)$	Cables / SF Suspension cable 2.5 Hanger 3.0 Stay cable 2.2
	Fatigue stress	$g_5 \sim g_6 = \lambda \times [f_{c,max} - f_{c,min}] - \frac{\Delta f_c}{\gamma_{Mf}} \le 0$ (λ : equivalent damage factor)	[Eurocode 1991-2 6.3.2] $\Delta f_c = 160\ Mpa$ $\gamma_{Mf} = 1.15$
Deck	Vertical displacement	$g_7 = \delta_y - L_m / 300 \le 0$	
	Stress	$g_8 = f_d - f_a \le 0$	
	Rotation angle	$g_9 = \Delta\theta_d - 0.0035\ (\text{rad}) \le 0$	for railway design

4.4 Cost Optimization Procedure

4.4.1 Optimization procedure

The cost optimization procedure for this study has a series of calculation process including a setting of the range of design variables, a generation of population, a structural analysis for live loads using the proposed simplified analysis model, an estimation of the objective function, and a genetic operation for the reproducing process by GA as shown in Figure 4.8.

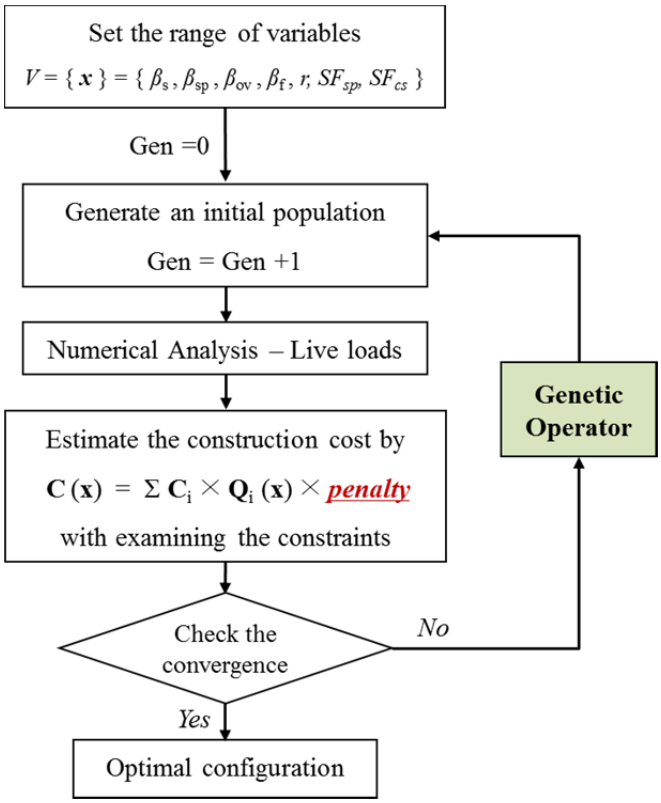

Figure 4.8 Flowchart of cost optimization

The genetic operator for reproduction, mutation, and crossover is employed to improve a fitness of the objective function during the optimization procedure. This research uses the genetic operator, built in MATLAB, and input parameters for the operator are a population of 100, a generation of 1,000, a crossover of 0.8, and a mutation fraction of 0.2, respectively. Also, the tolerance for convergence is 10^{-6} as listed. Also, an example of the progress to find the best fitness by MATLAB is plotted in Table 4.6

Table 4.6 Input parameters for Genetic Algorithm

Input parameter		Example of the optimization progress
Population	100	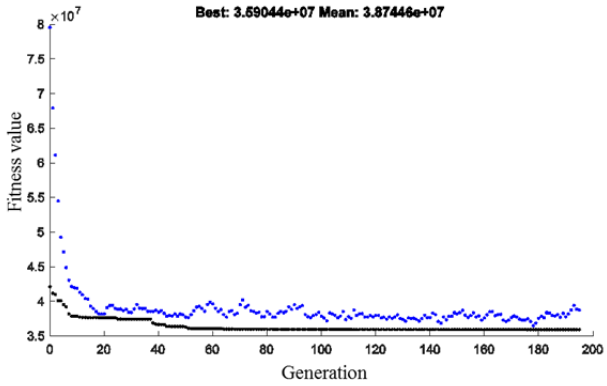
Generation	1,000	
Tolerance	10^{-6}	
Crossover	0.8	
Mutation	0.2	
Selection	Elite count=5	

4.4.2 Penalty in objective function

In the flowchart of the optimization procedure in Figure 4.8, a penalty is applied to the objective function, and the penalty is the important parameter which imposes an additional cost on the objective function based on the design constraint violation. In this research, the penalty is varied from 1.5 to 10,000, and the optimization process is

carried out. As the penalty increases, it tends to increase the number of generation for convergence, but the increment is not significant. Also, the optimal cost is not affected to the variation of the penalty as shown in Figure 4.9.Thus, the penalty of 2 is used in this study.

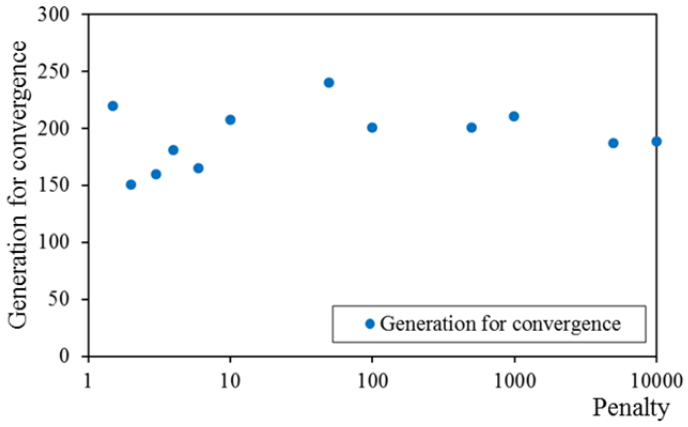

(a) Effect of a penalty on the generation for convergence

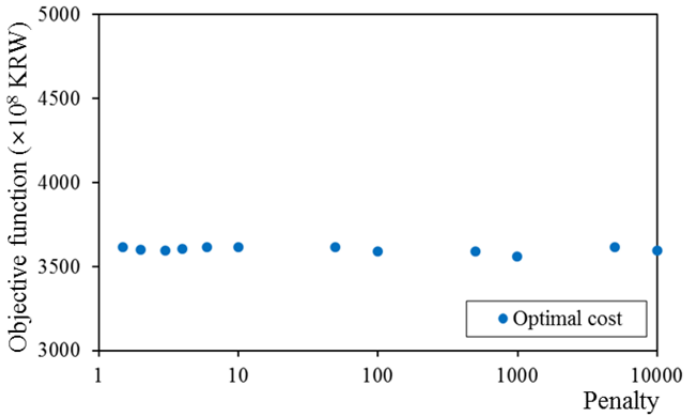

(b) Effect of a penalty on the optimal cost

Figure 4.9 Effect of a penalty on the objective function

4.5 Optimal Cable System for a Road-railway Bridge

4.5.1 Design conditions

The optimization procedure presented in the previous chapter is applied to a road-railway bridge with a cable-stayed suspension cable system. The bridge has a various main span length from 1,500 m to 2,500 m. The deck has eight lanes for traffic and two tracks for train, and the area of the cross section is assumed as 2.8 m^2 as illustrated in Figure 4.10. The material properties are listed in Table 4.7.

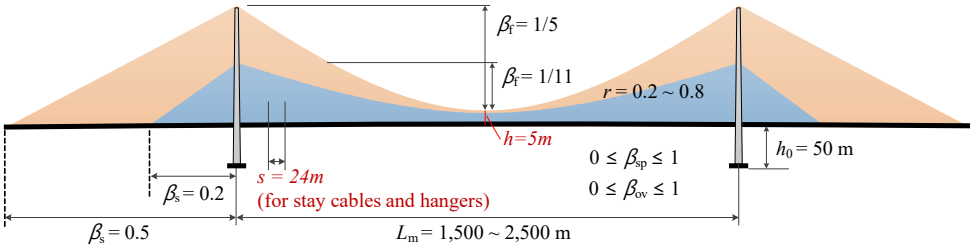

Lane / Load	DL (kN/m)	LL (kN/m)
8 lanes for traffic + 2 tracks for train	420	48

Figure 4.10 Scheme of design conditions for a road-railway bridge

Table 4.7 Material properties for example cases

Material	γ (kN/m³)	E (GPa)	f_u (MPa)	f_a (MPa)	f_{ck} (MPa)	Remarks
Suspension cable	77	200	1,960	784	-	
Hanger	77	200	1,770	590	-	
Stay cable	77	200	1,960	890	-	
Steel	77	200	-	210	-	SM520
Concrete	25	30	-	-	40	C40

For the design of cable system, the height from the foundation to deck is assumed as 50m. The height of suspension cable from deck at the center of main span is 5m. Other dimensions to define a cable system – a side span length (L_s), a suspension section length (L_{sp}), an overlapping length (L_{ov}), a sag(f) – are design variables as listed in Table 4.8.

Table 4.8 Lower and upper bounds of the design variables for example cases

Variables	Definition	Lower bound	Upper bound
β_s	L_s / L_m	0.2	0.5
β_{sp}	L_{sp} / L_m	0	1
β_{ov}	$2L_{ov}$ /(L_m - L_{sp})	0	1
β_f	f / L_m	1/11	1/5
r_1	W_{cs} / W_g	0.2	0.8
r_2	W_{cs} / W_g	0.2	0.8

The live load for a railway bridge is a uniformly distributed load of 48 kN/m on the entire span and two train loads of LM71 as illustrated in Figure 4.5. The length of train is 270m. For examining the structural safety and design criteria, the load combination is defined as the serviceability limit state (SLS) as expressed in Equation 4.20.

$$1.0D + 1.0L_T + 1.0L_R \tag{4.20}$$

where D is the dead load, and L_T is the uniformly distributed load. For the rail load, two different load cases are considered in the optimization procedure. The rail load is loaded at the center of the span in Load case 1, and it is loaded at the quarter location of the span in Load case 2 as illustrated in Figure 4.11. Therefore, all results by both load cases are checked by the design criteria in the optimization procedure.

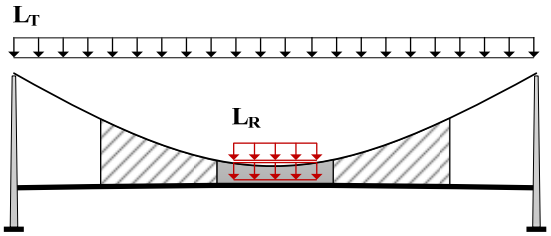

(a) Load case 1 : rail load at the center

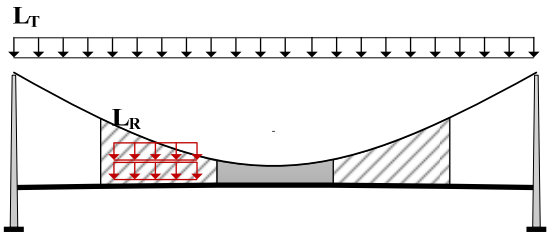

(b) Load case 2 : rail load at the quarter position

Figure 4.11 Load cases of the optimization procedure for a road-railway bridge

4.5.2 Optimal cable system

As mentioned in the previous chapter, although the angular change of suspension cable is very sensitive to the design variation and leads a large secondary stress in the cross section, the calculation of the secondary stress is not clear at present. In this study, therefore, two constraints for the angular change are considered to decide the reasonable design criteria for a cable-stayed suspension bridge.

Firstly, the secondary stress is calculated by Wyatt's equation and Lee's equation as expressed in Equation 4.15 and Equation 4.16. The design criteria use the limitation of the allowable stress of suspension cable with considering the secondary stress by the safety factor of 2.0.

$$f_1 = \frac{T_{sp,liveload}}{A_{cable}} \le f_a = \frac{f_u}{SF} \quad (here, SF = 2.0) \tag{4.21}$$

Table 4.9 shows the optimal cable system for a road-railway bridge with a main span length of 1,500 m by the design criteria for the secondary stress of suspension cable. Since, Wyatt's equation overestimates the secondary stress and Lee's equation tends to underestimate the secondary stress, the optimal cable system by Wyatt's equation has a longer suspension section, a longer overlapping section, a higher cable sag, and a lower dead load distribution factor to reduce the angular change of suspension cable. As a result, the optimized construction cost by Wyatt is higher, and the maximum angular change by Wyatt's equation is 0.66 degree that is the same as 28% of the result by Lee's equation. These discrepancies are very fatal to propose a reasonable optimal solution.

Table 4.9 Optimal cable system using the criteria for the secondary stress of suspension cable

Eq.	*Wyatt*'s equation	*Lee*'s equation
Configuration	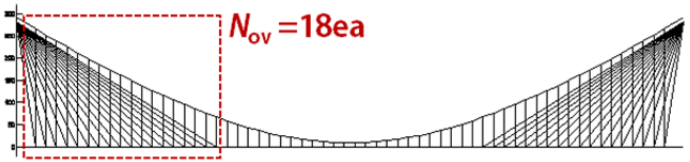	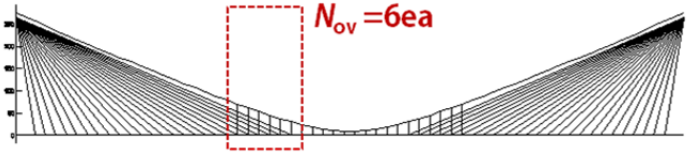
	β_s = 0.2, β_{sp} = 0.39, β_{ov} = 1.00, β_f = 0.188, r = 0.65	β_s = 0.2, β_{sp} = 0.17, β_{ov} = 0.21, β_f = 0.176, r = 0.77
	Area of suspension cable = 0.355 m^2	Area of suspension cable = 0.164 m^2
	Diameter of suspension cable = 0.752 m	Diameter of suspension cable = 0.512 m
Cost	6,874 $\times$ 10^8 KRW	6,290 $\times$ 10^8 KRW
Max. angular change	*0.66 deg*	*2.37 deg*
Max. vertical displacement	2.91 m (= L_m/515)	2.95 m (= L_m/510)

Secondly, the optimization procedure is performed by the design criteria using the angular change of the suspension cable. The criteria for the angular change are varied from 0.1 degree to 3.0 degree, and the optimized construction costs for a main span length of 1,500 m and 2,000 m are plotted in Figure 4.12. When the criteria is lower than 0.5 degree, any combination of the design variables cannot satisfy the design criteria, and the optimized construction cost is very high due to the penalty. Also, when the criteria is over 1.5 degree, it is clear that the optimized cost is converged. On the other hand, the secondary stress calculated by both equations according to the criteria for the angular change is plotted in Figure 4.13. For applying the Lee's equation as expressed in Equation 4.16, the friction coefficient between wires (μ_w) and the inner pressure by wrapping pressure (p_0) refer to the Lee's experimental results (Lee, 2016).

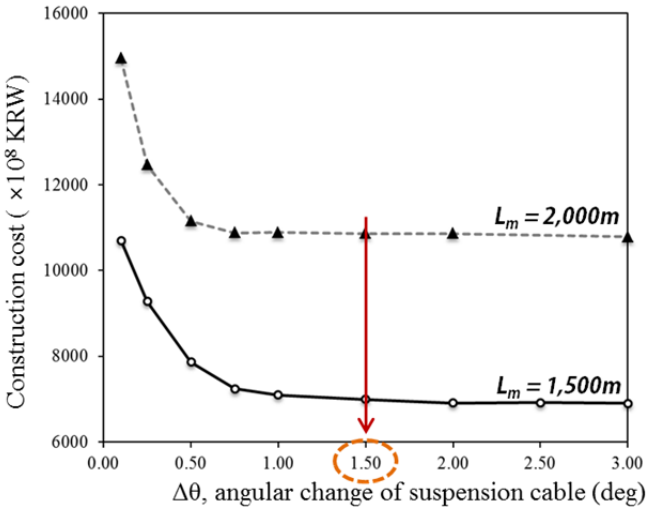

Figure 4.12 Optimized construction cost according to various criteria for angular change

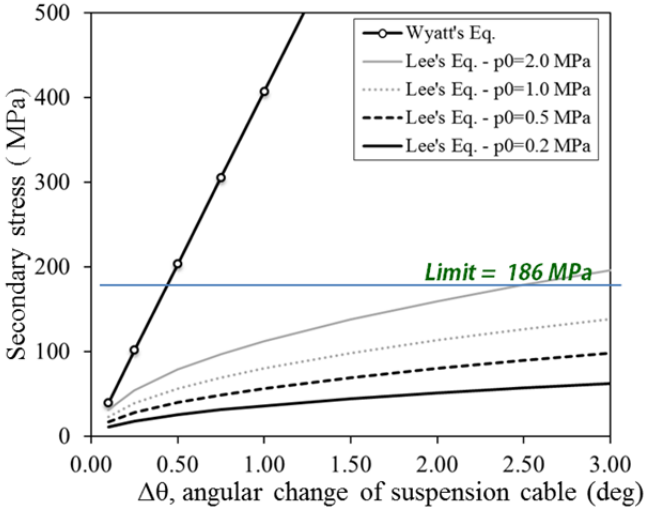

(a) secondary stress when $\mu_w = 0.23$, and various p_0

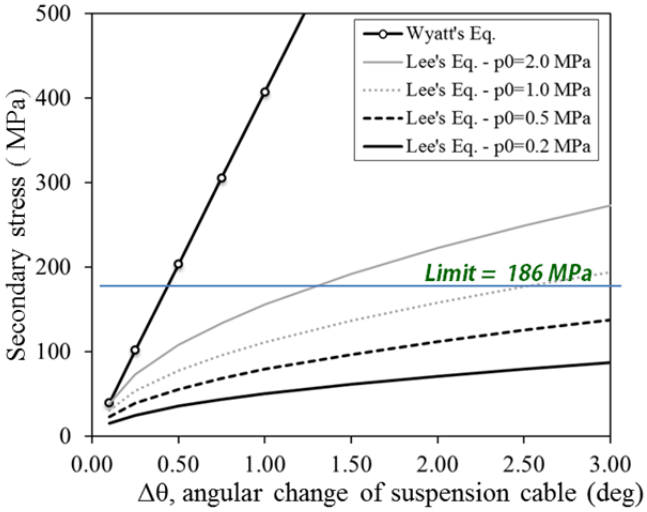

(b) secondary stress when $\mu_w = 0.45$, and various p_0

Figure 4.13 Secondary stress by both equations for a road-railway bridge

From the experimental result, the friction coefficient is about 0.23, and the inner pressure is from 0.2 MPa to 2.0 MPa. To investigate the effect of change of the

friction coefficient on the secondary stress, this study uses two friction coefficients, 0.23 and 0.45. The limit of the secondary stress is 186 MPa since the safety factor considering the secondary stress is 2.0. As expected, the secondary stress by Wyatt's equation is very larger, although the stress by Lee's equation is increased as the friction coefficient increases. Therefore, it is clarified that the constraint by the calculation of secondary stress is not clear to find an optimal solution, and this study suggests a constraint by the angular change. Also, the angular change of 1.5 degree is reasonable when considering the convergence of the optimized cost and the secondary stress. The optimal cable system by the constraint of the angular change of 1.5 degree under the design condition in the sub-chapter 4.5.1 is illustrated in Figure 4.14. It shows that the optimal cable system by the proposed constraint is between the result by Wyatt's equation and the result by Lee's equation.

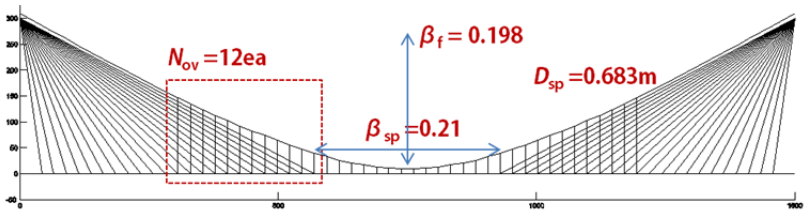

Eq.	*Wyatt*'s equation	Proposed : $\Delta\theta \leq 1.5^\circ$	*Lee*'s equation
Configuration	Asp= 0.355 m², Dsp = 0.752 m β_{sp} = 0.39 N_{ov} = 18 EA	Asp= 0.293 m², Dsp = 0.683 m β_{sp} = 0.21 N_{ov} = 12 EA	Asp = 0.164 m², Dsp = 0.512 m β_{sp} = 0.17 N_{ov} = 6 EA
Cost	6,874 × 10^8 KRW	6,678 × 10^8 KRW	6,290 × 10^8 KRW
Max. angular change	*0.66 deg*	*1.02 deg*	*2.37 deg*
Max. vertical displacement	2.91 m (= L_m/515)	2.44 m (= L_m/615)	3.25 m (= L_m/460)

Figure 4.14 Optimal cable system of a road-railway bridge with L_m of 1,500 m

As a result, the optimal cable system by the proposed optimization procedure using the constraint for the angular change of suspension cable is illustrated in Figure 4.15. As the main span length increases, the ratio of the suspension section length is increased, and the sag ratio is decreased. However, the number of hangers in the overlapping section is not affected by the variation of L_m, and the dead load distribution factor is 0.74 regardless of L_m, too. The optimized ratio of side span length is 0.2 for all cases.

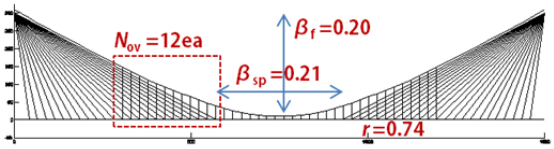

(a) Optimal cable system with L_m = 1,500m

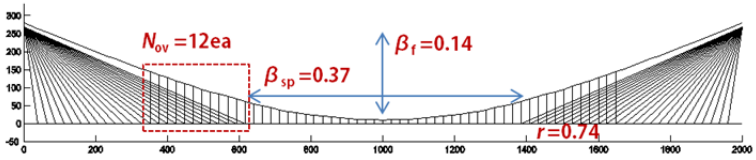

(b) Optimal cable system with L_m = 2,000m

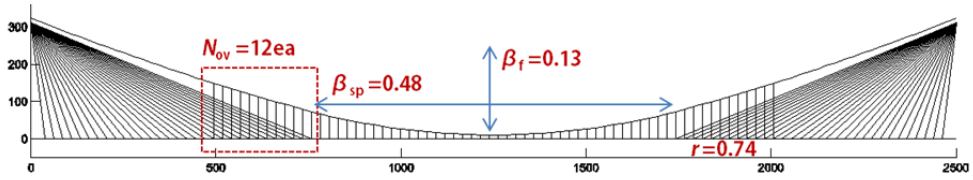

(c) Optimal cable system with L_m = 2,500m

Figure 4.15 Optimal cable system for a rail load with various main span length

At present, the limitation of the span length for a long-span cable-stayed bridge is known as 1,500 m when considering the structural behavior and economic feasibility. As shown in Figure 4.15, the length of the stayed section including the overlapping section has a range from 1,200 m to 1,500 m. Namely, it is efficient to reduce the quantity of suspension cable by extending the cable-stayed section.

In addition, the cable quantities and the construction cost of the optimal cable system are compared with the results of the suspension system with the same span length. The comparison is plotted in Figure 4.16, and Q_{sp}-CSSB means the quantity of suspension cable for the optimal cable-stayed suspension bridge. Q_{sp}-SP means the quantity of suspension cable for the suspension system with the same L_m. As shown in Figure 4.16, it is clarified that the cable-stayed suspension bridge can reduce the construction cost by 15% by reducing the cable quantity.

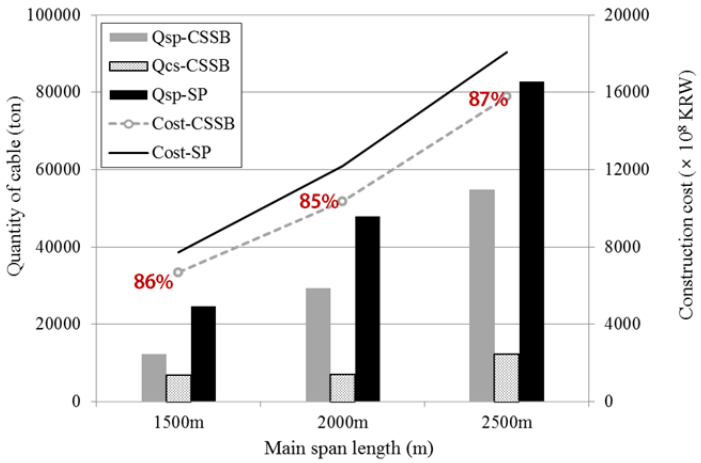

Figure 4.16 Comparison of quantity and cost with suspension system for railway

4.5.3 Sensitivity analysis

To investigate the sensitivity of the design variables near the optimal point, the sensitivity analysis is performed. The sensitivity is defined as the variation of the construction cost by the objective function according to the variation of the design variables as expressed in Equation 4.22.

$$S_{c,i} = \frac{\partial C}{\partial \beta_i} \quad \beta_i = \{ \quad \beta_s, \quad \beta_{sp}, \quad \beta_{ov}, \quad \beta_f, \quad r \quad \} \tag{4.22}$$

The result of sensitivity analysis for the optimal cable system with the main span length of 1,500 m is plotted in Figure 4.17. The suspension section length is very dominant to the optimal result, and the proposed objective function is sensitive in order of cable sag, side span length, and overlapping length.

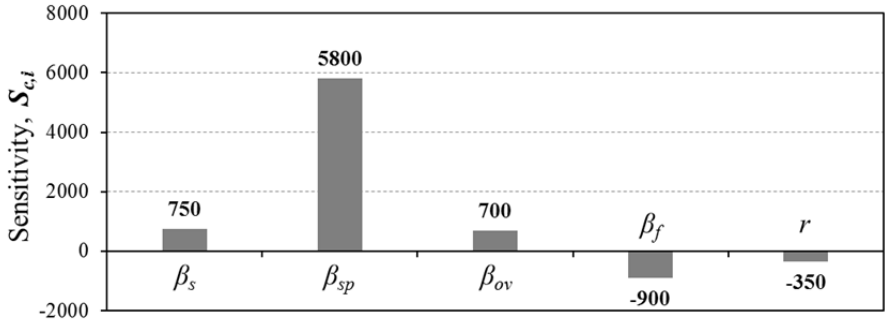

Figure 4.17 Sensitivity for construction cost of a road-railway bridge with L_m=1,500 m

In addition, the sensitivities for the angular change of suspension cable and the vertical displacement of deck are investigated. The sensitivity is defined as the variation of the deformation according to the variation of the design variables as expressed in Equation 4.23 and Equation 4.24. The result of sensitivity analysis for the optimal cable system with the main span length of 1,500 m is plotted in Figure 4.18. The suspension section length is very dominant to the deformation likewise the sensitivity of construction cost, and the cable sag and the overlapping length is sensitive to the deformation of the optimal cable system under live loads.

$$S_{\Delta\theta,i} = \frac{\partial\left(\Delta\theta_{sp}\right)}{\partial\beta_i} \qquad \beta_i = \{ \quad \beta_s, \quad \beta_{sp}, \quad \beta_{ov}, \quad \beta_f, \quad r \quad \} \tag{4.23}$$

$$S_{y,i} = \frac{\partial V_y}{\partial\beta_i} \qquad \beta_i = \{ \quad \beta_s, \quad \beta_{sp}, \quad \beta_{ov}, \quad \beta_f, \quad r \quad \} \tag{4.24}$$

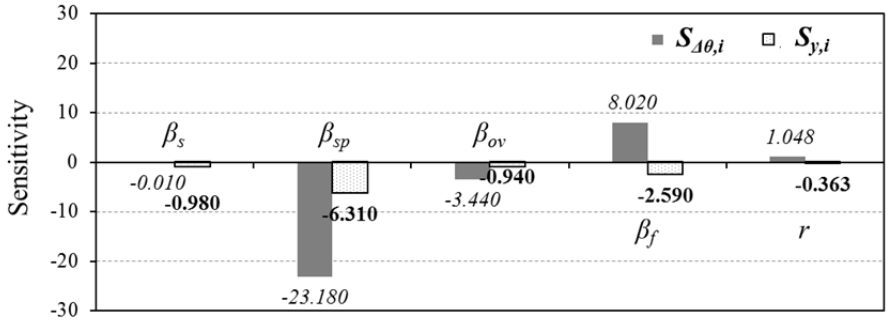

Figure 4.18 Sensitivity for deformation of a road-railway bridge with L_m=1,500 m

4.6 Optimal Cable System for a Roadway Bridge

4.6.1 Design conditions

The optimization procedure presented in the previous chapter is applied to a roadway bridge with a cable-stayed suspension cable system. The bridge has a various main span length from 1,500 m to 2,500 m. The deck has six lanes for traffic, and the area of the cross section is assumed as 1.6 m^2 as illustrated in Figure 4.19. The material properties for design are the same as Table 4.8 in the sub-chapter 4.5.1 applied to the road-railway bridge.

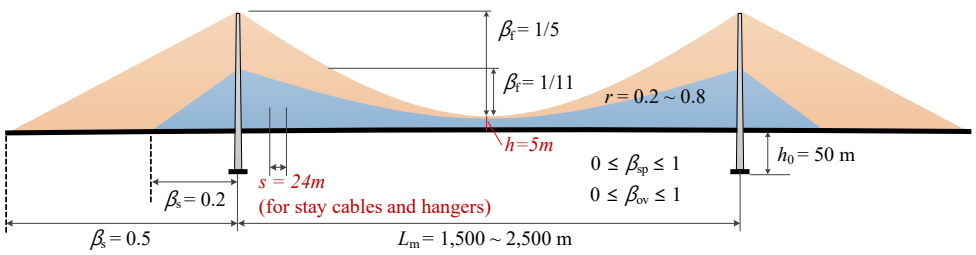

Lane / Load	DL (kN/m)	LL (kN/m)
6 lanes for traffic	240	36

3.5m

Figure 4.19 Scheme of design conditions for a roadway bridge

For the design of cable system, the height from the foundation to deck is assumed as 50m. The height of suspension cable from deck at the center of main span is 5m. Other dimensions to define a cable system – a side span length (L_s), a suspension section length (L_{sp}), an overlapping length (L_{ov}), a sag(f) – are design variables as

illustrated in Figure 4.19 and listed in Table 4.8. The live load for a roadway bridge is a uniformly distributed load of 36 kN/m on the entire span. For examining the structural safety and design criteria, the load combination is defined as the serviceability limit state (SLS) as expressed in Equation 4.25.

$$1.0D + 1.0L_T \tag{4.25}$$

where D is the dead load, and L_T is the uniformly distributed load for traffic.

4.6.2 Optimal cable system

The optimal cable system for a roadway bridge by the design criteria of Table 4.10 is calculated. The constraint for the angular change of suspension cable uses the limitation of 1.5 degree as described in the previous chapter. As a result, the optimal cable system is illustrated in Figure 4.20. As the main span length increases, the ratio of the suspension section length is increased, and the sag ratio is decreased. However, the number of hangers in the overlapping section is not significantly affected by the variation of L_m. For a roadway bridge with a combined cable system, three to five hangers are enough to control the structural discontinuity at the overlapping section. The number of overlapping hangers is clearly smaller than the number in case of the railway bridge. Also, the dead load distribution factor is 0.68 regardless of L_m, too. The optimized ratio of side span length is 0.2 for all cases.

Table 4.10 Summary of design criteria for a roadway bridge

ITEM		Equation for Constraints	Remarks
Cable	Axial stress	$g_1 \sim g_3 = \frac{T_c}{A_c} - \frac{f_u}{SF} \le 0$ $g_4 = \Delta\theta$ (Angular change) – 1.5 (deg) ≤ 0	Cables / SF Suspension cable / *2.5* Hanger / *3.0* Stay cable / *2.2*
	Fatigue stress	$g_5 \sim g_6 = \lambda \times [f_{c,max} - f_{c,min}] - \frac{\Delta f_c}{\gamma_{Mf}} \le 0$ (λ : equivalent damage factor)	[Eurocode 1991-2 6.3.2] $\Delta f_c = 160\ Mpa$ $\gamma_{Mf} = 1.15$
Deck	Vertical displacement	$g_7 = \delta_y - L_m / 600 \le 0$	
	Stress	$g_8 = f_d - f_a \le 0$	

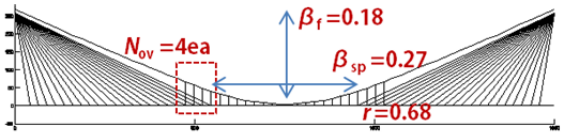

(a) Optimal cable system with L_m = 1,500m

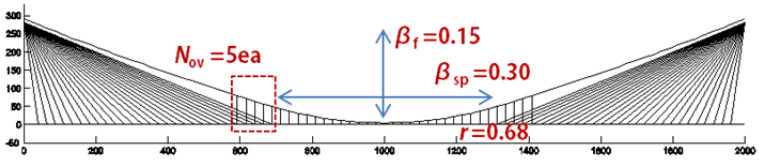

(b) Optimal cable system with L_m = 2,000m

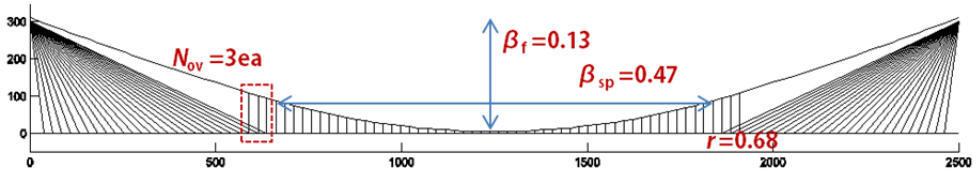

(c) Optimal cable system with L_m = 2,500m

Figure 4.20 Optimal cable system for a road load with various main span length

Likewise the case of the road-railway bridge, the length of the stayed section including the overlapping section has a range from 1,200 m to 1,500 m. Namely, it is efficient to reduce the quantity of suspension cable by extending the cable-stayed section. In addition, the cable quantities and the construction cost of the optimal cable system are compared with the results of the suspension system with the same span length. As shown in Figure 4.21, it is clarified that the cable-stayed suspension bridge can reduce the construction cost by 21% by reducing the cable quantity, but the

reduction rate is increased as L_m increases.

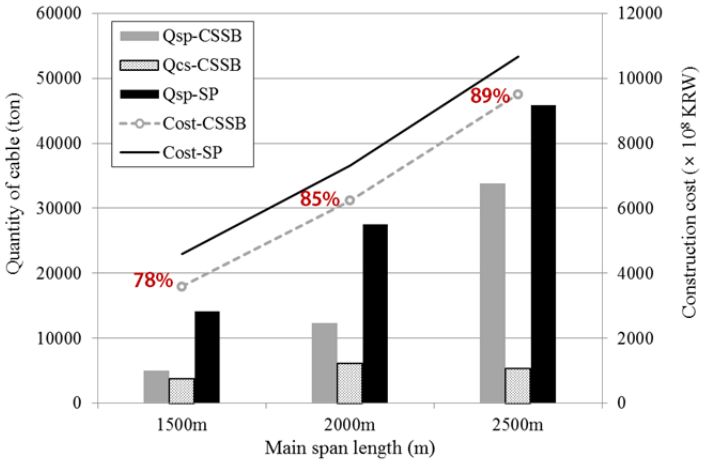

Figure 4.21 Comparison of quantity and cost with suspension system for roadway

4.6.3 Sensitivity analysis

The sensitivity of construction cost calculated by Equation 4.22 for the optimal cable system with the main span length of 1,500 m is plotted in Figure 4.22. Likewise the case of the road-railway bridge, the suspension section length is very dominant to the optimal cost, and the proposed objective function is sensitive in order of side span length, cable sag, and overlapping length.

In addition, the sensitivities for the angular change of suspension cable and the vertical displacement of deck are investigated. The sensitivity is defined as the variation of the deformation according to the variation of the design variables as

expressed in Equation 4.23 and Equation 4.24. The result of sensitivity analysis for the optimal cable system with the main span length of 1,500 m is plotted in Figure 4.23. The suspension section length is very dominant to the deformation likewise the sensitivity of construction cost, and the cable sag and the overlapping length is sensitive to the deformation of the optimal cable system under live loads.

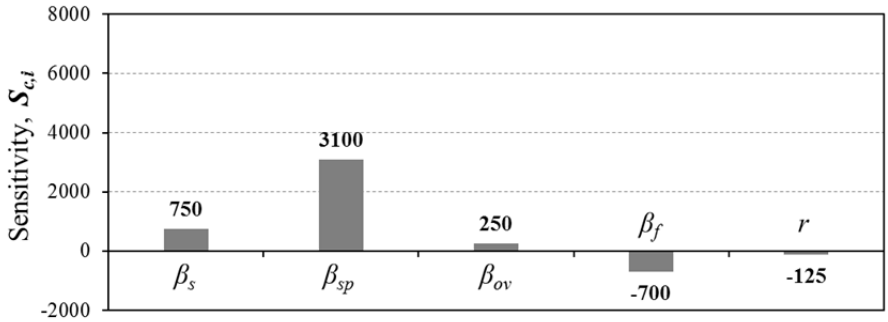

Figure 4.22 Sensitivity for construction cost of a roadway bridge with L_m=1,500 m

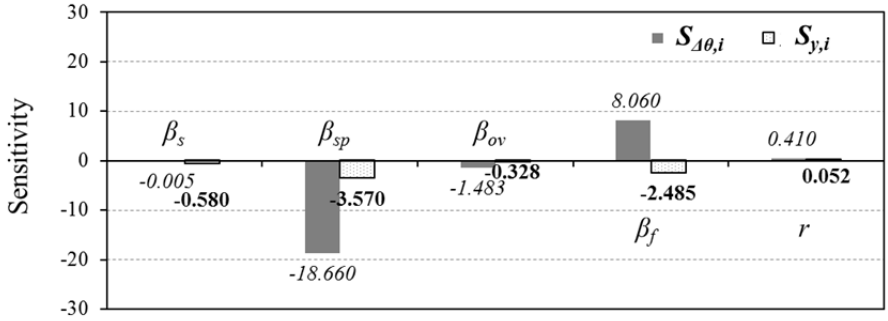

Figure 4.23 Sensitivity for deformation of a roadway bridge with L_m=1,500 m

5. CONCLUSIONS

An optimization procedure to find an optimal cable system with minimized construction cost of superstructures for a cable-stayed suspension bridge is presented. Using the optimization procedure, the optimal cable systems for a roadway bridge and a railway bridge are proposed. The optimal variables are expressed in terms of the side span length (L_s), the suspension section length (L_{sp}), the overlapping length (L_{ov}), the cable sag (f), and the dead load distribution factor (r). To reduce the time consumption for iterative calculations and improve the efficiency of the optimization procedure, a new simplified analysis model using truss elements and equivalent horizontal cable spring is proposed. In addition, parametric investigation is performed to understand the effects of design modifications on the structural behavior under live loads by the proposed analysis model.

First of all, the proposed simplified analysis model for a cable-stayed suspension bridge uses two-dimensional truss elements considering the geometric nonlinearity and replaces the cables in the side span and the pylon with an equivalent horizontal cable spring at the top of the pylon. This simplified analysis model can be easily built using five design variables, which are namely the side span length, the suspension section length, the overlapping length, the sag and the dead load distribution factor in the overlapping section. To verify and confirm the accuracy and adequacy of the proposed simplified analysis model, a suspension bridge with main span length of 850 m and a cable-stayed suspension bridge with main span length of 1,408 m are analyzed by two methods – the proposed model and a three-dimensional frame model

by a commercial FEM software, RM Bridge. As a result, the maximum discrepancy in cable tension, geometry, and deformation between both methods is about 4.0 %, but the proposed model reflects the structural behavior including the stress in the cross section and the global deformation under live loads very well. The proposed procedure is efficient and reasonable enough to develop a conceptual design in the preliminary design stage which needs numerous iteration works. In this study, by applying the simplified analysis model to the optimization procedure, the time consumption for assembling and analyzing is remarkably reduced.

Secondly, the effects of design modifications including the change of L_s, L_{sp}, L_{ov}, f, and r on the structural behavior are investigated by the proposed analysis model. The 3rd Bosphorus Bridge with main span length of 1,408 m in Turkey is employed for the parametric investigation, and the stress of cable, the angular change of suspension cable, and vertical displacement and curvature of deck are analyzed under traffic load and rail load. Through the sensitivity analysis with normalized results, it appears that the considered variables influence the structural behavior in both road cases in the following order: L_{sp}, L_{ov}, f, r, and L_s. Here, when L_{sp} and L_{ov} expand, the stress and deformation for cables and deck are decreased, and when r increases, the results are increased. Also, if the sag, f, increases, the stress and angular change of suspension cable are increased, but the stress of stay cables, hangers, deck and the deformation of deck are decreased. The effects of L_s on the stress and deformation are insignificant. Meanwhile, the most sensitive behavior recorded under the design modifications is the angular change of suspension cable which leads to large secondary stress, followed by the vertical displacement and curvature of deck. Therefore, the design criteria for the

angular change of suspension cable and the deformation of deck have an important role when deciding the optimal cable system in the optimization procedure.

Finally, this study proposes the optimized cable system for a cable-stayed suspension bridge with main span lengths of 1,500 m, 2,000 m, and 2,500 m under road and rail loads. The optimization procedure uses Genetic Algorithm, and the objective function minimizes the construction cost of the superstructure including cables, decks, pylons, and anchorages. For a roadway bridge, the suspension section length is increased when the main span length enlarges, and the ratio of L_{sp} to the main span length is 0.27, 0.30 and 0.47 for main span length of 1,500 m, 2,000m and 2,500 m, respectively. The overlapping length between the suspension section and the stayed section is not affected by the variation of the main span length, and three to five hangers are enough to control the structural discontinuity at the overlapping section. Also, the ratio of the sag to the main span length is 0.17, 0.15, and 0.12 for main span length of 1,500 m, 2,000m and 2,500 m, respectively. The dead load distribution factor is about 0.70 regardless of the main span length. On the other hand, for a railway bridge, the ratio of L_{sp} to the main span length is 0.21, 0.37 and 0.48 for main span length of 1,500 m, 2,000m and 2,500 m, respectively. Twelve hangers are recommended to control the structural discontinuity at the overlapping section. Also, the ratio of the sag to the main span length is very similar to the roadway bridge case. The dead load distribution factor is about 0.75 regardless of the main span length. From the optimal cable system, the railway bridge needs three times longer overlapping length to control the angular change of suspension cable and the vertical displacement of deck. The sensitivity analysis shows that the cost sensitivity of each

design variable predominates in the order of L_{sp}, f, and L_{ov} for both bridges. The optimized construction cost of a cable-stayed suspension bridge is lower than the cost of a suspension bridge, and the cable-stayed suspension bridge can save the cost by 15 % when the main span length is shorter than 2,000 m.

The proposed optimization procedure and simplified analysis model for a cable-stayed suspension bridge is so efficient and reasonable that they can be applied to the practical design process efficiently. Also, designers can avoid heavy iteration works to find the optimal cable system of a combined system with consuming much time, cost and manpower.

References

Aschrafi, M. (1998) Comparative investigations of suspension bridges and cable-stayed bridges for spans exceeding 1000m, *Proceedings of the IABSE Symposium, Long-Span and High-Rise Structures*, Kobe, Japan, 79, 447-452.

Arie, R., Reza, S., and David, V.G. (2008) Parametric study on static behaviour of self-anchored suspension bridges, *Steel Structures*, 8, 91-108.

Bruno, D., Greco, F., and Lonetti, P. (2009) A parametric study on the dynamic behavior of combined cable-stayed and suspension bridges under moving loads, *International Journal for Computational Methods in Engineering Science and Mechanics*, 10(4), 243-258.

Buonopane, S. (2006) The Roeblings and the stayed suspension bridge: Its development and propagation in 19th century United States, *Proceedings of The Second International Congress on Construction History*, Cambridge, England, 441-460.

Carine, M. (2010) Optimal design of bridges for high-speed trains, Master thesis, Royal Institute of Technology, Sweden.

Cho, Y., Son, Y., and Yoo, D. (2011) Optimum span-ratio of cable stayed-suspension bridge, *Proceedings of the Conference of KSCE 2011*, South Korea, 1008-1011.

Cho, Y., Son, Y., and Yoo, D. (2013) Parametric analysis for systemic behavior of cable stayed-suspension bridge, *Proceedings of the Conference of KSCE 2013*, South Korea, 1062-1065.

Choi, D., Lee, S., Gwon, S., and Yoo, H. (2013) Initial equilibrium state analysis and buckling analysis using a fictitious axial force for cable-stayed suspension bridge, *Proceedings of the Conference of KSCE 2013*, South Korea, 1066-1069.

Choi, D., Gwon, S., and Na, H. (2014) Simplified analysis for preliminary design of towers in suspension bridges, *Journal of Bridge Engineering*, 19(3), 04013007.

Choi, J., Hwang, I., and Kim, M. (2012) Initial shape analysis for bridges supported with stayed and suspended cables by initial force method, *Proceedings of 2012 KSSC Annual Conference*, South Korea, 25-26.

Choi, H., Moon, J. and Koh, H. (2016) Static behavior of cable-stayed suspension bridge with a transition zone, *Proceedings of 19th IABSE Congress 2016*, Stockholm, Sweden.

De ville de goyet, V., Virlogeux, M., Klein, J.F., and Duchene, Y. (2015) The behavior of the third Bosporus bridge related to wind and railway loads, *Proceedings of the 38th IABSE Symposium 2015*, Geneva, Switzerland, 2109-2116.

Drago, F., Tortolini, P., and Petrangeli, M. (2015) The kamaro suspension bridge in Madagascar, *Proceedings of the 38th IABSE Symposium 2015*, Geneva, Switzerland, 2010-2017.

Envico Consultants Co., Ltd. (2011) *The 3rd yearly report*, Super Long Span Bridge R&D Center.

Fatema, S. and Shunichi, N. (2015) Study on serviceability of cable-stayed bridges with new stay systems, *Proceedings of the School of Engineering Tokai University*,

Series E40, 21-28.

Gimsing, N.J. and Georgakis, C.T. (2012) *Cable supported bridges concept and design, 3rd ed.*, New York, John Wiley & Sons Ltd.

Gregor, P.W. (2001) Preliminary analysis of suspension bridges, *Journal of Bridge Engineering*, 6(4), 227-233.

Kim, N., Koh, H., and Hong, S. (2014) Exploration of structural form of hybrid cable-supported structures, *Proceedings of the 37th IABSE Symposium 2014*, Madrid, Spain, 1353-1360.

Kim, K. (2011) Initial equilibrium configuration analysis for bridges supported with stayed and suspended cables, Master thesis, Seoul National University.

Kim, S. (2011) A study on initial shape finding of cable-stayed suspension bridges, Master thesis, Hanyang University.

Kivi, E. (2009) Structural behavior of cable-stayed suspension bridge structure, Doctoral dissertation, Tallinn University of Technology.

Konstantakopoulos, T.G. and Michaltsos, G.T. (2010) A mathematical model for a combined cable system of bridges, *Engineering Structures*, 32(9), 2717-2728.

Lee, M. and Kim, H. (2016) Angular change and secondary stress in main cables of suspension bridges, *International Journal of Steel Structures*,16(2), 573-585.

Lonetti, P. and Pascuzzo, A. (2014) Optimum design analysis of hybrid cable-stayed suspension bridges, *Advances in Engineering Software*, 73, 53-66.

Maeda, K., Nakamura, H., Nomura, K., and Narita, N. (2002) Static and dynamic structural characteristics and economic efficiency of ultra long-span cable-stayed suspension bridges, *Journal of JSCE*, 55(707), 177-194.

Moon, J.H. (2008) Methods for numerical analysis and configuration control of the main cable of suspension bridges considering the curvature of the earth surface, Doctoral dissertation, Seoul National University.

Nagai, M., Fujino, Y., Yamaguchi, H., and Iwasaki, E. (2004) Feasibility of a 1,400 m Span Steel Cable-Stayed Bridge, *Journal of Bridge Engineering*, 9(5), 444-452.

Narita, N., Nakamura, H., Maeda, K., and Nomura, K. (1998) Applicability of Dischinger-type to ultra-long span bridges, *Proceedings of the IABSE Symposium, Long-Span and High-Rise Structures*, Kobe, Japan, 79, 137-142.

Olfat S.Z. (2012) Comparison between three types of cable stayed bridges using structural optimization methods, Master thesis, The University of Western Ontario.

Sato, Y., Sasaki, S., Morohashi, K., and Suzuki, N. (2003) Construction of Nagisa bridge hybrid system of cable-stayed pc bridge and steel suspension bridge, *Proceedings of 19th US-Japan Bridge Engineering Workshop*, Tsukuba, Japan.

Savaliya, G.M., Desai, A.K., and Vasanwala, S.A. (2015) Static and Dynamic Analysis of Cable-stayed Suspension Hybrid Bridge & Validation, *International Journal of Advanced Research in Engineering and Technology (IJARET)*, 6(11), 91-98.

Seo, J., Kim, H., Kim, G., Kim, M., Lee, J., and Kim, K. (2013) Initial shape finding of a cable-stayed suspension bridge, *Proceedings of the Conference of KSCE 2013*,

South Korea, 1070-1071.

Sun, B., Cai, C.S., and Xiao, R. (2013) Analysis strategy and parametric study of cable-stayed-suspension bridge, *Advances in Structural Engineering*, 16(6), 1081-1102.

Venkat, L., Akhil, U., and Krishna, K.S. (2011) Genetic algorithms-based optimization of cable stayed bridge, *Journal of Software Engineering & Application*, 4, 571-578.

Wang, H., Wang, J., and Wei, H. (2014) Case study on 4000m-span cable-stayed suspension bridge, *Research Journal of Applied Sciences, Engineering and Technology*, 7(15), 2998-3001.

Zhang, X.J. and Sun, B.N. (2005) Aerodynamic stability of cable-stayed-suspension hybrid bridges, *Journal of Zhejiang University SCIENCE*, 6(8), 869-874.

초 록

본 연구에서는 사장교와 현수교가 혼합된 교량형식인 사장-현수교에 대해서 케이블 설계 시, 상부구조의 건설비용 최소화를 통한 케이블 시스템의 최적화 절차를 제시하고 차량 하중 및 철도 하중에 대한 최적 케이블 시스템의 설계를 제안한다. 이 때, 제안된 최적의 케이블 시스템은 측경간장(L_s), 주경간장(L_{sp}), 사장교 구간과 현수교 구간의 중첩구간 길이(L_{ov}), 주케이블 새그(f) 및 고정하중 분담율(r) 등의 변수로 결정되고, 최적화 수행에는 다수의 설계변수를 포함하는 최적화 문제에 효율적인 유전자 알고리즘(GA)를 적용하였다.

일반적으로 다수의 설계변수를 다루는 최적화 절차는 과다한 비용, 시간 및 인력이 소모되는 많은 반복 계산을 필요로 하므로, 이 연구는 사장-현수교에 대한 간략화 구조해석모델을 제안하여. 반복 계산에 소요되는 비용, 시간 및 인력을 감소시키고자 하였다. 제안된 간략화 해석모델은 비선형성을 고려한 2차원 트러스 요소를 사용하고, 측경간의 사장 케이블 및 현수 케이블은 주탑 상단의 등가 수평 케이블 스프링으로 대체된다. 제안된 해석 모델의 검증을 위하여 상용 소프트웨어를 이용한 FEM 해석과 비교를 실시하고, 제안된 해석모델의 케이블 지지교량의 구조해석에 대한 적용 가능성을 검증한 후 최적화 절차에 적용하였다. 이를 통하여, 사장현수교의 구조해석모델을 작성 및 분석에 대한 소요시간이 현저히 줄어들었다. 한편, 간략화 해석모델의 적용성 검토에 적용된 예제 교량을 사용하여 측경간장의 변경, 현수구간 길이, 중첩구간 길이, 케이블 새그 및 고정하중 분담율의 변화가 사장-현수교의 구조적 정적거동 특성에 미치는 영향을 분석하였다. 이 연구에서는 주경간장 1,408m 인 제3보스포러스 교량을 예제 교량으로 채택 하였다. 이러한 변수연구 조사의 결과는 제안된 최적화 절차에서 설계 변수의 범위를 설정하는 데 적용되었다.

사장-현수교의 케이블 시스템 설계에 대한 최적화 문제는 상부구조의 최소 건설 비용을 찾는 비용 최적화로 정의되며, 최적화 과정 중 설계변수 조합에 대한 사장-현수교 해석 모델의 설계 적정성을 판별하기 위해 도로교 설계기준 및 Eurocode의 설계기준을 통하여 구조 안전성을 검사하였다. 차량 하중 및 철도 하중에 대한 최적의 케이블 시스템이 제안되었으며, 민감도 분석을 수행함으로써 최적 결과에 대한 설계제약조건 및 변수의 민감도를 조사하였다. 그 결과, 구속조건 중 현수 케이블의 각도 변화($\Delta\theta_{sp}$)와 설계변수 중 현수교 구간 길이(L_{sp})rk 케이블 시스템의 최적 설계에 가장 지배적이다.

간략화 해석모델을 적용한 사장-현수교의 최적 케이블 시스템을 찾기 위한 최적화 절차는 매우 합리적이고 효율적이어서 실제 설계업무 시 발생되는 많은 반복작업에 소요되는 시간, 비용 및 인력을 감소시킬 수 있다. 또한, 도로 교량과 철도 교량을 위해 제안된 최적의 케이블 시스템은 예비 설계단계에서 개념설계를 찾기 위해 소요되는 반복적인 해석작업을 감소시킬 것이다.

주요어 : 케이블 시스템, 사장-현수교, 비용 최적화, 간략화 해석모델, 변수해석, 민감도 해석, 유전자 알고리즘

학 번 : 2011-30985